Fall 2014

An electrospinning apparatus for the production of heterogeneous scaffolds and their application in cartilage regeneration

Andrew Ryan Hollingsworth
New Jersey Institute of Technology

Copyright Warning & Restrictions

The copyright law of the United States (Title 17, United States Code) governs the making of photocopies or other reproductions of copyrighted material.

Under certain conditions specified in the law, libraries and archives are authorized to furnish a photocopy or other reproduction. One of these specified conditions is that the photocopy or reproduction is not to be "used for any purpose other than private study, scholarship, or research." If a, user makes a request for, or later uses, a photocopy or reproduction for purposes in excess of "fair use" that user may be liable for copyright infringement,

This institution reserves the right to refuse to accept a copying order if, in its judgment, fulfillment of the order would involve violation of copyright law.

Please Note: The author retains the copyright while the New Jersey Institute of Technology reserves the right to distribute this thesis or dissertation

Printing note: If you do not wish to print this page, then select "Pages from: first page # to: last page #" on the print dialog screen

ABSTRACT

AN ELECTROSPINNING APPARATUS FOR THE PRODUCTION OF HETEROGENEOUS SCAFFOLDS AND THEIR APPLICATION IN CARTILAGE REGENERATION

by
Andrew Ryan Hollingsworth

The human body contains a vast array of soft and hard tissues, each with their own unique set of physical, chemical, mechanical, and electrical properties. It is the combination of these tissues that allows the human body to function as it does. However, these tissues are subject to wear, fatigue, and injury and thus can potentially limit the functions of the body. Therefore, tissue engineering has sought various natural and synthetic materials that can be used for fabrication of cellular scaffolds that have the ability to promote cellular attachment, proliferation, differentiation, and eventual whole tissue formation for replacement and repair of damaged human tissues.

The objective of this thesis is to develop an apparatus that is capable of producinga gradedheterogeneous fiber scaffold, and its subsequent application towards the development of a scaffold which mimics the cartilage-bone ECM interface. The scaffold is a combination of fibers made from three separate solutions: 1) gelatin-NaCS in dH_2O and ethanol, 2) gelatin-NaCS-HA/β-TCP in dH_2O and ethanol, and 3) PCL-HA/β-TCP in methylene chloride and dimethylformamide.The fibers produced from the electrospinning of these solutions are intended to mimic the extracellular matrix of hyaline cartilage, calcified cartilage, and subchondral bone, respectively. A co-electrospinning technique, utilizing a grounded rotating mandrel, is used to create the fiber grade through the depth of the scaffold.

A combination of light microscopy, scanning electron microscopy (SEM), Fourier transform infrared spectroscopy (FTIR), and fluorescence microscopy are used to determine several scaffold parameters including: fiber diameter, inter-fiber spacing, fiber alignment, the presence of specific material components, and the confirmation of the presence of two distinct sides to the scaffold. Ideally,the scaffold has the potential of promoting cellular differentiation of mesenchymal stem cellsinto chondrocytes and osteoblasts on separate halves of the same scaffold. However, several hurdles remain that could impede complete differentiation of two cell types on the scaffold, the largest being the absence of a differentiation media that is both osteogenic and chondrogenic. Nevertheless, this work serves as a foundation for the development of electrospun scaffolds that look to generate more than one tissue type.

AN ELECTROSPINNING APPARATUS FOR THE PRODUCTION OF HETEROGENEOUS SCAFFOLDS AND THEIR APPLICATION IN CARTILAGE REGENERATION

by
Andrew Ryan Hollingsworth

A Thesis
Submitted to the Faculty of
New Jersey Institute of Technology
in Partial Fulfillment of the Requirements for the Degree of
Master of Science in Biomedical Engineering

Department of Biomedical Engineering

January 2015

APPROVAL PAGE

AN ELECTROSPINNING APPARATUS FOR THE PRODUCTION OF HETEROGENEOUS SCAFFOLDS AND THEIR APPLICATION IN CARTILAGE REGENERATION

Andrew Ryan Hollingsworth

Dr. George Collins, Advisor Research Professor of Biomedical Engineering, NJIT	Date
Dr. Treena L. Arinzeh, Committee Member Professor of Biomedical Engineering, NJIT	Date
Dr. Bryan J. Pfister, Committee Member Associate Professor of Biomedical Engineering, NJIT	Date
Dr. Bruno A. Mantilla, Committee Member University Lecturer of Biomedical Engineering, NJIT	Date

BIOGRAPHICAL SKETCH

Author: Andrew Ryan Hollingsworth

Degree: Master of Science

Date: January, 2015

Undergraduate and Graduate Education:

- Master of Science Biomedical Engineering,
  New Jersey Institute of Technology, Newark, NJ, 2015

- Bachelor of Science Biomedical Engineering,
  New Jersey Institute of Technology, Newark, NJ, 2013

Major: Biomedical Engineering

I dedicate this thesis to my family for their unwavering support and encouragement; to Dr. George Collins, for his expert guidance and relentless emphasis on "clarity of thought and expression;" to Dr. Bruno Mantilla for his advice and challenging me to think outside my mental boundaries; and to all those in the NJIT CHEN labs who lent their knowledge and time.

ACKNOWLEDGEMENT

This thesis would not have been possible without the guidance and advice of several important individuals who have gracefully lent their knowledge, expertise, time, and advice. First, I would like to extend the utmost gratitude to Dr. George Collins, whose teachings and mantras have inspired me to challenge the status quo through deep philosophical and scientific thought. His calm, strategic, and yet engaging presentation style is one that I look to model my own after. I would also like to thank Dr. Bruno Mantilla, for his planning advice regarding my thesis and all the constructive criticism he has provided when analyzing data. Thanks as well to Dr. Treena Arinzeh, for allowing me to access her laboratory for fluorescence microscopy. Thank you to Dr. Bryan Pfister, for his feedback regarding the preliminary writing of this thesis. I would like to extend a special thanks to Dr. Yuki Imura, for his input regarding my electrospinning device setup, as well as his generosity when it came to listening to my concerns and lending me equipment. I also extend my gratitude to Dr. Gloria Portocarrero-Huang, for her patience and instruction regarding cell staining and fluorescence imaging.Many thanks, to Amir Hossein Rajabi Zamani, for all his help with FTIR analysis andtroubleshooting the electrospinning of the gelatin solutions. Thanks to Khady Guiro, for the SEM imaging of my scaffolds. Thank you to Amy Cilento, for taking the time to tirelessly review my work and lend me her support. Lastly, I would like to thank my family, for pushing me to become the individual I am today. Their undying love, support, and encouragement have given me the courage to tackle some of life's most difficult challenges.

TABLE OF CONTENTS

TABLE OF CONTENTS
(Continued)

LIST OF TABLES

LIST OF FIGURES

LIST OF FIGURES
(Continued)

LIST OF FIGURES
(Continued)

LIST OF FIGURES
(Continued)

LIST OF DEFINITIONS

ECM	Extracellular matrix
PG	Proteoglycan
CS	Chondroitin sulfate
GAG	Glycosaminoglycan
PCL	Polycaprolactone
HA	Hydroxyapatite
HC	Hyaline cartilage
CCZ	Calcified cartilage zone
SCB	Subchondral bone
β-TCP	Beta tri-calcium phosphate
MC	Methylene chloride
DMF	Dimethylformamide
dH_2O	Deionized water
EtOH	Ethanol
NaCS	Sodium cellulose sulfate
ISDGE	Isosorbide diglycidyl ether
MSC	Mesenchymal stem cell(s)
ESC	Embryonic stem cell(s)
SEM	Scanning electron microscopy/microscope
FTIR	Fourier transform infrared spectroscopy

CHAPTER 1

INTRODUCTION

1.1 Objective

Cartilage (specifically hyaline cartilage) is an avascular tissue responsible for ensuring smooth movement of articulating joints. Over the span of an individual's life, this lining of cartilage over the bone can deteriorate, resulting in painful bone on bone rubbing. Between 2010-2012 approximately 52.5 million (22.7%) adults in the US alone were diagnosed as having some form of arthritis – the second largest cause of disability(Control, 2014). It is the loss of this thin lining of cartilage which results in around $128 billion a year in medical care (Control, 2014). In the most drastic circumstances, total joint replacements of the knee and hip are required to eliminate pain. This procedure is extremely taxing on the body and doesn't completely eliminate the problem. Patients can be exposed to metal or plastic wear debris (sometimes toxic) and will eventually develop stress shielding – resorption of bone tissue surrounding the implant, necessitating yet another surgery(Huiskes, 1993). Re-growth of cartilage tissue would eliminate the need for drastic and inherently problematic joint replacement surgeries. This not only means a reduction in medical care spending but also reduced recovery time, increased quality of life, and most importantly a solution for the actual problem.

To address this problem, this thesis will concentrate on the development of an electrospinning apparatus capable of co-electrospinning several different polymer solutionsto create graded fiber scaffolds, which have the potential to mimic complex

ECM, such as the cartilage-bone interface. One polymer solution and set of electrospinning parameters (voltage, flow rate, humidity, temperature, etc.) will be used to create fibers for one half of the scaffold. A second polymer solution (with a different set of spinning parameters) will be electrospunsimultaneouslyto create fibers for the other half. By varying the polymer injection rateforthe polymer solutions separately over time, the amount of each type of fiber deposited onto the mandrel can be controlled. This method allows for the generation of a grade of two differing fibers through the depth of the scaffold.

Ideally, two or more defined sections within these scaffolds wish to be seen. These sections could then contain fibers with varying material or bioactive components, as well as distinct fiber orientation or density. When these scaffolds are tailored for specific applications, such as mimics for the cartilage-bone interface, it would be anticipated that mesenchymal stem cells seeded on the graded scaffold would differentiate into bone progenitor cells on one half of the scaffold and chondrocytes on the otherhalf. Future work can begin on refining the scaffold to further tailor it to the tissue types of interest. A positive outcome could prove very promising for the engineering of non-regenerative tissues. In the area of cartilage regeneration, specifically, this work could lead to highly specialized ECM mimics that model the entire hyaline cartilage ECM, or the cartilage-bone interface. Additionally, modeling of the entire cartilage-bone interface could solve issues surrounding integration of newly formed cartilage with bone tissue, as well ashow the engineered scaffold is integrated with a patient's existing bone, since the presence of bone tissue on half of the scaffold couldallow for grafting onto the patient's bone at the joint.

1.2 Articular (Hyaline) Cartilage

Hyaline cartilage remains an elusive tissue to generate in cell cultures, on scaffolds, and in vivo. Previous scaffolds have focused on the regeneration of adult hyaline cartilage, despite the fact that adult cartilage is not generative. Instead, direction can be focused on the generation of fetal cartilage, which eventually develops into adult hyaline cartilage. Fetal cartilage, although similar in material components to adult cartilage, possesses different quantities of collagen, GAGs, and proteoglycans as well as differences in structural organization.

1.2.1 Function

Articular cartilage is a thin layer of connective tissue found on the ends of bones in diarthrodial joints. This avascular tissue provides a low-friction, load-bearing surface on which jointed bones can glide. It is this cartilage that provides all joints with several biomechanical functions including wear resistance, load bearing capabilities, and shock absorption (Lu & Mow, 2008).The absence of this thin layer of tissue causes increased friction within the joint, thus hindering motion and causing painful bone-on-bone rubbing. This often occurs in those who have received traumatic injury to a joint, suffer from an autoimmune disease such as rheumatoid arthritis, or those who place high static compression on the joint up to physiological strain magnitudes. Joint immobilization often leads to chondrocyte death and loss of proteoglycan content. Therefore, regular loading and mobilization of the joint is necessary to maintain cartilage density; however,

the magnitude, rate, and frequency of the loading will determine the effect on the cartilage tissue (Lu & Mow, 2008).

1.2.2 Composition

Cartilage is often defined as a viscoelastic material, as it is comprised of three distinct phases, each with its own unique physical and mechanical properties.The first phase is a solid phase, which is comprised of collagens II, III, VI, IX, X, XI, XII, and XIV (collagen II being the main constituent) (Eyre, 2002).These collagens form a fibrillar network with embedded proteoglycans (Figure 1.1). The exact orientation of the collagen fibers changes throughout the cartilage tissue, depending upon their location relative to the articulating surface (Figure 1.2). Normally, collagen comprises 15-22% by wet weight, and PGs 4-7% by wet weight (Lu & Mow, 2008).The second phase is a fluid phase, which is comprised of <80% by wet weight of water. Water, in conjunction with PGs, accounts for most of cartilage's compressive strength. The last phase is an ion phase which accounts for less than 1% by wet weight of cartilage. This phase contains numerous positively and negatively charged ions such as Na^+, Ca^{2+}, and Cl^-.

When cartilage is compressed, fluid is able to flow within or out of the collagen-PG network due to the created pressure gradient. The movement of fluid through the

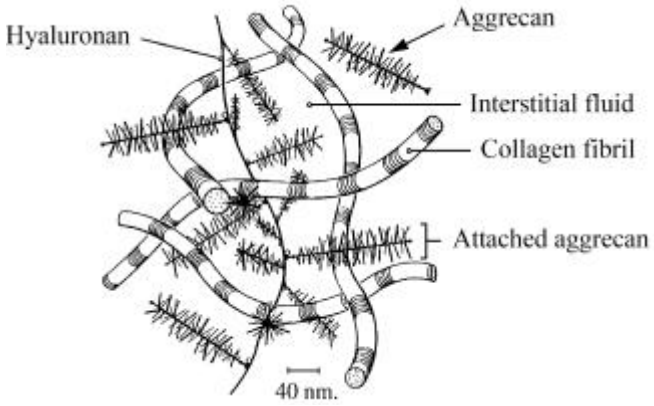

Figure 1.1 Schematic representation of porous collagen and PG network.

Source: (Lu & Mow, 2008)

solid matrix generates very high frictional resistance due to the non-covalent interactions between the negatively charged PGs and the charged ions present in the water. This fluid movement is the primary mechanism that gives rise to the frictional dissipation and viscoelastic behavior of cartilage (Lu & Mow, 2008).

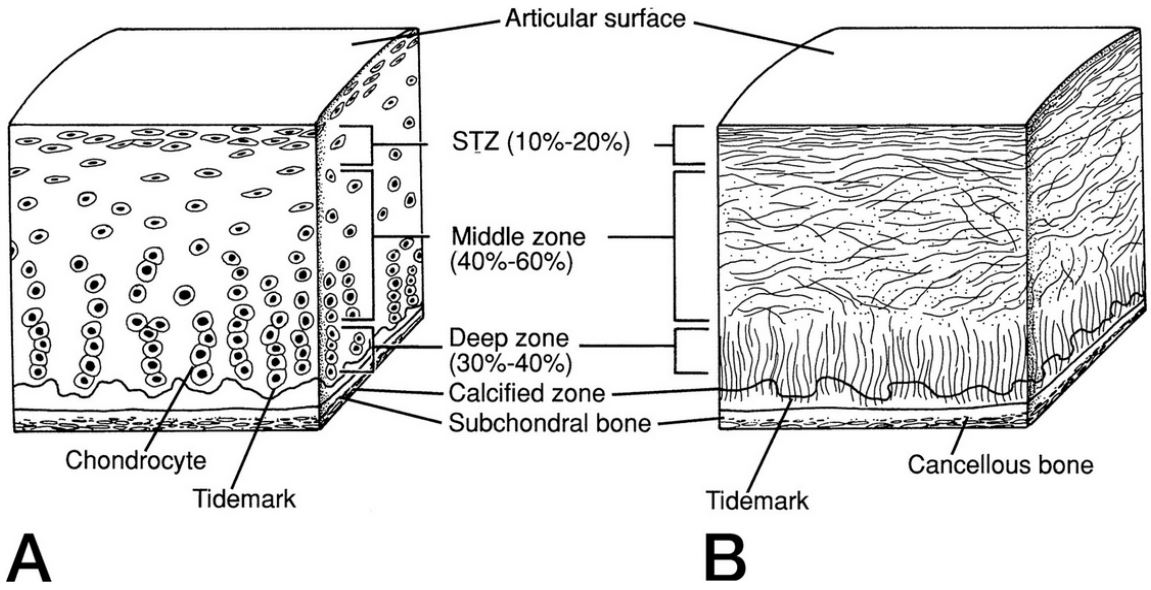

Figure 1.2 Schematic of chondrocyte localization (A), and collagen fiber orientation (B).

Source: (Buckwalter, Mow, & Ratcliffe, 1994)

1.2.2.1 Collagen and Collagen II. Generally, collagen is comprised of a glycine-X-Y amino acid sequence, where X and Y can be any other amino acid (although typically glycine-proline-hydroxyproline). These sequences of amino acids then form α-chains, which are then arranged into left-handed α-helices (coiled-coil), making them rather resilient to proteolytic degradation except by specific metalloproteinases (Cremer, Rosloniec, & Kang, 1998). A number of different types of collagen (I, II, III, V, XI) spontaneously form fibular structures *in vivo*; however, only collagen II, VI, IX, X, and XI are found in sufficient quantity in cartilage.

These collagens comprise a large portion of the cell's extracellular matrix, giving soft tissue its mechanical strength in addition to imparting useful extracellular information to bound cells via integrin binding. In hyaline cartilage alone, collagen II comprises 80-85% of the total collagen (Cremer et al., 1998). This is due mostly to collagen II's structural motif – which refers to the protein's super-secondary structure that consists of several secondary structures to form coiled-coils, parallel β-sheets, anti-parallel β-sheets, Greek keys, helical bundles, and more – and residues – which refers to specific amino acids or their side chains that comprise the primary protein structure. It is collagen II's high hydroxylysine content and helical α_1II chains, which allow for glycosylation, that subsequently makes it an ideal component for the hydrophilic cartilage tissue (Cremer et al., 1998).

The α_1II chains in collagen II form a homotrimer that twists around a central axis to create the coiled-coil motif. Coiled-coils can be found in collagen XI, IX, or X as well, however they are either homotrimers of a different α-chain (such as α_1X) or heterotrimers of α-chains (Cremer et al., 1998). These coiled-coils are quite stable due to numerous secondary bonding forces within the core of the coiled-coil, and allow for the formation of long collagen fibers. The presence of hydrophilic residues in collagen II, such as lysine, allow for hydroxylation, modifying lysine groups into hydroxylysine.This hydroxylation is needed for eventual glycosylation of the hydroxylysine, crosslinking, and the eventual formation of the triple helix and the protein as a whole. More specifically, "the hydroxyl groups of hydroxylysine residues have two important functions: they serve as attachment sites for carbohydrates and they play a crucial role in stabilizing intra- and intermolecular crosslinks" (Wang, 2002).

Additionally, theα_1II chains that make up collagen II are comprised of a von Willebrand factor (type C) domain near the N-terminus (extending from the 32nd to 90th AA position), a fibrillar domain near the C-terminus (extending from the 1,252nd to 1,487th AA position), and seven triple helix repeats (scattered over the 117th to 1,216th AA positions) (EMBL-EBI). It is within the fibrillar domain, from the 1301st to the 1309th AA position that metal binding (Ca^{2+}) can occur. These calcium binding regions then allow collagen II to bind to integrin binding domains on cells. Integrins $\alpha_1\beta_1$, $\alpha_2\beta_1$, and $\alpha_3\beta_1$ act as the major cell surface receptors for collagen (Tuckwell, Ayad, Grant, Takigawa, & Humphries, 1994).The β_1 domain contains a Rossman dinucleotide binding fold, as well as two metal binding sites; the β-propeller domain contains four Ca^{2+} binding sites which are "solvent exposed and may be involved in allosteric regulation of the integrin ligand binding"; and the α_1 domain contains a conserved cation binding site (Tulla, 2007). The presence of a metal cation (either Mg^{2+}, Mn^{2+}, or Ca^{2+}) mediates the binding of collagen with the $\alpha_1$domain of the integrin (Figure 1.3). The aspartate (D151

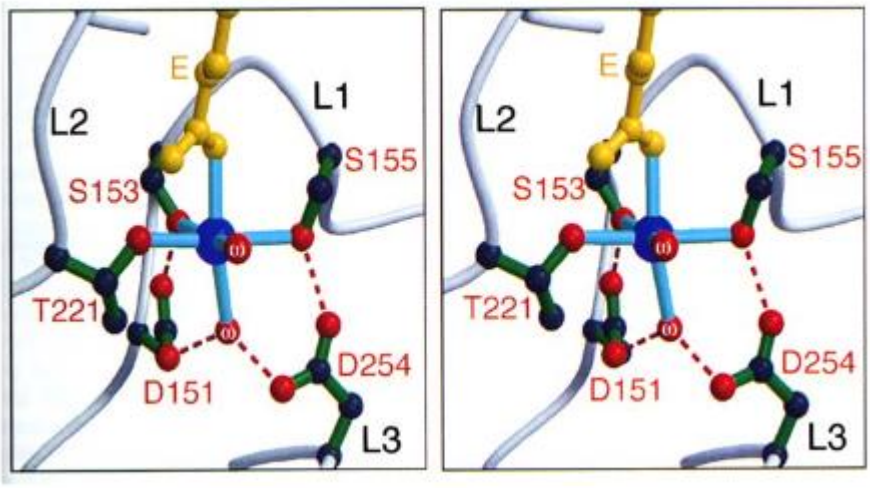

Figure 1.3 Image of α_1 domain bound to glutamate residue of collagen (yellow). Cation is colored blue, oxygen colored red, water colored red and marked with "ω", carbon colored black, and loops of the α_1 domain colored grey.

Source: (Tulla, 2007)

in Figure 1.3) bonds to the metal cation via a water molecule, while threonine (T221) and the serines (S153, S155) directly bond via hydroxyl oxygen; two acid residues (D254, E256) then bond to the cation via water; lastly glutamate from collagen will bind to the cation with the help of two water molecules (Tulla, 2007).

1.2.2.2 Proteoglycans. A proteoglycan consists of a protein core with various attached polysaccharide side chains called glycosaminoglycans. Several glycosaminoglycans are foundthroughout the body; however the most prominent in cartilage are chondroitin sulfate, keratin sulfate, and hyaluronic acid(Muir, 1978; Roughley, 2006). Hyaline cartilage is characterized by its high proteoglycan aggrecan – which is a combination of proteoglycan aggregates, hyaluronic acid, and link protein (Figure 1.1) (Roughley, 2006).The interaction between the core protein of the aggrecan and hyaluronic acid is very strong (binding affinity of $10^{-7} – 10^{-8}$ M), and combined with link protein's ability to bind both the aggrecan core and HA, a "tripartite linkage" is made that is "essentially non-dissociating and non-displaceable under physiological conditions" (C. Knudson & Knudson, 2001). The negatively charged sulfated GAGs present in these aggregate complexes impart a high charge density. Since these aggregates are non-displaceable, there are a large number of fixed negative charges. As previously described in Section 1.2.2, these proteoglycan aggrecans are surrounded by a fluid environment containing water and various ions (Na^+ and Ca^{2+}). Therefore, in order to maintain electrical neutrality within the tissue, each fixed negative charge will require the presence of a positive ion moving through the aqueous cartilage ECM. This then leads to an imbalance of these mobile aqueous ions within and without the aqueous cartilage

environment, creating a pressure difference. Subsequently, the pressure difference causes an influx of fluid into the cartilage tissue, creating high fluid pressure in the tissue (Lu & Mow, 2008). It is this osmotic swelling that further lends to cartilage's viscoelastic behavior.

1.2.2.2.1 Keratin Sulfate. Keratin sulfate is a repeating disaccharide comprised of N-acetylglucosamine and galactose (Figure 1.4). Keratin sulfate is highly variable in its chain length and degree of sulfation when compared to chondroitin sulfate(Muir, 1978). The sulfate groups present impart localized negative charges.

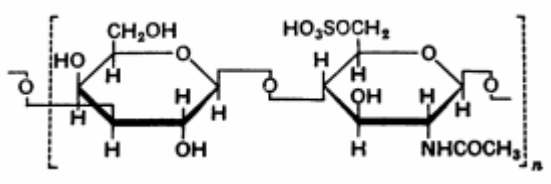

Figure 1.4 Repeating disaccharide structure of keratin sulfate.

Source: (Muir, 1978)

1.2.2.2.2 Chondroitin-4 and -6 Sulfate. Chondroitin sulfate is a repeating disaccharide comprised of N-acetylgalactosamine and glucuronic acid. The degree of

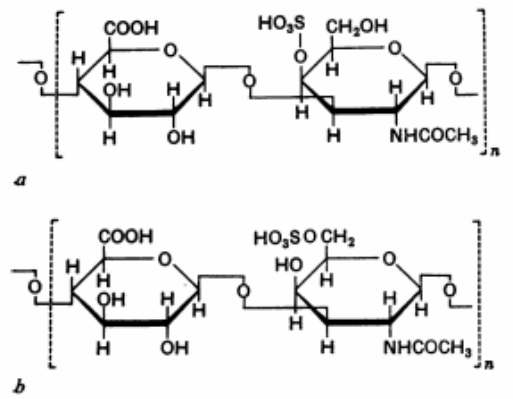

Figure 1.5 Repeating disaccharide of chondroitin-4 sulfate (a) and chondroitin-6 sulfate (b).

Source: (Muir, 1978)

sulfation is relatively constant in chondroitin sulfate, with one sulfate unit per disaccharide unit. However, the sulfate group will present itself at one of two isomeric positions – C_4 or C_6 (Figure 1.5). Again, the sulfate groups impart localized negative charges, allowing interaction with surrounding ions in the aqueous cartilage environment. It is proposed that since the sulfate group in CS6 projects farther from the repeating chain than in CS4, that CS6 may interact more strongly with the surrounding cartilage environment (Muir, 1978).

1.2.2.3 Chondrocytes. Chondrocytes are responsible for the production of collagen and proteoglycans within the cartilage environment. These cells do not form cell-cell contacts – preferring contact with surrounding collagen binding integrins instead (W. Knudson & Loeser, 2002). The distribution of chondrocytes within the cartilage matrix varies depending upon the distance from the articulating surface (Figure 1.2). The density of chondrocytes decreases moving from the superficial zone to the deep zone. Additionally, chondrocytes changefrom a flattened discoidal shape, to spherical, and then ovular shape when in the superficial, middle, and deep zones respectively (Izadifar, Chen, & Kulyk, 2012).

Since cartilage is an avascular tissue, chondrocytes do not receive nutrients from blood vessels. In order to exchange nutrients and waste, these cells rely upon mass transfer through the porous fiber ECM. Pore size, porosity, surface area, and interconnectivity of the pores affect whether the transport of nutrients, wastes, and signaling molecules within the ECM is primarily diffusive or convective(Lanza, Langer, & Vacanti, 2013).

1.2.2.3.1 Chondrocyte–Integrin Binding. The ability of a chondrocyte to sense its spatio-mechanical environment is reliant upon contact-dependent signaling between a cell surface integrin and ECM proteins such as collagen (W. Knudson & Loeser, 2002). The interaction between the integrin domains, the cytoskeleton, and ECM proteins provides a way in which integrins can mediate a variety of cellular activities such as cell shape, gene expression, differentiation, cell growth, and matrix remodeling.

Integrins mediate cell-matrix and cell-cell adhesion through an alpha and beta subunit which are bound non-covalently to form a heterodimer (Tulla, 2007). The two dimers (the alpha and beta subunits) can be further divided into three families: β_1, β_2/β_7, andβ_3/α_V(Reactome, 2013). Each family is geared toward a specific function. The β_1 subunit can bind to 12 other α subunits to create a variety of integrins for RGD, collagen, and laminin binding as well as identification of matrix and vascular ligands (Reactome, 2013). The β_2/β_7 family regulates leukocytes and mediates cell-cell over cell-matrix interactions, while the β_3/α_V family is dedicated to RGD reception (Reactome, 2013). The integrin pictured in Figure 1.6 is comprised of a α_2 and β_1 dimer – again the association of different dimers produces different integrin roles. Of all the integrins found within the body, the $\alpha_1\beta_1$, $\alpha_2\beta_1$, $\alpha_{10}\beta_1$, and $\alpha_{11}\beta_1$ integrins serve as receptors for collagen (White et al., 2004). Depending upon the integrin domains present and the type of bound collagen, various types of cellular signaling can occur including increase in proliferation, reduction/increase in collagen synthesis, and increase in collagenase synthesis– although not all signaling events are known for each integrin subunit (White et al., 2004).

The binding of integrin with an ECM protein such as collagen is mediated through the presence of a metal cation (Mg^{2+}, Mn^{2+}, or Ca^{2+}) as both integrin and collagen fibers contain metal cation binding sites (Tulla, 2007; UniProt, 2013a).The aspartate (D151 in Figure 1.3) bonds to the metal cation via a water molecule, while threonine (T221) and the serines (S153, S155) directly bond via hydroxyl oxygen; two acid residues (D254, E256) then bond to the cation via water; lastly glutamate from

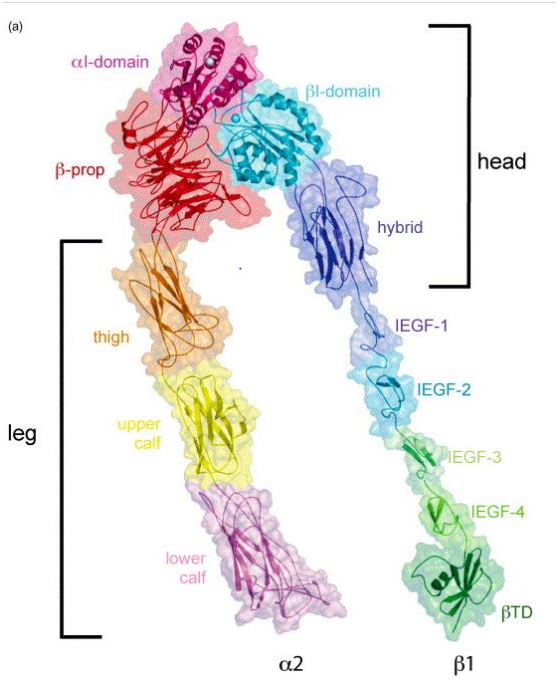

Figure 1.6 Model of a $\alpha_2\beta_1$integrin – a heterodimer of a $\alpha_2$and β_1 subunit.

Source: (White, Puranen, Johnson, & Heino, 2004)

collagen will bind to the cation with the help of two water molecules (Tulla, 2007).This metal cation binding and coordination results in a conformational change of the integrin structure. The activation of the α_1 domain on the integrin (via cation binding) causes an α_7 helix within the α_1 domain to push out, moving the β-propeller; a similar phenomenon occurs for the β_1 domain when a cation binds, except that the hybrid domain is moved instead of the β-propeller (White et al., 2004). In either case, the movement of the β-

propeller or hybrid domain causes the α_2 or β_1 legs (respectively) to open, putting the integrin in an active conformation (seen in Figure 1.6).

After the binding of the collagen and metal cation (the primary messenger) to the integrin, the integrin is then able to carry out several interactions with varying cytosolic proteins (secondary messengers). Integrin acts as a bi-directional bridge, binding to extracellular collagen and intracellular cytoskeletal proteins. Phosphorylation of RAP1[1]'s bound GDP via GEF yields an activated RAP1, which now has bound GTP[2]. Subsequent coordination between the GTP-bound RAP1, PIP2, and RIA[3] then allows for the binding of Talin[4]. The binding of Talin to RIAM causes RIAM and Talin to then dissociate from RAP1 and PIP2. The dissociated RIAM-Talin complex is then able to bind to the α or β subunit leg on an activated integrin. The activation of the integrin with bound Talin then causes the binding and activation of SRC - a non-receptor protein tyrosine kinase responsible for the activation of other tyrosine kinase families (UniProt, 2013b) – thus, binding and activating the tyrosine kinase FADK1. FADK1 is known to have roles in regulating cell migration, proliferation, adhesion, spreading, cytoskeletal actin reorganization, focal adhesion assembly/disassembly, cell cycle progression, and apoptosis (UniProt, 2013h). If FADK1 activates a tyrosine-protein kinase (SYK) actin polymerization could be an end result. If instead, FADK1 binds and activates a docking protein (p130CAS), which then activates another adapter protein (CRK), the cell may undergo cytoskeletal reorganization – this is because the CRK adaptor protein contains

[1] RAP1 – a GTPase acting as a cellular switch (UniProt, 2013f)
[2] GTP – Guanosine triphosphate
[3] RIAM – GTPase activator for the RAP1 protein, which converts the active RAP1 with bound GTP to its inactive state with a bound GDP (UniProt, 2013f)
[4]Talin – protein involved in the connection of major cytoskeletal structures (such as actin) to the plasma membrane (UniProt, 2013g)

SH2 and SH3 domains (SRC homology domains) which positively and negatively (respectively) regulate assembly of specific protein complexes (UniProt, 2013d, 2013e). Still, if FADK1 binds and activates a growth factor receptor-bound protein (GRB2), GRB2 can then complex with a gene encoding guanine nucleotide exchange factor (SOS) thus activating a MAPK (mitogen-activated protein kinase) pathway which can regulate gene expression, differentiation, mitosis, and protein production (UniProt, 2013c).

1.3 Bone

1.3.1 Function

Bone is a highly specialized tissue characterized by its rigidity, hardness, and ability to regenerate. Primarily,bone is responsible for providing the supporting framework of the human body; however it is also responsible for production of marrow (blood forming and fat storage), the storage of crucial minerals such as calcium, storage of growth factors and cytokines, and maintenance of acid-base balance (Kini & Nandeesh, 2012). Bone is constantly undergoing remodeling – a state of bone resorption and deposition – in response to tissue damage and biomechanical forces.

1.3.2 Composition

Bone has two main components – cortical bone which is the dense outer layer, and trabecular (or cancellous) bone which is the soft, porous inner layer containing the bone marrow. Cortical bone is further divided into an outer periosteal surface and an inner endosteal surface. The periosteal surface is comprised of fibrous connective tissue, blood vessels, nerve fibers, osteoblasts, and osteoclasts (Kini & Nandeesh, 2012). The

endostealsurface behaves like a membrane, covering the inner surface of the cortical and cancellous bone, as well as the Volkmann's canals. The type of bone found within the

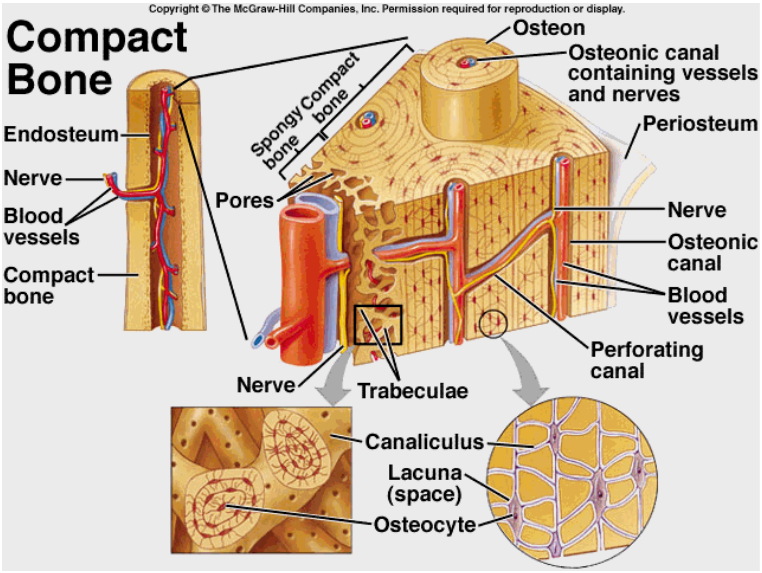

Figure 1.7 Cross sectional view of compact bone.

Source: (Shier, Butler, & Lewis, 2009)

osteons of cortical bone is further divided into woven and lamellar bone, both of whichare characterized by the organization of their collagen fibers. Woven bone has a disorganized arrangement of collagen fibers, making it relatively weak. This type of bone is rapidly formed by osteoblasts during bone repair and growth and eventually is converted into lamellar bone. Lamellar bone has highly aligned collagen fibers in sheets, making it much stronger mechanically (Kini & Nandeesh, 2012).

Bone itself is a combination of organic and inorganic components, comprising 22% and 69% of the bone matrix, respectively.Hydroxyapatite accounts for 99% of the inorganic components, while calcium and inorganic phosphate (amorphous calcium phosphate later matures into hydroxyapatite) make up the remainder. Collagen accounts for 90% of the organic components (90-95% of which is collagen I), with the remainder being proteoglycans, sialoproteins, glacontainingproteins, and 2HS-glycoprotein (Kini &

Nandeesh, 2012). The remainder of the bone matrix contains functional components such as cytokines and various other growth factors.

1.3.2.1 Hydroxyapatite. Crystalline hydroxyapatite is the main inorganic mineral component of bone, occupying roughly one fourth the volume and one half the mass of adult bone (Kini & Nandeesh, 2012). In this crystalline form, $Ca_{10}(PO_4)_6(OH)_2$, hydroxyapatite alone is brittle and relatively fragile in tension (Oyefusi et al., 2014).However, in bone, hydroxyapatite is deposited along the collagen fibers, lending to the overall strength of the bone tissue matrix.

1.3.2.2 Osteoblasts/Osteoclasts. The two main mesenchymal stem cell derived cell types found within bone are osteoblasts and osteoclasts. These cells are responsible for the maintenance and growth of the bone matrix. Osteoblasts regulate osteoclasts and are responsible for the deposition of the bone matrix. During maturation osteoblasts develop the ability to secrete bone matrix; however, they often will surround themselves in their own matrix. As a result, the osteoblasts will halt bone matrix secretion and develop into osteocytes – the most abundant cell in bone, responsible for communicating with other osteocytes, the surrounding matrix medium, and osteoclasts (Kini & Nandeesh, 2012). The osteoclasts are then responsible for dissolving the bone tissue. Primarily, osteoclast activity takes place on the endosteal surface (inner surface of the cortical bone next to the marrow cavity). This then allows the marrow cavity to enlarge at a pace equivalent to the growth of the circumference of the bone shaft (Sherwood, 2007).

1.4 Calcified Cartilage

In Sections 1.2 and 1.3 the function and composition of two primary tissues of interest, hyaline cartilage and bone, were discussed. Individually, the function and composition of these tissues is apparent; however, what is not is the relationship between the two – specifically the transition from bone to hyaline cartilage. Cartilage does not simply lie upon the ends of bones in diarthrodial joints like a sheet. Although it is easy to think of cartilage and bone as being completely separated tissues with a clear and abrupt transition, this is not the case. Between subchondral bone and hyaline cartilage there exists a transitional area in which deep zone regions of cartilage can undergo endochondral ossification to become calcified(Lyons, McClure, Stoddart, & McClure, 2006). This region of calcified cartilage is known as the calcified cartilage zone (CCZ) or the chondro-osseous junctional region.

1.4.1 Function

The calcified cartilage zone (seen in Figure 1.8) is a thin region of mineralized or calcified cartilage roughly 70-250μm thick – depending upon the joint location, age, and health of the patient (Lane & Bullough, 1980). This CCZ is responsible for attaching hyaline cartilage to the subchondral bone, providing transmission of force across the joint, limiting molecular diffusion from subchondral bone, and transfer of interstitial fluid between tissue layers (Oegema, Carpenter, Hofmeister, & Tompson, 1997; Zhang et al., 2012).

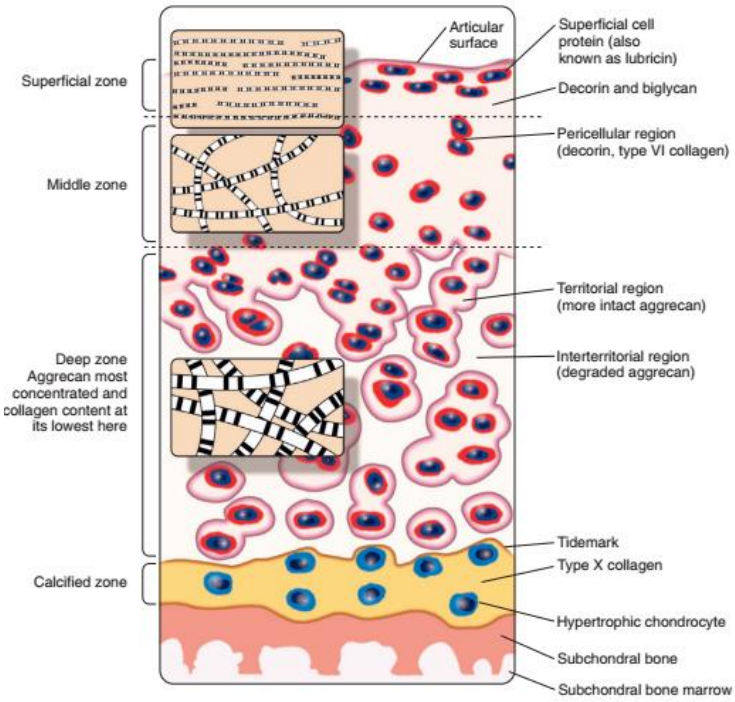

Figure 1.8 Structure of hyaline cartilage, including superficial, middle, and deep zones as well as the calcified zone and subchondral bone. Note the changes in collagen and architecture as well as cell morphology.

Source: (Goldring, 2009)

This CCZ also serves as an ossification front for further bone growth and remodeling. The endochondral ossification occurs when vessels in the underlying subchondral bone invade the CCZ. The presence of blood vessels allows for the advancement of osteoblasts into the CCZ (this zone is normally avascular, much like in hyaline cartilage). Osteoblasts in close proximity to these invading vessels are then able to remodel the surrounding ECM and create bone tissue (Bullough & Jagannath, 1983).These cells are able to increase mineralization through the production of enzymes which locally increase calcium and phosphate concentration, as well as ECM vesicles which allow for hydroxyapatite deposition (Bullough & Jagannath, 1983). Consequently, the conversion of calcified cartilage into bone tissues causes a thinning of the CCZ. In

order to maintain the CCZ, calcification advances into the deep layers of hyaline cartilage, gradually reducing the thickness of the hyaline cartilage. The thickness of the CCZ can vary based upon age and joint loading. Loss of CCZ and hyaline cartilage thickness can be seen with increasing age. The exact rate of CCZ thickness loss is variable, but rate of loss remains relatively steady until the age of sixty, at which the loss in CCZ thickness accelerates (Lane & Bullough, 1980). It was also found that joint immobilization increases CCZ thickness, and that remobilization can reduce CCZ thickness back to normal, suggesting that calcification and tidemark advancement is linked to resorption (Oegema et al., 1997). It is also interesting to note that, as previously mentioned, joint immobilization is a cause for cartilage loss. It can now be seen that this is most likely the case due to the increased thickness of the CCZ after immobilization, forcing un-calcified deep zone cartilage to become mineralized.

1.4.1.1 The Tidemark. Directly abutting the CCZ and the deep layer of hyaline cartilage is the tidemark. The tidemark serves as a junction between the calcified cartilage (CCZ) and the un-calcified hyaline cartilage. It marks the extent of the ossification front and plays a role in the transduction of mechanical forces (collagen fibers here are able to resist both direct compression and lateral shear)between hyaline cartilage and the underlying CCZ and bone (Broom & Poole, 1982). Additionally, this region is not inert – it is metabolically active as a zone of regulation, halting uncontrolled vascular invasion and subsequent mineralization of cartilage tissue (Lyons et al., 2006). This region also plays a role in joint nutrition, as it is permeable to low molecular weight solutes, allowing

nutrient access to the deep zones of the avascular hyaline cartilage (Arkill & Winlove, 2008).

1.4.2 Composition

Calcified cartilage is comprised of organic and inorganic constituents. The organic portion CCZ is comprised primarily of collagen, specifically collagen II and X. Just as in hyaline cartilage, collagen II is responsible for imparting tensile strength and is the major component of collagen fibrils. Unlike hyaline cartilage, which has a collagen II content of 15-22% by wet weight or ≈61% by dry weight, calcified cartilage has a lower collagen II content of ≈20% by dry weight (Zhang et al., 2012). Type X collagen is present within this calcified zone as well, providing support for endochondral ossification. In fact, collagen X is a hypertrophic chondrocyte marker, as 45% of collagen produced by mature hypertrophic chondrocytes is type X (Shen, 2005).In addition to collagen II and X, GAGs are also present (similar to un-calcified hyaline cartilage), as well as alkaline phosphatase (Hoemann, Lafantaisie-Favreau, Lascau-Coman, Chen, & Guzman-Morales, 2012).

The inorganic portion of the CCZ contains several components including calcium, phosphorous, potassium, sulfur, zinc, and strontium(Hoemann et al., 2012). These inorganic components and minerals account for roughly 60% of the CCZ dry weight, compared to bone's 80%; however, the main component is a low crystallinity hydroxyapatite (comprised of calcium and phosphorous). As an inorganic compound, HA comprises roughly 65% by dry weight, compared to the ≈86% found in bone (Zhang et al., 2012).

1.4.2.1 Collagen X. Collagen type X is believed to play an important role in the regulation of the ossification front in calcified cartilage due to its association with hypertrophic chondrocytes; however, the exact mechanism through which collagen X regulates calcification is not completely known, but there are some educated speculations. The first proposed way in which collagen X regulates mineralization is through matrix vesicles[5], which serve as the starting point for hydloxyapatite formation. These matrix vesicles are formed by chondrocytes in a collagen II and X ECM within the hypertrophic zone. These vesicles then become trapped in this zone and serve as nucleation points for mineralization. A similar phenomenon is seen in the growth plate, where these matrix vesicles associate themselves with proteoglycans and can subsequently bind to collagen II and X (Shen, 2005).

The second proposed way in which collagen X regulates mineralization follows closely with matrix vesicle entrapment. Matrix vesicles contain three proteins similar to annexin V, which is a Ca^{2+} dependent acid phospholipid binding protein (Shen, 2005).Annexin V is found to bind to collagen X independent of Ca^{2+} content (Wu, Lark, Chun, & Eyre, 1991). In doing so, annexin V's Ca^{2+} ion channels open, allowing uptake of Ca^{2+} into the matrix vesicle. Therefore, the local increase of calcium ions in hypertrophic CCZ is a result of matrix vesicle and collagen X binding.

Lastly, collagen X is believed to regulate mineralization through compartmentalization of cartilage ECM components. This is a result of collagen X's matrix vesicle entrapment and binding. Due to collagen X's hexagonal lattice structure and its affinity proteoglycans and other collagen fibrils, it is able to act as a fiber web,

[5]Matrix vesicles contain mineral and alkaline phosphatase and are part of the ECM microstructure (Shen, 2005).

snaring essential components for mineralization (such as matrix vesicles and proteoglycans)(Shen, 2005). Without the presence of collagen X, there is not a high localized content of the necessary components to initiate mineralization. As a result, collagen X effectively dictates the location of the hypertrophic or calcified cartilage zone.

1.5 Tissue Engineering

Tissue engineering is amultifaceted field of research combining the areas of organic chemistry, materials science, physiology, mechanics, and cells to develop therapies and organ transplants for patients suffering from injury and disease. All essential elements of tissue engineering must be considered when constructing an ECM for implantation: the seeded cells, signaling between cells, the material base of the artificial ECM, the design parameters of the ECM (fiber diameter, density, orientation, etc), vascularization after implantation, proper bioreactor environment, maintaining efficacy during storage and transportation, and ensuring that the host can remodel the site of implantation, all without eliciting any life threatening immune responses (Sipe, 2002). Consideration must be given to the cell source (either autologous, allogenic, xenogenic) and cell type as well.

In the past several years tissue engineering devices have moved to include more than one active material component, often incorporating several different materials, biological agents, and drugs. A proper substrate alone is not enough to cause cells to differentiate and develop into functioning tissue. Cells need multiple chemical, mechanical, electrical, and environmental cues to guide their growth. Tissue engineers are putting more focus on their cell sources, preservation of cells, type of biomaterial (synthetic or natural), sterilization, and large-scale culturing (Langer, 1993). This is

because the biocompatibility of a device no longer refers to its immediate toxicity after implantation, but rather the integrity and performance of the device for its intended application throughout the entire span of the device's life – from fabrication, to transportation, to storage, to use.

1.5.1 Biomaterials and Biological Function

Biomaterials can be defined as "any substance or combination of substances, synthetic or natural in origin, which can be used for any period of time, as a whole or as part of a system which treats, augments, or replaces any tissue, organ, or function of the body" (Dee et al., 2002). Natural biomaterials have the advantage of potentially inherently containing the molecular structure and composition needed for cellular attachment,

Table 1.1 Basic Characteristics of Natural and Synthetic Materials

Biological/Natural Materials	**Synthetic Materials**
Cellular	Acellular
Hydrous	Anhydrous
Anisotropic	Isotropic
Heterogeneous	Homogeneous
Viscoelastic	Elastic
Capable of self-repair	Inanimate

Source: (Dee, Puleo, & Bizios, 2002)

differentiation, and proliferation. However, they also have the potential of carrying disease and being immunogenic. On the other hand, synthetic biomaterials can be tailored to have specific chemical, mechanical, and electrical properties. The disadvantage of

these materials is that they often lack the proper cellular binding regions, and have the potential to decompose or be metabolized into toxic byproducts.

The selection of a biomaterial depends on the application it is being used for, but ideally all biomaterials should be biocompatible. The definition of "biocompatible" is not easy to define, as the biomaterial and biological systems are often quite complex. A simple definition of "biocompatability" would be: the ability of a biomaterial to be introduced into a biological system without the degradation or disruption of the normal physiological processes. However, this definition only takes into account the effect of the biomaterial on body. In actuality, the biomaterial and the biological system are constantly interacting. The biomaterial affects the ability of the biological system to function just the same as the biological system affects the ability of the biomaterial to carry out its intended purpose. Instead of using the term "biocompatibility," a more fitting term, biological function, should be used. Biological function can be defined as the ability of a biomaterial to be introduced into a specific biological system with a specific intended function without the degradation or disruption of the normal biological responses of the host, or the degradation of the biomaterial's ability to perform said intended function. It is critical that a biomaterial be selected with a specific intention in mind in order to adequately judge its performance within a biological system.

1.5.1.1 Gelatin. Gelatin is a natural polymer derived from the hydrolysis of collagen (Figure 1.9a, b). It is commonly used in pharmaceutics and medical applications because of its ability to be degraded by natural metabolic processes, ease of modification, and its biocompatibility within a biological environment(Young, Wong, Tabata, &

Mikos, 2005).The physical properties of gelatin largely determine its applications, and this structure can vary slightly depending upon the source of the gelatin. Roughly 46% of

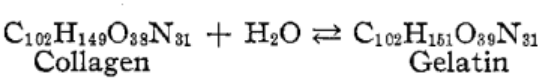

(A)

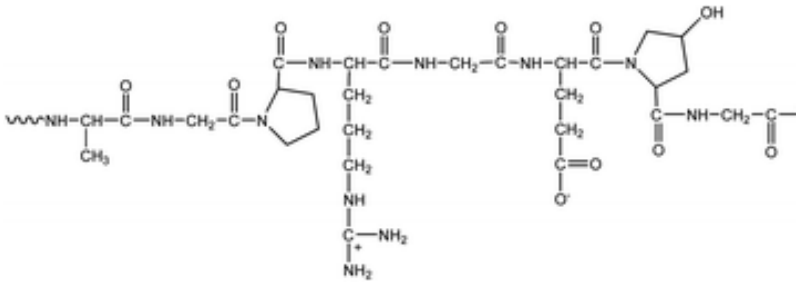

(B)

Figure 1.9 Chemical equation depicting hydrolysis of collagen into gelatin (A) and resulting chemical structure of gelatin (B).

Source: (Bogue, 1923)

all gelatin is gathered from porcine skin, 29.4% from bovine hide, 23.1% from porcine and bovine bones, and 1.5% from fish (Gómez-Guillén, Giménez, López-Caballero, &Montero, 2011). These sources can produce gelatin with varying rheological properties, such as gelation temperature and thermal stability, as well as variances in swelling, solubility, emulsion formation, adhesion, cohesion, colloid function, and film-forming capacity (Gómez-Guillén et al., 2011).

The ease at which gelatin can be degraded *in vivo* can be a problem when designing tissue engineering constructs, especially if the construct must persist within the biological environment for an extended period of time. In order to tailor the rate at which gelatin degrades *in vivo*, chemical or physical crosslinking is employed. This greatly enhances gelatin's uses as a functional tissue engineered scaffold or drug delivery

system. However, care must be given to the form of crosslinking and crosslinking agent used. Particular chemical crosslinkers are highly cytotoxic or become cytotoxic when present in high amounts (Haitang, Qiang, & Heng, 2014).

1.5.1.2 Sodium Cellulose Sulfate. Cellulose sulfates, including sodium cellulose sulfate, have several uses in tissue engineering applications, including cell/drug encapsulation and mimics for ECM proteoglycans (Bohlmann, Schneider, Andresen, & Buchholz, 2002). Cellulose is derived from the cell walls of plants and certain types of algae, with primary sources being wood, cotton, flax, and hemp (Klemm, Schmauder, & Heinze, 2004). The sulfation of cellulose is the most important step in the creation of cellulose sulfate, especially when used as a mimic for ECM proteoglycans. Cellulose contains three free hydroxyl groups at the carbon 2, 3, and 6 positions, which are subsequently used for bonding of sulfate groups (Figure 1.10) (Klemm et al., 2004).

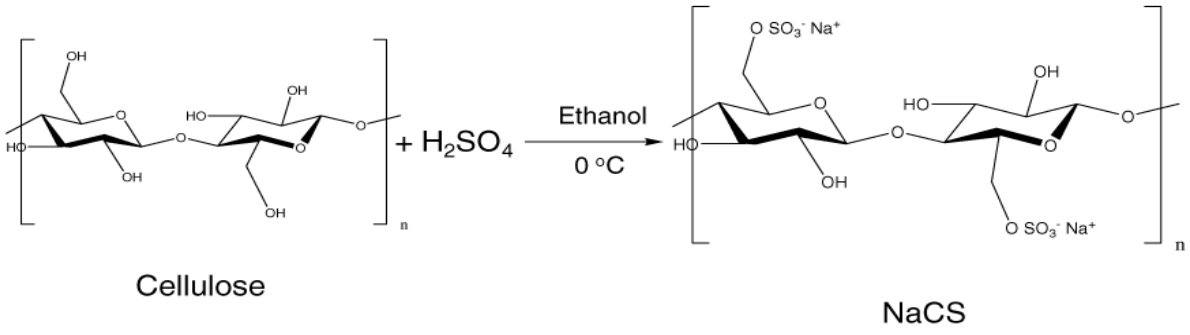

Figure 1.10 Schematic of NaCS synthesis.

Source: (Zeng et al., 2013)

1.5.1.2.1 Similarity between NaCS and Cartilage Proteoglycans. The purpose of including NaCS in tissue engineering scaffolds for cartilage regeneration is to mimic the proteoglycans naturally found within the cartilage ECM. As previously stated, the cartilage ECM contains PGs such as keratin sulfate, chondroitin-4 sulfate, and chondroitin-6 sulfate.NaCS mimics these PGs through its core structure of repeating disaccharide units, in addition to containing active functional groups such as $–SO_3–$, which provide biological functions useful for cartilage repair (Oprea et al., 2010). However, NaCS does differ from these PGs in degree of sulfation. The PGs found within the cartilage ECM are partially sulfated, meaning that not all of their reactive hydroxyl (R–OH)groups obtain sulfate (SO_3^{2-}). NaCS has the potential to be fully sulfated (in which all R–OH groups become $R–OSO_3^-$). The degree of NaCS sulfation depends greatly upon the process of chemical conversion of cellulose to cellulose sulfate.

1.5.1.3 Polycaprolactone. Polycaprolactone is a hydrophobic, semi-crystalline polymer used for a variety of tissue engineering designs in need of resorbable polymers, ECM scaffold structures, and drug delivery systems. PCL has a low melting point (59-64^oC); good blend compatibility; alterable degradation kinetics; alterable mechanical properties; can be easily shaped and manufactured; and has the ability to be co-

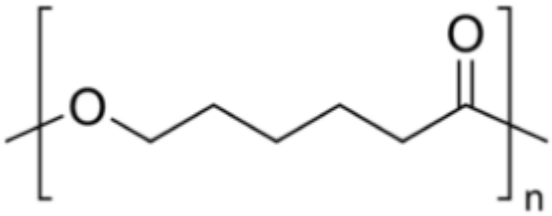

Figure 1.11 Chemical structure of polycaprolactone.

Source: (Sigma-Aldrich, 2014)

polyermized to adjust hydrophobicity, adhesiveness, and biocompatibility (Woodruff & Hutmacher, 2010). Due to PCL's hydrophobic nature, it is not soluble in polar solvents such as water. Therefore, in order to obtain a PCL solution, solvents such as dichloromethane and dimethylformamide are used. PCL is not resorbable within the biological environment of humans due to lack of proper enzymes; however, PCL is biodegradable. The resorption of PCL is on a large time scale (2-4 years), proceeding first through non-enzymatic hydrolytic cleavage of its ester groups and then through intracellular degradation (Woodruff & Hutmacher, 2010).

1.5.1.4 Hydroxyapatite. The hydroxyapatite used for many tissue engineering constructs issimilar to the natural bone apatite found within the bone ECM. HA is prepared through the precipitation and high temperature sintering (>1000^{o}C) of calcium phosphate ceramics to obtain a calcium to phosphate ratio of 1.67 (Ogose et al., 2004). When pure HA constructs are implanted into bone defects, neither postoperative infection nor toxicity is seen; and radiolucent zones around the bone defect disappear in 16 weeks. Additionally, increased density around HA implant sites is seen in subsequent follow-ups, but no evidence of HA biodegradation is seen even at 130 months post-op (Ogose et al., 2004).

1.5.1.5 β-Tricalcium Phosphate. Beta tricalcium phosphate is not naturally found within the bone matrix, however β-TCP does mimic the amorphous calcium and phosphate precursors to bone mineral such as bone apatite (hydroxyapatite), with a stoichiometric calcium-phosphate ratio of 1.5 (Ogose et al., 2004). Since calcium phosphate can manifest as HA, β-TCP, biphasic calcium phosphate, HA/β-TCP, or

calcium-deficient apatite ($(Ca,Na)_{10}(PO_4)_6(OH)_2$), it is important to ensure that the intended type of calcium phosphate is being used.When pure β-TCP constructs are implanted in bone defects, no postoperative infection or toxicity is observed. Radiolucent zones at the implantation site disappeared after 4-16 weeks, with β-TCP being resorbed and replaced by healthy bone tissue (Ogose et al., 2004).

1.5.2 Stem Cells

Just as the human changes from childhood to adulthood, so too do the cells that make them up. Cells can change in a variety of ways with respect to their ability to proliferate, differentiate, or regenerate. These changes in the cell throughout its life can have a profound effect on how tissue engineering attempts to tackle disease and tissue regeneration treatment.

One broad family of cells that has become of great interest to tissue engineers is the stem cell. These cells may be defined "as cells that must choose between alternative fates of self-renewal and differentiation at each division" (Ying, Nichols, Chambers, & Smith, 2003). Within the stem cell tree there are two large categories: embryonic stem cells and adult stem cells. ESCs are harvested from the blastocyst of an embryo before it is implanted on the uterine wall. These cells are termed "totipotent" as they are able to differentiate into cells and tissues of all three germ layers[6], both *in vitro* and *in vivo*(Takahashi & Yamanaka, 2006; Ying et al., 2003). Not only are these cells able to become any cell type found within the body, but if cultured correctly, can undergo symmetrical proliferation indefinitely (Takahashi & Yamanaka, 2006). However, since the behavior of cells is regulated by numerous chemical signals and growth factors, the

[6] Mesoderm, ectoderm, and endoderm

totipotency of embryonic stem cells may not always be retained. Several transcription factors (Oct3/4, sox2, and Nanog) were found to "function in the maintenance of pluripotency in both early embryos and ESCs" while the genes Stat3, E-Ras, c-myc, Klf4, and β-catenin were found to contribute to the "long-term maintenance of the ESC phenotype and the rapid proliferation of ESCs in culture" (Takahashi & Yamanaka, 2006).

After the embryo has developed into the fetus and eventually an adult human, ESCs are no longer able to be harvested from that individual. However, in several adult tissues (adult) stem cells are maintained to either continuously generate new cells or to respond to injury (Clarke et al., 2000). These adult stem cells are termed "multipotent" and are found in bone marrow, skeletal muscle, the cerebral cortex, olfactory bulb, placenta, gastric epithelium, retina, inner ear, and hair follicle bulge – they are able to only differentiate into certain cell lines (Barrilieaux, Phinney, Prockop, & O'Connor, 2006). Since the function of these adult stem cells is determined by the niche they are in, the "maintenance of their stem-like properties may depend on adhesion to non-stem cells" (Barrilieaux et al., 2006). This creates two problems: first this makes it difficult to separate adult stem cells from neighboring cells based on surface markers; and second, by taking the adult stem cell out of its environment there is the possibility that it may lose its potency.

Currently the graded scaffold this thesis discusses does not use MSCs, however, future work looks to observe whether the scaffold is viable and can induce differentiation of chondrocytes and osteoblasts. It is possible a final implantableconstruct could contain MSCs to speed bone fusion and cartilage growth. If stem cells are used for an implantable

construct, autologous MSCs will be chosen over ESCs. Despite the fact that ESCs are totipotent, they are harvested from an embryo with surfaces markers that are different from the patient who will receive the ESCs. These foreign surface markers on the ESCs will trigger an unwanted immune response in the host. By using MSCs (which have the ability to differentiate into chondrocytes and osteoblasts) derived from the patient's own tissue, these cells will have the same surface markers and not be targeted for destruction by the patient's immune system. The use of MSCs also eliminates one of the largest ethical issues surrounding ESC use – the destruction of potential human life. Despite this, some may find the external culturing of MSCs to be against their beliefs or religion. With implantation of autologous MSCs on the scaffold, these cells should differentiate into chondrocytes and osteoblasts and begin to remodel the implanted scaffold by resorbing the existing artificial ECM and depositing their own.

1.5.3 Fiber Scaffolds

An artificial fibrous ECM must not only have a fibrous architecture constructed from material that mimics that found in the natural ECM of bone and cartilage, for example, but also have proper fiber spacing, orientation, and density – all of which will affect how cells attach, grow, differentiate, and receive proper spatio-mechanical signals. ECM construction is further complicated by the fact that being successful in an *in vitro* environment (such as a bioreactor) is not enough. In a bioreactor nutrients and waste are delivered and shuttled away in the medium. However,*in vivo* tissues and cells aren't supplied nutrients from nebulous fluid surrounding them but through blood vessels that have infiltrated the tissue. Therefore, a tissue engineered scaffold must also accommodate

gas exchange and vascularization when placed *in vivo*, then gradually degrade and be metabolized so the patient's own cells/tissue fill the space of the scaffold.

1.5.3.1 Electrospinning. One of the simplest approaches to producing micro- and nano-scale fibers with relatively uniform diameter, diverse composition, long length, and varying interior structure (hollow or solid) is the process of electrospinning. The formation of fibers via electrospinning is based on "the uniaxial stretching of a viscoelastic jet derived from a polymer solution or melt" (Li & Xia, 2004).The stretching and drawing of the polymer jet is accomplished through the injection of charge into the polymer, which in turn creates electrostatic repulsion between the surface charges. As the solution is pulled out of the needle, the solvent evaporates, leaving a solid polymer fiber.

The electrospinning setup (Figure 1.12) is relativelysimple; however the physics behind it and the mechanism of polymer jet formation is rather complex and not fully understood.As the infusion pump pushes the polymer solution through the needle, a small

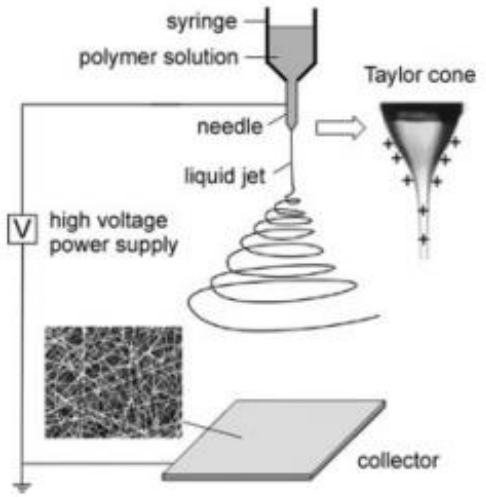

Figure 1.12 Basic electrospinning setup consisting of a high voltage power source, grounded collection plate, conducting or non-conducting needle, syringe, polymer solution, and infusion pump (not shown).

Source: (Li & Xia, 2004)

droplet forms at its tip. The high voltage source electrifies the polymer droplet and evenly distributes charge over its surface. At this point, the polymer droplet experiences electrostatic repulsion between neighboring surface charges, and Coulombic force by the external electric field between the charged needle tip and the grounded collection plate (Li & Xia, 2004). These forces will subsequently shape the polymer droplet into what is known as the Taylor cone (Figure 1.12).Then once the electrostatic forces are able to overcome the surface tension of the polymer solution, the polymer stream is ejected from the nozzle in a whipping motion, leading to the evaporation of the solvent and the deposition of elongated polymer fibers on the collection plate. The whipping motion and elongation of the polymer fiber is believed to be attributed to the electrostatic field and forces present; however, the exact mechanism through which the micro- and nano-scale fibers are created after ejection from the polymer droplet/Taylor cone is unclear.

1.5.3.2 Chemical Crosslinking. Crosslinking is often employed as a way to increase the thermal, mechanical, and degradation properties of the final fiber scaffold. Crosslinking is especially useful in electrospinning of gelatin scaffolds, since gelatin has relatively weak mechanical and degradation properties. There are two methods of crosslinking that can be used for gelatin: physical crosslinking or chemical crosslinking.

Physical crosslinking employs methods such as UV-irradiation and dehydrothermal treatment. Although these methods can be additive free and introduce surface functionalization, they are often inefficient and make it difficult to control crosslinking density (Haitang et al., 2014; Young et al., 2005).Since the crosslinking density can greatly affect the viscosity of a polymer solution, and practical

electrospinning requires a solution with a specific viscosity, physical crosslinking is not employed in the fabrication of the proposed functionally graded fiber scaffold.

The second method of crosslinking, chemical crosslinking, employs the use of various synthetic or naturally derived reagents in order to stabilize a polymer structure while preserving its mechanical properties (Haitang et al., 2014). Greater control can be obtained over the crosslinking density; however, chemical crosslinkers can be cytotoxic to cells at varying concentrations.

Chemical crosslinkers can be divided into main groups: zero-length and non-zero length. Zero-length crosslinkers, such as acyl azides and water-soluble carbodiimides, use carboxylic acid residues to react with an amine group on an adjacent polymer chain – without the need of an additional molecule to directly bridge the crosslinked polymer residues. Non-zero length crosslinkers, such as formaldehyde, glutaraldehyde, glyceraldehyde, polyepoxides, and isocyanates, are poly-functional and act as a bridge between free carboxylic acid or amine groups on polymer chains (Young et al., 2005).

The crosslinker used for the stabilization of gelatin in this study is isosorbide diglycidyl ether (Figure 1.13). This crosslinker is an expoxy compound, thus making it a non-zero length crosslinker. As such, ISDGE will react with carboxylic acid and amine groups on adjacent polymer chains to bridge them (Figure 1.14).

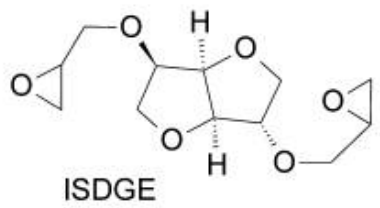

Figure 1.13 Chemical structure of ISDGE.

Source: (Lukaszczyk, Janicki, & Frick, 2012)

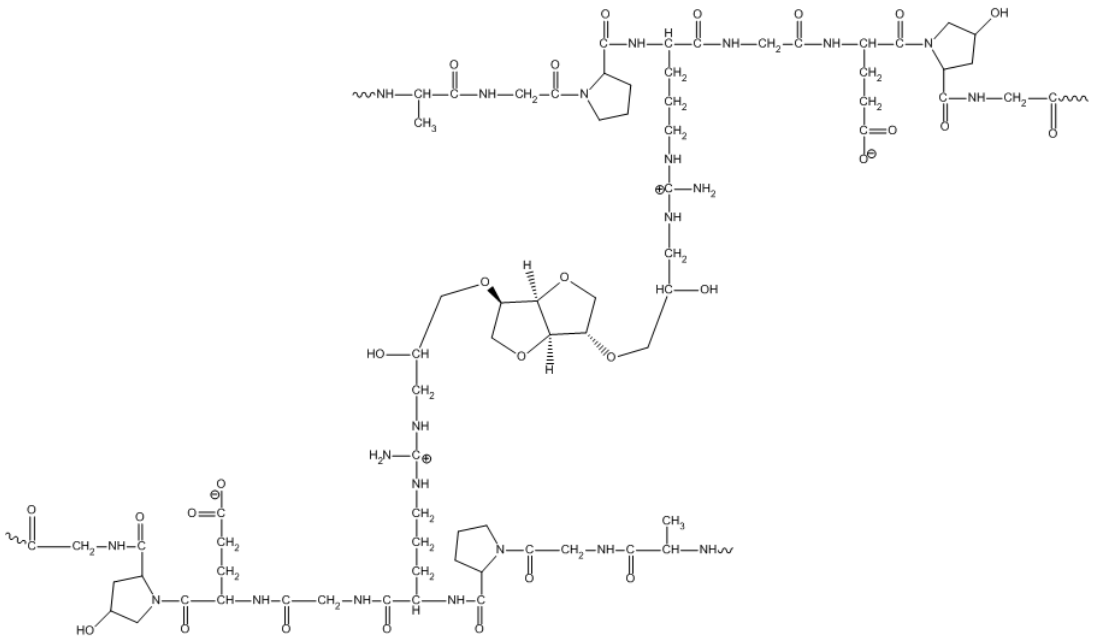

Figure 1.14 ISDGE crosslinking gelatin chains via the primary amine group of the amino acidarginine.

Source: Andrew Hollingsworth

CHAPTER 2

MATERIALS AND METHODS

2.1 Electrospinning Apparatus Setup

The electrospinning of this fiber scaffold entailed co-spinning two polymer solutions. As a result, the typical electrospinning set up (previously seen in Subsection 1.4.3.1) had to be modified. This modification entailed the use of a grounded, rotating mandrel, two voltage sources, two syringe holders (one polyethylene, the other wood), air pump, heater, syringes, and two syringe pumps (Figure 2.1). The rotating mandrel consists of a motor attached to a plastic coated hollow metal rod. Half way up the rod is an attached metal cylinder which acts a collection plate for the electrospun scaffolds. To ground this open cylinder, a wire is soldered to the inside of the cylinder and then runs through the hollow metal rod to the end distal the motor. At the distal end is a slip ring which allows

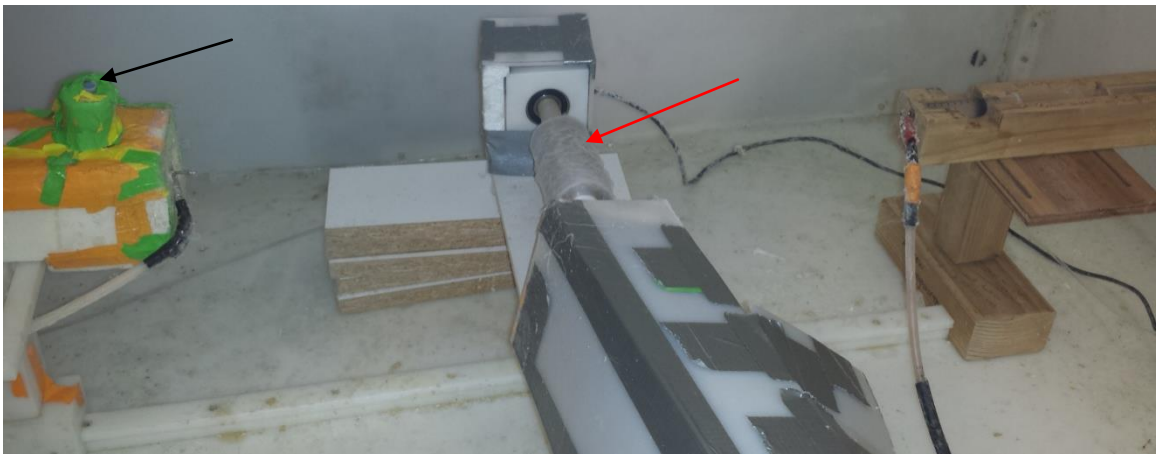

Figure 2.1 Picture of electrospinning setup. *Left* – polyethylene syringe holder which holds the gelatin based solutions. This syringe holder is housed within a Styrofoam housing to maintain a constant air temperature. The heated air line is fed through the hole in the top (arrow). *Right* – wooden syringe holder containing the PCL based solution. *Middle* – rotating mandrel with motor and slip ring ground connection covered by polyethylene sheets. The collection plate is identified by a red arrow. Note: the infusion pumps and voltage sources are not shown in this picture.

for electrical connection between the rotating rod and cylinder, and the grounded stationary nub (Figure 2.2). The hollow metal rod and wires are insulated with electrical tape, while the motor and grounded end of the mandrel is shielded with polyethylene sheets. This ensures that the electrospun fibers deposit only on the surface of the metal cylinder. Additional information regarding the rotating mandrel and electrospinning setup can be found in appendices A and B.

Figure 2.2 Picture of the slip ring with a protruding eye hook to allow for attachment of the grounding wire clip. This grounded eye hook is shielded by polyethylene housing.

2.2 Fabrication of Scaffold

In this study, gelatin from bovine skin (type B), sodium cellulose sulfate, isosorbide diglycidyl ether, deionized water, polycaprolactone, methylene chloride, dimethylformamide, hydroxyapatite, and beta-tricalcium phosphate are used to create the polymer solutions used for electrospinning of the fiber scaffold. Gelatin was provided by Sigma-Aldrich (USA, Lot # MKBQ1929V); sodium cellulose sulfate was provided by

Dextran Products (Canada, Lot# SCS 020R); isosorbide diglycidyl ether was synthesized in the Medical Device Concept Laboratory by Dr. W. Hammond (Newark, NJ); 3mm polycaprolactone pellets were provided by Sigma-Aldrich (Mn 70,000-90,000, USA, Lot# MKBK2903V); methylene chloride was provided by Fisher Scientific (USA, Lot# 123054); dimethylformamide was obtained from Sigma-Aldrich (USA); hydroxyapatite was provided by Berkeley Advanced Biomaterials Inc. (USA, BABI-HAP-N100); and beta-tricalcium phosphate was provided by Berkeley Advanced Biomaterials Inc. (USA, BABI-TCP-N100).

2.2.1 Solution Preparation

Three different polymer solutions are prepared in order to create the fiber scaffolds for the cartilage-bone interface: gelatin-NaCS in deionized water and ethanol (hyaline cartilage mimetic), gelatin-NaCS-HA/β-TCP in deionized water and ethanol (calcified cartilage zone mimetic), and PCL-HA/β-TCP in methylene chloride and dimethylformamide (subchondral bone mimetic). The determination of solute components varied between the three polymer solutions. The formation of the gelatin solutions relied upon weight-weight percentages, while the PCL solution relied upon weight-volume percentages. The difference between weight-weight percent and weight-volume percent used here can be seen in Equations 2.1 and 2.2.

$$\%({}^{w}/_{w})_{gelatin} = \frac{weight\ of\ gelatin}{weight\ of\ solvents + weight\ of\ gelatin} * 100 \quad \textbf{(2.1)}$$

$$\%(^{w}/_{v}) = \frac{total\ weight\ of\ solutes}{total\ volume\ of\ solvent} * 100$$

(2.2)

The proportion of solutes needed in the gelatin-NaCS solution (HC mimetic)is first obtained by assuming a percentage of the grams of gelatin in grams of solvent (deionized water and ethanol). A ratio between the amount of dH_2O and EtOH is varied from 60:40, to 50:50, to 40:60 depending upon the humidity. Lower humidity requires a 60:40 dH_2O to EtOH ratio to ensure the solvent doesn't vaporize too fast. A higher humidity requires a 40:60 dH_2O to EtOH ratio to ensure the solvent vaporizes after formation of the Taylor cone.Then, by using solvent densities and Equation 2.1, the grams of gelatin needed are calculated. With a final desired percent of 24, the weight of solutes can be computed. From here, 5% crosslinker and 1% NaCS is computed based off the gelatin weight. Table 2.1 depicts the proportions of materials needed for varying solvent volumes.

Table 2.1 Gelatin-NaCS Solution Components for Varying Solvent Ratios

Total Solvent Weight (g)	dH_2O (mL)	EtOH (g)	Gelatin (g)	NaCS (g)	Crosslinker (g)	%(w/w)
9.156	6	4	2.8914	0.0289	0.1446	24
8.945	5	5	2.8247	0.0282	0.1412	24
8.734	4	6	2.7581	0.0276	0.1379	24

The proportion of solutes needed for the gelatin-NaCS-HA/β-TCP solution (CCZ mimetic) is very similar to that of the gelatin-NaCS solution. The same amount of NaCS

(1%) and crosslinker (5%) is used – the only difference is the addition HA and β-TCP to the solution. A total ceramic percentage of 0.85%, based off the gelatin weight, is used to ensure that these fibers will contain a lower amount of ceramic than the fibers of the SCB mimetic. Of the total ceramic weight, 60% is HA and 40% is β-TCP. Table 2.2 depicts the solution components for varying dH_2O and EtOH ratios.

Table 2.2 Gelatin-NaCS-HA/β-TCP Solution Components for Varying Solvent Ratios

Total Solvent Weight (g)	dH_2O (mL)	EtOH (mL)	Gelatin (g)	NaCS (g)	HA (g)	β-TCP (g)	Crosslinker (g)	%(w/w) $_{gelatin}$
9.156	6	4	2.8914	0.0289	0.0148	0.0098	0.1446	24
8.945	5	5	2.8247	0.0282	0.0144	0.0096	0.1412	24
8.734	4	6	2.7581	0.0276	0.0140	0.0094	0.1379	24

The proportion of solutes needed for the PCL-HA/β-TCP solution (SCB mimetic) was based upon a weight-volume ratio, and determined by assuming total solvent volume of 10mL, with a desired solution weight-volume percent of 13. Although an 80%MC/20%DMF solvent ratio is used, the total solvent volume is used for the determination of the solute components. This 80%/20% ratio of MC to DMF is used because it was found that it produces the best dispersion of the ceramic particles in the solution (Patlolla, Collins, & Livingston Arinzeh, 2010). Using the total solvent volume and the weight-volume percent, the solute weight is computed. From here, 98% of the solute weight will be PCL, with the remaining 2% being ceramic particles. Of the 2%

ceramic particles, an 80%/20% ratio of HA to β-TCP is used. The proportions of each component for varying total solvent volumes can be seen in Table 2.3 below.

Table 2.3 PCL Solution Components for Varying Total Solvent Volumes

Total Solvent Volume (mL)	80% MC (mL)	20% DMF (mL)	PCL (g)	HA (g)	β-TCP (g)	%(w/v)
10	8	2	1.274	0.0208	0.0052	13
8	6.4	1.6	1.019	0.0166	0.0042	13
6	4.8	1.2	0.764	0.0125	0.0031	13

2.2.2 Fiber Production

The production of nano- and micro-scale fibers employed the use of the electrospinning apparatus mentioned in Section 2.1. In order to produce a graded scaffold two polymer solutions are spun at once, from opposite sides of the rotating mandrel. Each solution has its own set of parameters, including: applied temperature, applied voltage, throw distance, and injection rate. Both solutions are electrospun inside the same ventilated polyethylene box, and therefore subject to the same environmental conditions such as humidity.

The creation of a highly aligned and relatively random fiber orientation is achieved by adjusting the speed at which the mandrel rotates. By setting the mandrel so that it rotates about100rpm or higher yields fibers that are aligned (with alignment increasing with increasing rotational speed). Setting the mandrel to rotate below 30rpm allows for the generation of fibers that are less aligned or random. Since this scaffold must be graded through the depth, the mandrel must remain rotating throughout the

electrospinning process with the current setup. Both aligned and unaligned scaffolds are able to be generated using the same solution and fiber preparation methods.

2.2.2.1 Gelatin-NaCS Fibers. Production of the gelatin-NaCS fibers begins with the addition of NaCS to a glass beaker containing dH_2O and EtOH. In order to ensure dispersion of the NaCS in the solvent and prevent the solution from being too viscous, the mixture of dH_2O/EtOH and NaCS is sonicated using a Branson Digital Sonicator at 22% amplitude for 10 minutes. Following sonication, gelatin from bovine skin type B is added. A magnetic stirrer is placed in the glass beaker and the beaker covered using paraffin wax. The beaker is then placed in a 50^{o}C water bath and stirred for 60 minutes. After 60 minutes of stirring and approximately 15 minutes before electrospinning, ISDGE crosslinker is added to the beaker and stirred in the 50^{o}C water bath for 10 minutes. At this time, the 10mL syringe and 14 gaugeneedle are submerged in the 50^{o}C water bath to ensure that the gelatin mixture does not begin coagulating in the syringe.

Electrospinning of the gelatin solution begins by placing the filled syringe with attached 14 gauge needle within the PE syringe holder and enclosing the syringe in a dense Styrofoam structure. Next, the electrode is attached to the needle and the infusion pumped checked to ensure that the infusion pump syringe plunger abuts the plunger of the gelatin-containing syringe, so that the gelatin solution just begins to come out of the needle. Then, the hot air line is placed in the Styrofoam structure, and the rotating mandrel is properly grounded. The location of the syringe pump holder is adjusted so that the needle tip and the surface of the mandrel collection plate are 25cm apart (this distance may vary from 20-25cm depending upon the environmental conditions). The infusion

pump is then set to dispense in units of ml/hr and the voltage source is set to 30kV (this can vary between 20-52kV based upon environmental conditions. The protocol regarding infusion rate is discussed in Subsection 2.2.2.4.

2.2.2.2 Gelatin-NaCS-HA/β-TCP Fibers. The production of the CCZ mimetic fibers is very similar to the Gelatin-NaCS fibers. NaCS and ceramic (HA and β-TCP) are added to a glass beaker containing dH_2O and EtOH. Again, in order to ensure proper dispersion and lower MW NaCS, the solution is sonicated at 22% amplitude for 10 minutes. After sonication, gelatin type B from bovine skin is added along with a magnetic stirrer, and the beaker placed in a 50^oC water bath to stir for 60 minutes. After 1 hour, and approximately 15 minutes before electrospinning, ISDGE is added and the solution left to stir for another 10 minutes. A 10mL syringe and 14 gauge needle are placed in the water bath to allow them to heat up.

Electrospinning begins by placing the filled syringe with attached 14 gauge needle in the non-conducting syringe holder and enclosing it within a dense Styrofoam cover. The electrode is attached to the needle tip and the infusion pump syringe plunger abuttedagainst the plunger of the solution filled syringe. The distance between the needle tip and collection plate is adjusted so that they are 25cm apart (this can vary from 20-35cm depending upon environmental conditions). The syringe pump is then set to dispense in units of ml/hr and the voltage source is set to 30kV (this can vary from 20-52kV). The protocol regarding infusion rate is discussed in Section 2.2.2.4.

2.2.2.3 PCL-HA/β-TCP Fibers. Production of the PCL/ceramic fibers requires preparation of two separate solutions which are later combined to form the final electrospinning solution. The first solution contains purely PCL and MC. First the required volume of MC is measured using a glass pipet (MC will dissolve polyethylene pipets) and deposited in a glass beaker. The measured amount of PCL beads are added to the MC solution and a magnetic stirrer is dropped in. The top of the glass beaker is securely sealed with paraffin wax to prevent the volatile MC from evaporating. The solution is then stirred for 2 hours at a medium-low speed. Approximately 30 minutes before the stirring of the MC and PCL solution is complete, the DMF and ceramic solution is prepared. This is done by measuring out the necessary volume of DMF using a glass pipet and depositing it in a glass beaker. The required amount of HA and β-TCP area added to the DMF and sonicated at 22% amplitude for 2 minutes to break up any ceramic aggregates. Once the MC and DMF solutions are prepared, the DMF solution is poured into the MC solution. Again, the beaker is covered with paraffin wax and the solution vigorously mixed for 30 minutes.

The electrospinning of the PCL/ceramic solution begins by filling up a 10mL syringe with the solution and attaching a 20 gauge needle to the syringe. The syringe is placed in the syringe holder and the infusion pump checked to ensure that the pump syringe plunger abuts the plunger of the PCL/ceramic-containing syringe, so that the PCL/ceramic solution just begins to come out of the needle. An electrode is attached from the second voltage source to the needle, and the syringe holder moved so that the needle tip and the surface of the mandrel collection plate are 18cm apart. The voltage

source is set to 20kV and the second infusion pump set to dispense in units of ml/hr. The protocol regarding infusion rate is discussed in Section 2.2.2.4.

2.2.2.4 Generationof the Scaffold & the Fiber Grade. The generation of a grade through the depth of the scaffold consisting of Gelatin-NaCS-ceramic and PCL-ceramic fibers is accomplished through the rotation of the grounded mandrel collection plate and the modification of the polymer solution infusion rates over the course of electrospinning. The adjustments to infusion rates are done stepwise in 15-40 minute intervals. A start and end infusion rate are chosen with divisions in between. Figure 2.3 depicts the layout for the change of infusion rate over the course of electrospinning of the scaffold. These rates are chosen based upon the desired electrospun fiber diameter and the intervals chosen based upon laboratory availability. A better continuously graded scaffold can be achieved through a greater number of rate changes, with slightly shorter intervals. Keep in mind that a greater number of rate changers or longer intervals will create a thicker scaffold. If a scaffold with a specific thickness is desired, a balance must be made between number of rate changes and the time spent electrospinning at each set of infusion rates.

It is important to note that the entire scaffold is not graded, but rather only a section, which is demonstrated in Figure 2.4c. This is the desired, complete scaffold which includes a sharp division (no grade) between the gelatin-NaCS and gelatin-NaCS-HA/β-TCP fibers, and a grading from the gelatin-NaCS-HA/β-TCP fibers to the PCL-HA/β-TCP fibers. The absence of a grade between the fibers in Figure 2.4a is meant to act as crude tidemark – a sharp division between the two fiber types that acts to halt further calcification. For characterization, scaffolds (A) and (B) in Figure 2.4 are created

to better visualize the fiber grade and the presence of two distinct regions on either side of the scaffolds.

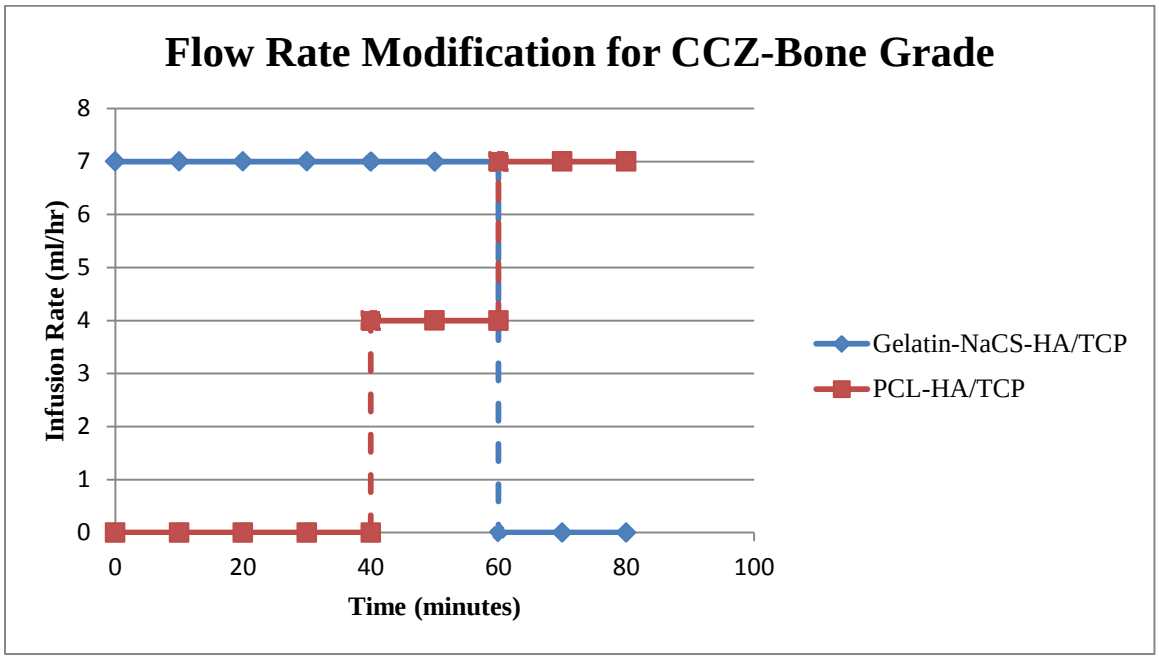

Figure 2.3 Graph representing the change in infusion rate over the course of electrospinning in order to generate a grade between two fibers.

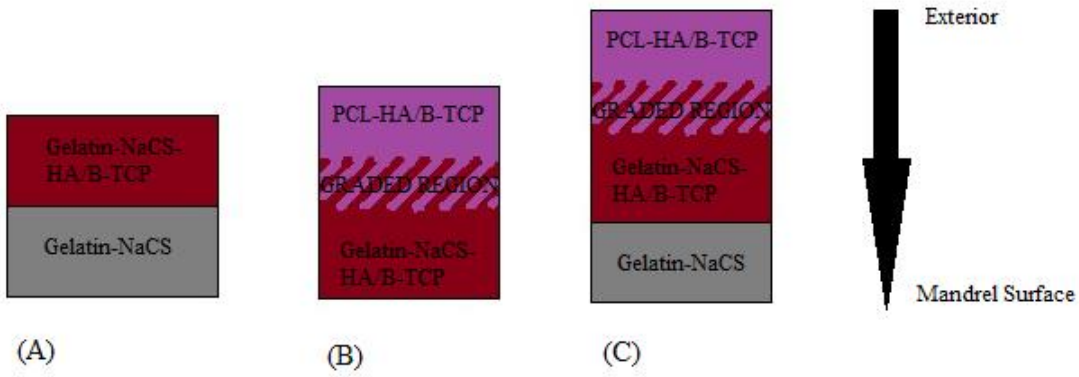

Figure 2.4 Schematic of scaffold architecture. (A) depicts only the HC and CCZ mimetic fibers. Note the sharp transition between the two that acts as a "tidemark" or clear divide between the two fiber types. (B) depicts the CCZ and SCB mimetic fibers. Here there are two distinct regions connected through a meshing of the two fiber types. (C) depicts the scaffold in its totality – a continuous combination of (A) and (B).

2.2.3 Crosslinking of Gelatin Fibers with ISDGE

As previously mentioned, isosorbide diglycidyl ether is added to the gelatin solutions in order to introduce increased mechanical properties. However, the addition of the ISDGE to the solution alone is not enough to ensure proper crosslinkage. To complete the crosslinking of the gelatin fibers, 6mm punches of scaffolds A and B (Figure 2.4a,b) are placed in a VWR Symphony oven at 150^{o}C for 5 hours. In addition, the heating of the scaffold removes any excess moisture or solvent from the fibers. These scaffolds are then later used for SEM imaging and observation in dH_2O.

2.3 Scaffold Characterization

A combination of light microscopy and SEM are used to identify fibers on the micro and nano scale. For those fibers which are on the micro scale, traditional light microscopy is sufficient; for those on the nano scale, SEM is required to obtain accurate fiber dimensions. Since the scaffolds being observed have two distinct sides, both sides of each scaffold will need to be imaged.

2.3.1 Assessment of Fiber Diameter

The assessment of micro scale fibers is carried out using a Dino-Lite USB digital microscope in conjunction with a computer running Dino Capture 2.0. This microscope has a magnification range of 10x to 240x (depending on working distance).A total of seven scaffold samples are imaged using this light microscope (Table 2.4). Each side of the scaffolds is imaged at low (~50x) and high (~200x) magnification.

Table 2.4 Scaffolds to be Analyzedin Order to Assess Fiber Properties

Scaffolds for Imaging					
	Components		Intended fiber orientation	Mandrel speed	Applied Heat
Scaffold	Side 1	Side 2			
1	Gelatin-NaCS-HA/β-TCP	Gelatin-NaCS	Random	15 rpm	N/A
2	Gelatin-NaCS-HA/β-TCP	PCL-HA/β-TCP	Random	15 rpm	N/A
3	Gelatin-NaCS-HA/β-TCP	Gelatin-NaCS	Random	15 rpm	150^{o}C @ 5hr
4	Gelatin-NaCS-HA/β-TCP	PCL-HA/β-TCP	Random	15 rpm	150^{o}C @ 5hr
5	Gelatin-NaCS	PCL-$CaCO_3$	Aligned	2340 rpm	N/A
6	Gelatin-NaCS	PCL-$CaCO_3$	Aligned	4250 rpm	N/A
7	PCL	PCL	Random/Aligned	15 rpm/2340 rpm	N/A

For fibers on the nano scale, SEM must be used to obtain accurate fiber dimensions. This imaging technique allows for high resolution photographs of the scaffold surface by focusing a condensed beam of electrons on the sample. With the help of scanning coils within the SEM, the beam is scanned across the surface. Each section of the scaffold that is bombarded by the condensed electron beam generates electromagnetic radiation in the form of secondary or backscattered electrons (Bozhilov, 2012). These secondary or backscattered electrons are collected by a detector and subsequently transformed into an image. The samples placed in the SEM are under vacuum, and therefore any samples containing liquid or volatile components cannot be directly viewed. Additionally, the sample must be conductive – if it is not it must be sputter-coated with a conducting metal such as gold, palladium, platinum, or carbon.

Due to financial and time restrictions, only two scaffolds (scaffolds 1 and 2 in Table 2.4) are imaged using SEM. Again, both sides are imaged separately. The samples are coated with gold using a BAL-TEC-MED 020 sputter coater. SEM is then conducted using a Gemini LEO 1530VP VPFE-SEM(working distance of 4mm, voltage of 3.00kV, 500x to 2,500x magnification)to obtain a high resolution picture of the scaffold surface.

Image analysis is conducted through ImageJ software to obtain fiber diameters and inter-fiber spacing for SEM and light microscope images. Seven random fibers and fifteen random inter-fiber distances are selected from each imaged side of the scaffold to determine an average.

2.3.2 Assessment of Fiber Alignment

For the scope of this thesis, only a qualitative assessment of fiber orientation is needed. SEM and light microscope images are used to determine whether the fibers are relatively aligned or random. In the future, if a more quantitative assessment is required, the slope of each fiber relative to defined axes can be obtained. If all the fibers have the same relative slope, it would be said that the fibers are aligned. Additionally, if a majority of the fibers have the same slope as the mean slope of all the fibers, it could beinferred that the fibers are aligned.

2.3.3 Assessment of Fiber Grade

The main advantage this scaffold has over other electrospun scaffolds is the ability to have separate yet distinct fiber regions within the same construct. Therefore, it is important to be able to detect that the electrospinning apparatus is capable of producing these scaffolds with distinct fiber sections. Ideally, identification of the fiber grade is done through fluorescent confocal microscopy, SEM energy dispersive x-ray analysis, and FTIR; however, due to limited resources, assessment is done through light microscopy, SEM imaging, and fluorescent light microscopy.

Identification of distinct fiber regions through SEM and light microscopy is done through observing significant differences in fiber morphology on each side of the scaffold. This identification is made easier if the fibers sizes are different by orders of magnitude (i.e. nano vs micro). SEM and light microscopy may also differentiate regions by identifying particular components (such as a ceramic) that should be present only on

one half of the scaffold. FTIR analysis of each side of the scaffold (Section 2.3.4) may further confirm the presence of particular components.

Fluorescent microscopy allows for the staining of specific proteins or molecules to make them readily identifiable. Since a confocal imaging technique is not used, interior sections of the scaffold will not be able to be imaged, leaving only surface images of each side of the scaffold. Regardless, staining for a particular molecule on one half of the scaffold but not the other should still allow for identification of two distinct surfaces on the scaffold. A simple way to determine if a fiber grade is produced with this technique is to create a scaffold that is comprised of organic fibers on one half, and inorganic fibers on the other. Here, a gelatin and PCL scaffold is created. Since gelatin is denatured collagen (a protein), and PCL is an inorganic polymer, staining for general protein easily delineates the two fiber types.

To stain for general protein, Alexa Fluor 488 dye is used, which fluoresces a bright green when bound to protein (in this case the gelatin). Two 6mm punch of the gelatin-PCL mat are obtained, along with two punches from a pure gelatin and two from pure PCL mat for controls. Before staining, a dye solution must be prepared. First, the Alexa Fluor 488 dye is removed from the freezer, covered in foil to protect from light and left out to thaw at room temperature. After thawing, the dye must be mixed in a 1:1000 ratio with 10µM sodium bicarbonate in a centrifuge tube (i.e. 0.5µL dye requires 500µL sodium bicarbonate) and centrifuged. Each sample is placedin a 1.5mL centrifuge tube, and 100µL of the dye/bicarbonate solution is added to each tube. It is important to ensure that the entire scaffold is submerged and then protected from light. After sitting in the solution for an hour, the dye solution is pipetted out and the scaffolds rinsed with 100µL

of PBS three times. At this point the scaffolds can be imaged immediately, or left in PBS and covered from light until ready.

2.3.4.1 Assessment of the Presence of NaCS and Ceramic Particles Ideally, SEM energy dispersive x-ray analysis is used in conjunction with FTIR analysis to determine not only the presence, but the dispersion of specific compounds across the scaffold. Unfortunately, due to available time and resources, only FTIR is used. A 6mm punch sample from scaffolds 1 and 2 in Table 2.4 are used for the FTIR analysis. To detect differences between one side and the other, each side is analyzed using a Perkin Elmer Spectrum 100 FT-IR Spectrometer (4000-500cm^{-1} range, resolution of 4cm^{-1}, 0.1cm/s scan speed, 20 scans). FTIR analysis of both sides of scaffold 1 will want to look for characteristic peaks pertaining to gelatin and NaCS, HA, and β-TCP on side 1; and on side 2, characteristic peaks pertaining to gelatin and NaCS. Analysis of scaffold 2 will look for characteristic peaks of gelatin, NaCS, HA, and β-TCP on side 1; and on side 2, characteristic peaks for PCL, HA, and β-TCP.

Table 2.5 Some Characteristic Wavenumbers for Identification of Functional Groups

Material	Wavenumber (cm^{-1})	Characteristic
PCL		
Asymmetric CH_2 stretch	2949	Larger peak, looks double w/ 2865
Symmetric CH_2 stretch	2865	Smaller peak, looks double w/ 2949
Carbonyl stretch	1727	Strong, sharp
C-O, C-C stretch	1293	Very sharp, looks double w/ 1240
Asymmetric C-O-C stretch	1240	Sharp, looks double w/ 1293
HA/β-TCP nanoparticles (phosphate focus)		
PO_4^{3-} bands	564, 603, 1031	(564, 603) Small sharp double, (1031) larger sharp jagged peak
NaCS (sulfate focus)		
SO_4^{2-}	1350-1450	Strong
Gelatin (peptide bond focus)		
C-N bond (non-aromatic)	1000-1250	Medium
Saturated keytone	1710-1720	Strong
2^o amine	3300-3400	Weak

Source: (Polini, Pisignano, Parodi, Quarto, & Scaglione, 2011; Reusch, 2005; Society, 2011)

2.4 Statistical Analysis

Data, regarding Dynoscope and SEM images,is analyzed using paired or unpaired T-tests and one-way analysis of variance (ANOVA). Significant differences between scaffold characteristics are determined using a level of significance equal to 0.05 or association with a p-value less than 0.05.

CHAPTER 3

RESULTS AND DISCUSSION

3.1Fiber Morphology

The electrospun mats produced to mimic the ECM of cartilage-bone interface ended up being very thin, which in turn created several problems in terms of characterization. This is due to the difficulty electrospinning gelatin based solutions in low humidity environments (those less than 20% relative humidity). In previous work conducted with Lina Loaiza, gelatin and gelatin-NaCS based solutions with ISDGE were found to electrospin very well at humidity levels between 25-30% (Loaiza, 2013). However, due to limited laboratory resources, humidity levels within the electrospinning enclosure were subject to environmental conditions. Since most spinning was conducted during the mid to late fall season, humidity wavered between 9-20%. Gelatin based solutions (those used to mimic HC and the CCZ) either did not electrospin at all, or would electrospin intermittently. PCL based solutions (mimic for SCB) had no issues electrospinning in these conditions.

The inability of gelatin to properly electrospin resulted in fibers larger than anticipated, especially when compared to PCL fibers (Figures 3.1-3.8, and 3.10). All fibers were intended to be on the nanometer scale, but gelatin fibers were in the micrometer range. When it came time to image the fibers using the SEM, due to the thinness of the mats and the high magnification, it became difficult to discern which fibers belonged to the intended side of the scaffold being imaged, and which were those that belonged to the other half – this was especially difficult for the HC and CCZ mimetic

scaffold since both fibers were of the same relative size (Figures 3.1, 3.2, 3.10). In an effort to ensure the incorrect fibers were being analyzed, only fibers in the foreground were chosen. Additionally, light microscope images using the Dynoscope were taken at lower magnification. These lower magnification images (200x compared to 1000-2500x) made it a little easier to discern the desired surface fibers from background fibers – those on the other surface of the scaffold (Figures 3.5-3.8).The fiber diameter measurements taken from the SEM and Dynoscope were then compared to see if there was any significant difference in the mean of the fiber diameters (Figure 3.9). With the exception of the PCL fibers[7], analysis showed, with 95% confidence, that there was no significant difference in the mean fiber diameters collected through either imaging technique. This lends a small degree of confidence to the results collected from the SEM images.

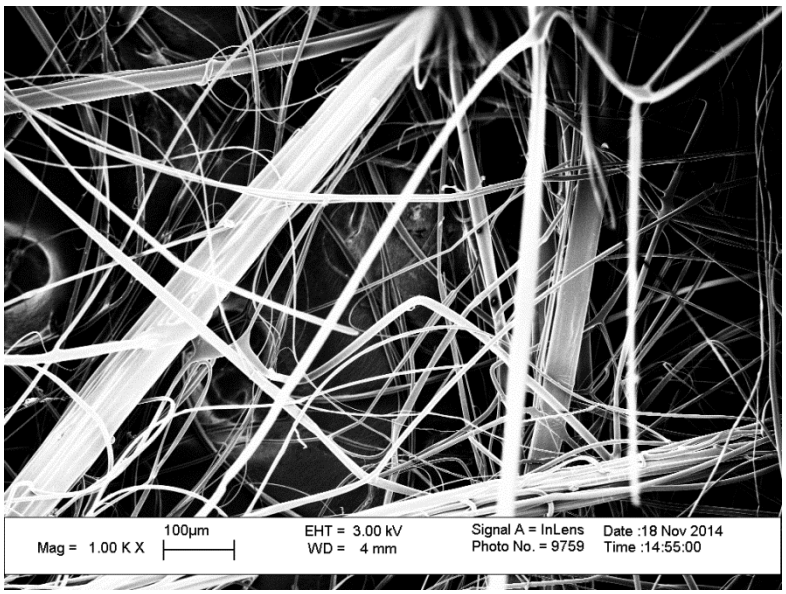

Figure 3.1 SEM image of the Gelatin-NaCS-HA/β-TCP side of the Gelatin-NaCS//Gelatin-NaCS-HA/β-TCP scaffold. Bright white fibers in the foreground are used for analysis.

[7]This was because the light microscope lacked sufficient magnification to obtain precise measurements of these small fibers.

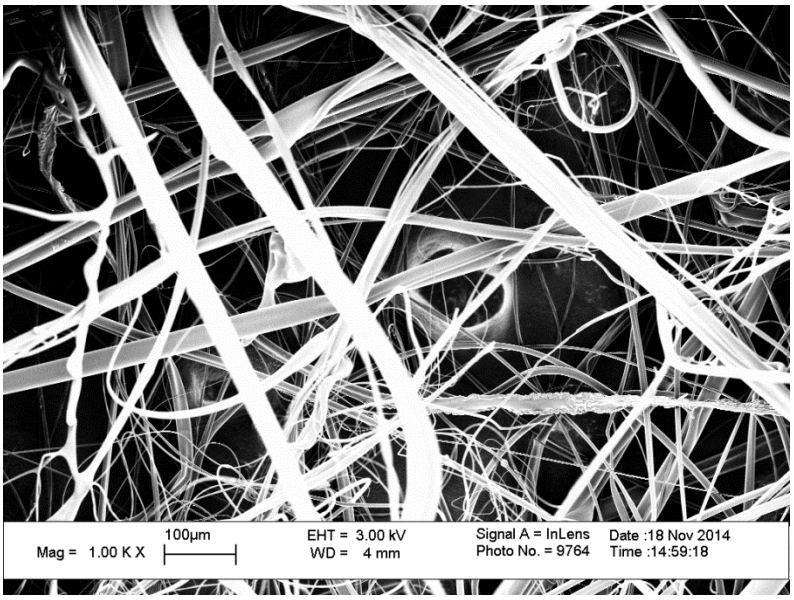

Figure 3.2 SEM image of Gelatin-NaCS side of the Gelatin-NaCS//Gelatin-NaCS-HA/β-TCP scaffold. Bright white fibers in the foreground are used for analysis.

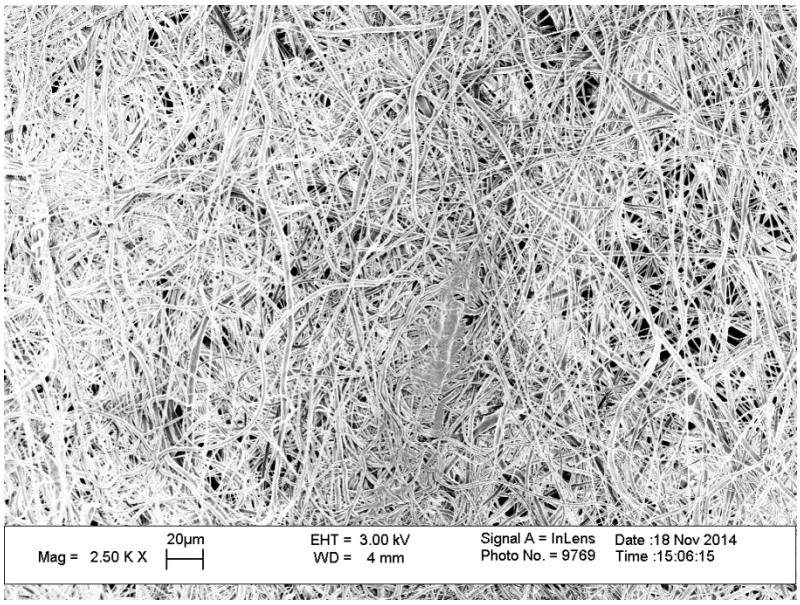

Figure 3.3 SEM image of the PCL-HA/β-TCP side of the Gelatin-NaCS-HA/β-TCP//PCL-HA/β-TCP scaffold. Fibers density is sufficient to obscure larger gelatin fibers on the other half of the scaffold.

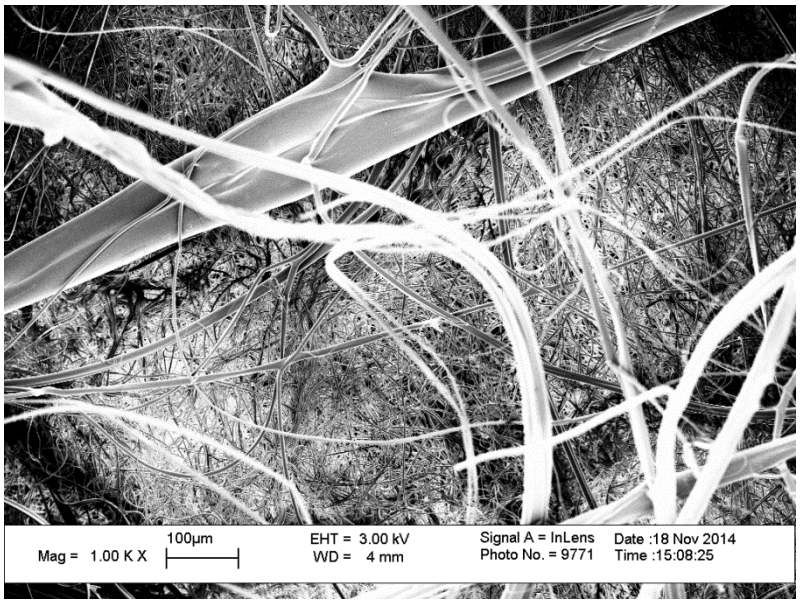

Figure 3.4 SEM image of the Gelatin-NaCS-HA/β-TCP side of the Gelatin-NaCS-HA/β-TCP//PCL-HA/β-TCP scaffold. Larger white fibers in the foreground are used for analysis. The smaller, denser volume of the PCL fibers can be seen in the background.

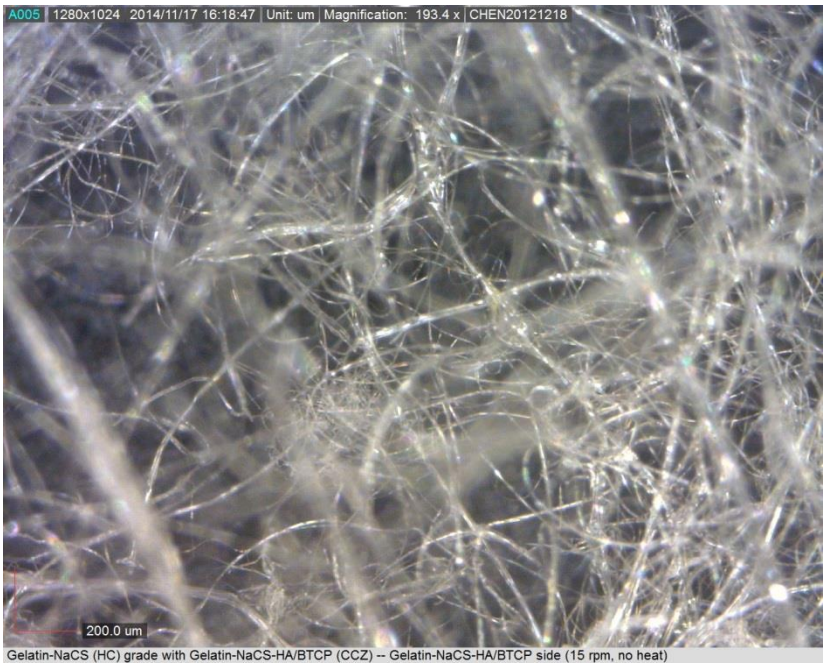

Figure 3.5 Light microscope image of the Gelatin-NaCS-HA/β-TCP side of the Gelatin-NaCS//Gelatin-NaCS-HA/β-TCP scaffold.

Figure 3.6 Light microscope image of the Gelatin-NaCS side of the Gelatin-NaCS//Gelatin-NaCS-HA/β-TCP scaffold.

Figure 3.7 Light microscope image of the PCL-HA/β-TCP side of the Gelatin-NaCS-HA/β-TCP//PCL-HA/β-TCP scaffold.

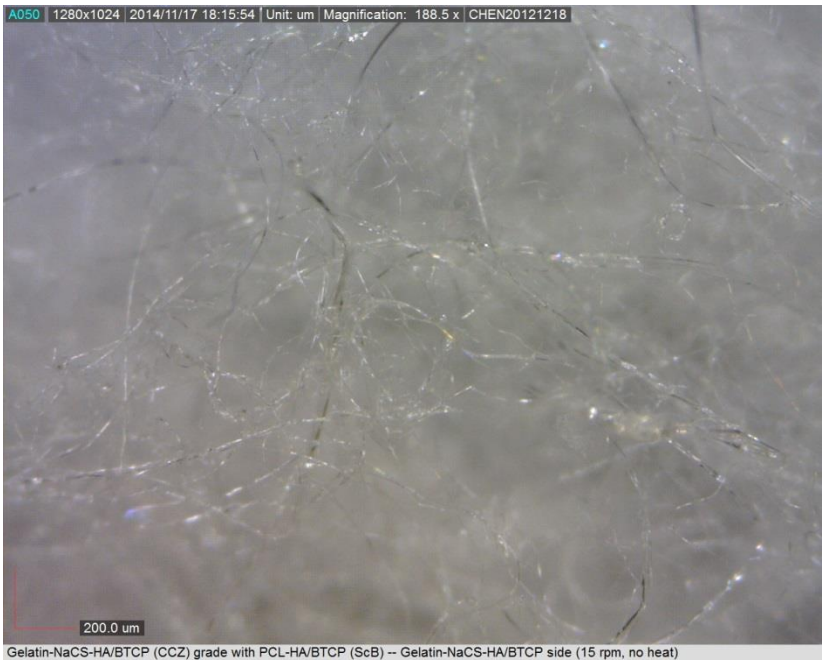

Figure 3.8 Light microscope image of the Gelatin-NaCS-HA/β-TCP side of the Gelatin-NaCS-HA/β-TCP//PCL-HA/β-TCP scaffold.

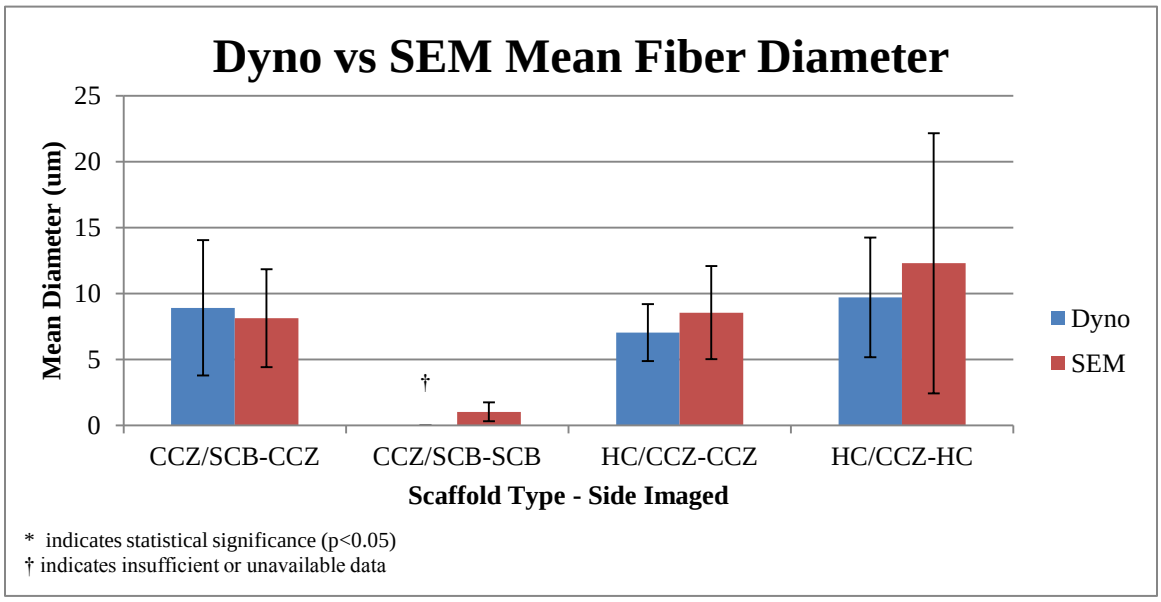

Figure 3.9 Graph showing comparison of fiber diameters collected through Dynoscope light microscopy and SEM. Bars represent standard deviation from the mean. No significant difference between mean diameters gathered from either microscope. No data collected from the light microscope for PCL fibers of the SCB side due to insufficient magnification.

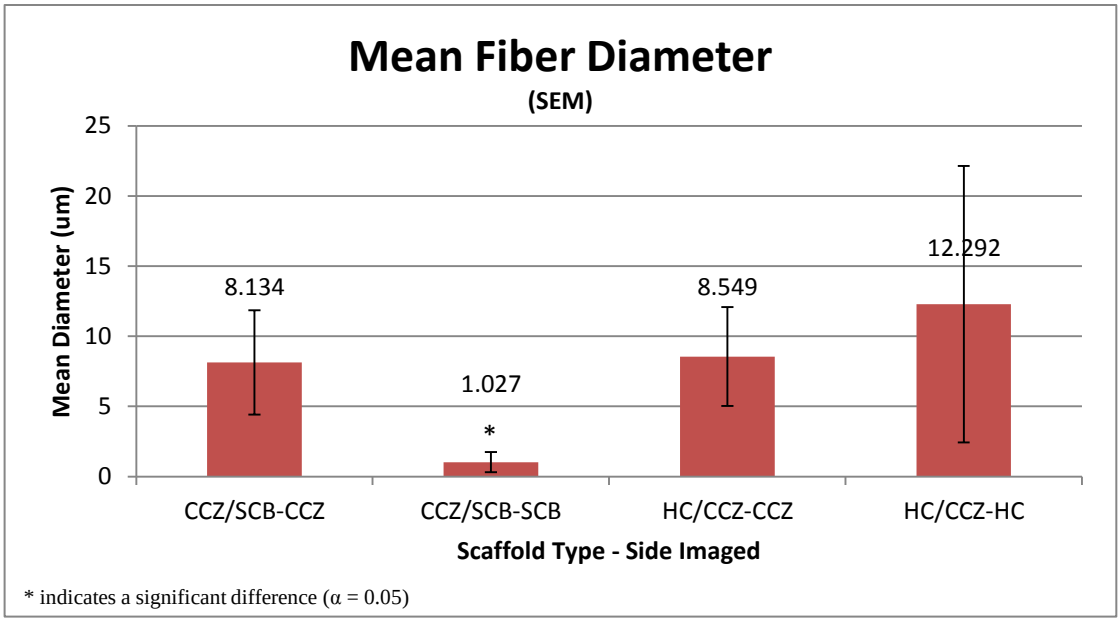

Figure 3.10 Graph of mean fiber diameters for the fibers both sides of the two scaffolds. Since no significant difference between the SEM and light microscopy images was found, SEM values will be of precedence. One-way ANOVA and post hoc tests showed no significant difference in mean fiber diameter between the gelatin fibers, but a significant difference in mean diameter between the PCL and all other gelatin fibers.

These results indicate that the electrospinning apparatus used is still able to achieve fiber diameters varying from hundreds of nanometers to tens of micrometers. Achieving fibers with nanoscale diameters is heavily reliant upon ideal environmental and electrospinning parameters – and it is this fiber diameter that is sought for cartilage regeneration. Although gelatin fibers in the hundreds of nanometers weren't achieved, it is possible that under more idealized electrospinning conditions, these smaller sized fibers may be produced using this electrospinning apparatus. With humidity as low as it was during electrospinning, the solvent often evaporated too fast, even with a shift from a 60:40 to 70:30 dH_2O to EtOH ratio. This prevented the polymer jet leaving the Taylor cone at the needle tip from properly thinning. It has been noted that a slower evaporating solvent allows for a longer fiber stretching process before jet solidification and final fiber

formation, resulting in a thinner fiber (Thompson, Chase, Yarin, & Reneker, 2007). Electrospun gelatin scaffolds with only dH_2O as the solvent were attempted due to its lower vapor diffusivity compared to ethanol or a water/ethanol mix. Nevertheless, these gelatin solutions were unsuccessful.

Volumetric charge density, throw distance, initial jet radius, relaxation time, and elongational viscosity are known to have the largest effects on final fiber diameter (Thompson et al., 2007). Although these can be easily controlled through modification in applied voltage, needle-to-plate distance, and solution viscosity, humidity can be strongly coupled to these parameters, thus indirectly altering the behavior of the electrospun solution. This could be how 100-400nm diameter gelatin and gelatin-NaCS fibers, with similar solution properties and electrospinning parameters employed herein, were easily electrospun at 25-30% relative humidity (Loaiza, 2013), but not at the 9-20% relative humidity.

3.1.1Change in Diameter Due to Heating

Scaffold samples were heated for 5 hours at 150^{o}C to complete crosslinking of the gelatin fibers, but also to observe any change in fiber diameter due to loss of moisture or excess solvent. Due to limitations, scaffold samples after heating were not able to be imaged with the SEM. Therefore diameter measurements for the heated and non-heated groups were accomplished through the Dynoscope (Figure 3.11). As a result, fiber diameters for the smaller PCL-HA/β-TCP fibers are unavailable. Despite the lack of fiber measurements, it is important to note that after heating, the CCZ/SCB scaffold shriveled significantly, to nearly half its original size. This is believed to be caused by

rearrangement and relaxation of the PCL polymer chains. Electrospinning causes the polymer chains to be stretched out during jet elongation and after fiber deposition. It is hypothesized that the high temperature needed to crosslink the gelatin with ISDGE, imparted enough thermal energy to allow the PCL polymer chains to reorient themselves in a lower potential state.

All gelatin based fibers appear to have a lower average diameter after heating, although the difference is not statistically significant. However, the large standard deviations seen throughout fiber diameter measurements could skew identification of any real significant differences between fibers. The cause for the large deviation in fiber diameter (in both heated an unheated fibers) is once again caused by the imperfect

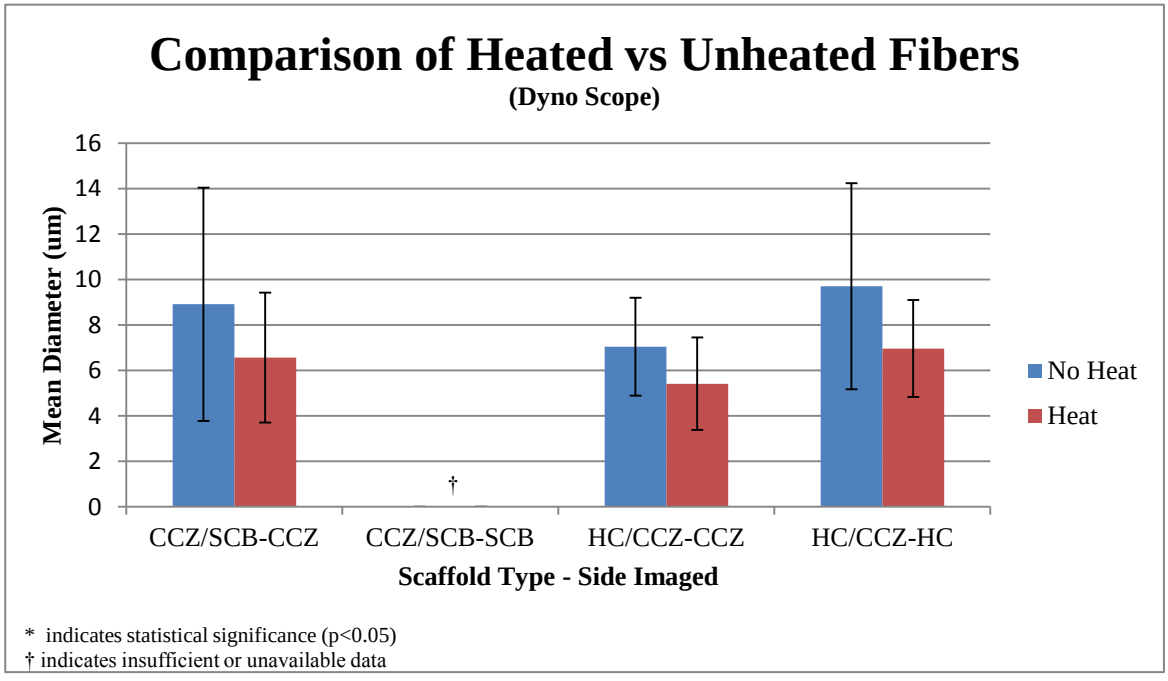

Figure 3.11 Graph depicting differences in average fiber diameter between heat treated and non-heat treated electrospun scaffolds. Measurements of PCL fibers on the SCB side of the CCZ/SCB scaffold were unable to be obtained accurately due to insufficient magnification.

electrospinning of the gelatin solutions. Electrospun gelatin fibers appeared to prematurely separate and deposit on the grounded mandrel before full elongation. This could be seen in the periodic start and stop of gelatin solution bead and jet formation, in which larger portions of the elongated gelatin jet would break off and land on the grounded mandrel. Figures 3.12-3.15 show scaffold samples after heating at 150^{o}C for 5 hours. SEM images of these scaffolds were not available at the time. In these images larger aggregates of gelatin solution can be seen due to the previously described electrospinning difficulties. Data regarding the PCL fibers weren't able to be collected due to their shrinkage after heating (especially due to the thinness of the scaffolds) and inability to distinguish the PCL based fibers from the gelatin based fibers with the Dynoscope.

Figure 3.12 Light microscope image of the Gelatin-NaCS-HA/β-TCP side of the Gelatin-NaCS//Gelatin-NaCS-HA/β-TCP scaffold after heating 5 hours at 150^{o}C. Gelatin aggregate is visible.

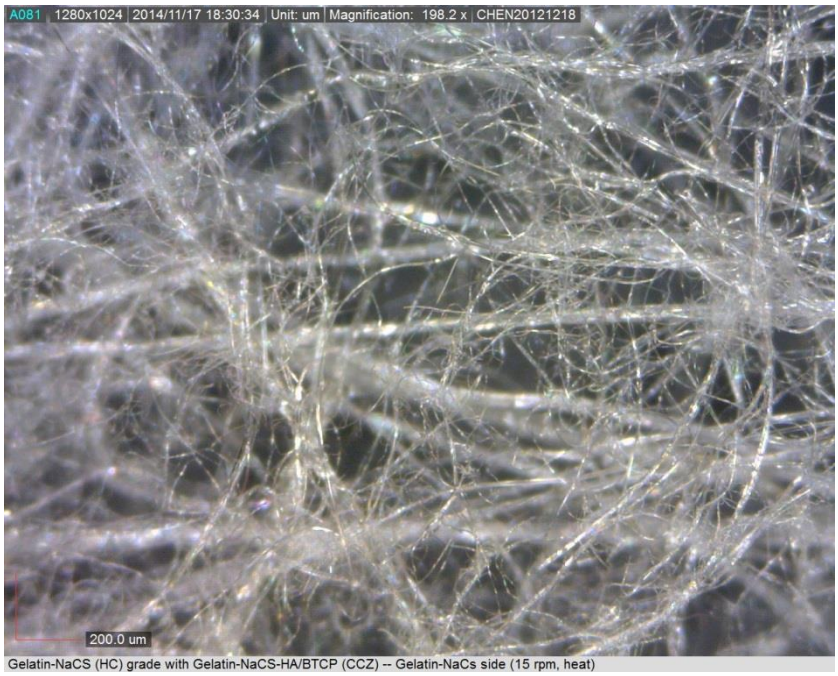

Figure 3.13 Light microscope image of the Gelatin-NaCS side of the Gelatin-NaCS//Gelatin-NaCS-HA/β-TCP scaffold after heating 5 hours at 150^{o}C.

Figure 3.14 Light microscope image of the PCL-HA/β-TCP side of the PCL-HA/β-TCP //Gelatin-NaCS-HA/β-TCP scaffold after heating 5 hours at 150^{o}C. Aggregates are visible.

Figure 3.15 Light microscope image of the Gelatin-NaCS-HA/β-TCP side of the PCL-HA/β-TCP //Gelatin-NaCS-HA/β-TCP scaffold after heating 5 hours at 150^{o}C. Aggregates are visible.

3.1.2 Interfiber Spacing

The electrospun scaffolds shown for cartilage-bone matrix mimics (Figures 3.1-3.8) ended up having very large variations in interfiber spacing. Measurements collected via the Dynoscope and SEM were compared again (Figure 3.16). This time significant differences were found between interfiber distances of the CCZ half of the SCB/CCZ scaffold and the HC half of the CCZ/HC scaffold. This could be due to issue involving discontinuous gelatin electrospinning. Since gelatin fibers weren't consistently electrospun, their distribution over the grounded mandrel is likely to be irregular or patchy. This can be seen in Figures 3.5, 3.6, and 3.8, where there are larger areas of sparsely packed fibers, adjacent to small areas of more densely packed fibers. When imaging at 1000x compared to 200x, it is easy to image an area which belongs to one of

these smaller, more densely packed regions – which may have happened for these two cases.

Since light microscope images of the PCL fibers weren't able to be accurately obtained, comparisons between interfiber spacing relied upon measurements from the SEM. Based on these SEM images, gelatin halves of scaffolds had mean interfiber spacing that ranged from roughly 40 to 60 micrometers, compared to the PCL fibers that wereroughly 4 micrometers apart on average (Figure 3.17). The spacing between PCL fibers was significantly smaller than all gelatin based fibers. The spacing between PCL fibers is the idealized spacing for a cartilage-bone matrix mimic, which was not achieved across the gelatin fibers. Again, this is most likely due to uncontrollable environmental factors at the time, specifically humidity, which led to the aforementioned problems

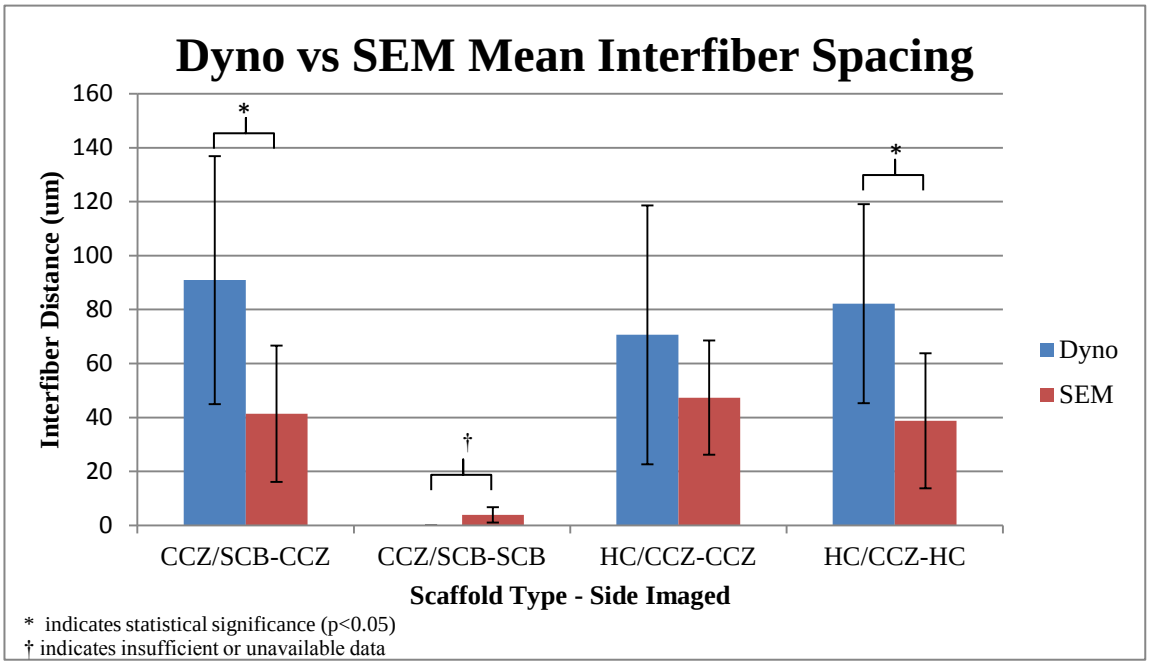

Figure 3.16 Graph of mean interfiber distance collected from Dynoscope and SEM images. A significant difference between means collected from the Dynoscope and SEM were found for two groups.

issues with gelatin electrospinning. Having a better controlled laboratory environment should enable the maintenance of ideal electrospinning parameters, enabling continuous gelatin fiber formation and subsequently, a more densely packed fiber scaffold.

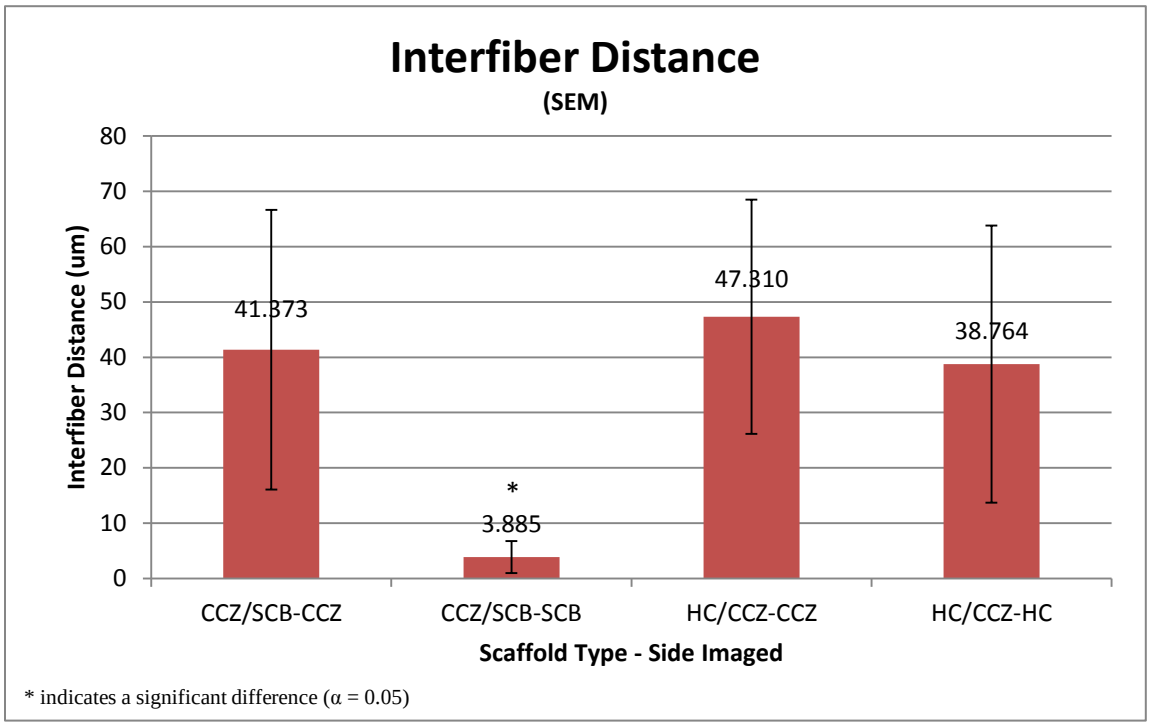

Figure 3.17 Graph of interfiber distances from SEM images. A significant difference in fiber spacing is found between the SCB PCL fibers and the gelatin fibers. No significant difference found between the gelatin fibers alone.

3.2 Fiber Alignment

A random fiber alignment was desired for fiber mats mimicking the cartilage-bone matrix interface. Therefore, during electrospinning, the rotating mandrel is set to rotate between 10 and 20 rotations per minute. Low magnification (500x) SEM images of the mats distinctly depict fibers on both halves of the scaffolds with a random alignment (Figure 3.18). When the speed at which the mandrel rotates is increased, fibers deposited on the mandrel are pulled along the circumference of the mandrel, aligning the fibers in the

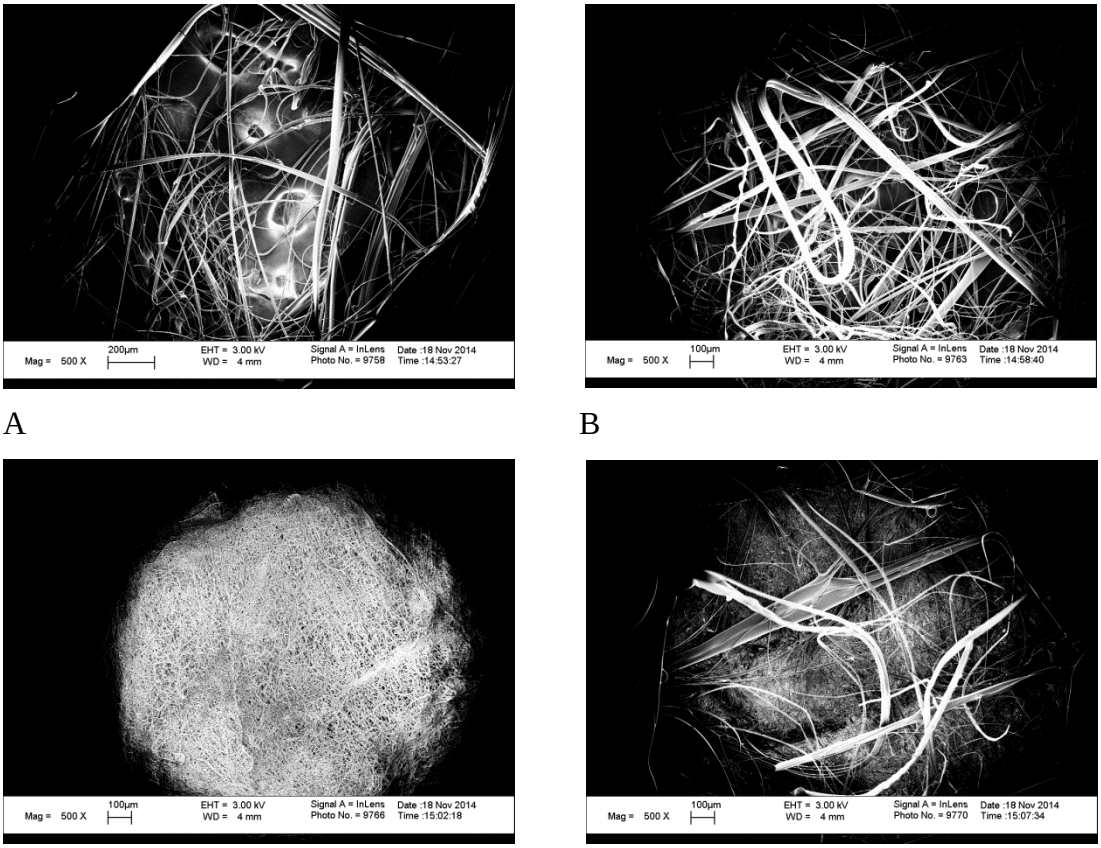

Figure 3.18 SEM images at 500x magnification of the CCZ side of the HC/CCZ scaffold (A), the HC side of the HC/CCZ scaffold (B), the SCB side of the CCZ/SCB scaffold (C), and the CCZ side of the CCZ/SCB scaffold (D).

direction of the rotation of the mandrel. This current electrospinning setup is also capable of producing aligned fibers in addition to unaligned fibers, which can be seen in Figure 3.19.

The ability for this electrospinning apparatus to produce both aligned and unaligned fibers opens the door for future applications in cartilage regeneration, but also for applications outside the realm of cartilage that require two distinct fiber architectures. Although not shown here, this apparatus can produce a fiber scaffold with highly aligned fibers on one half and random fibers on the other half of the scaffold, simply but

increasing the rotational speed of the mandrel after electrospinning random fibers at low speeds. Random fiber orientation is best achieved using rotational speeds under 20rpm, whereas very highly aligned fibers were achieved using rotational speeds above 2000rpm. When rotation was increased to over 4000rpm, no large noticeable difference was found in degree of alignment. That is not to say there is no difference in interfiber spacing or fiber diameter though. The exact effects variance in rotational speed has on electrospun fibers, outside alignment, is not discussed here, however, it would be interesting to study these effects.

(A)

(B)

(C)

Figure 3.19 (A) Gelatin//PCL scaffold with mandrel at 2300rpm, (B) Gelatin//PCL scaffold with mandrel at 4200rpm, and (C) the CCZ/SCB scaffold previously discussed which was electrospun onto a 15rpm mandrel.

3.3 Fiber Grade

The novelty of this electrospinning apparatus setup is its ability to create a single electrospun scaffold with two or more distinct fiber regions, able to have their own set of functional components, fiber diameters, fiber alignment, and fiber spacing. The presence of two distinct fiber diameters, alignment and spacing is seen in the figures in previous sections. Figure 3.20 is able to more clearly show the presence of two distinct sides comprised of different polymer fibers via fluorescent staining and microscopy. Here two

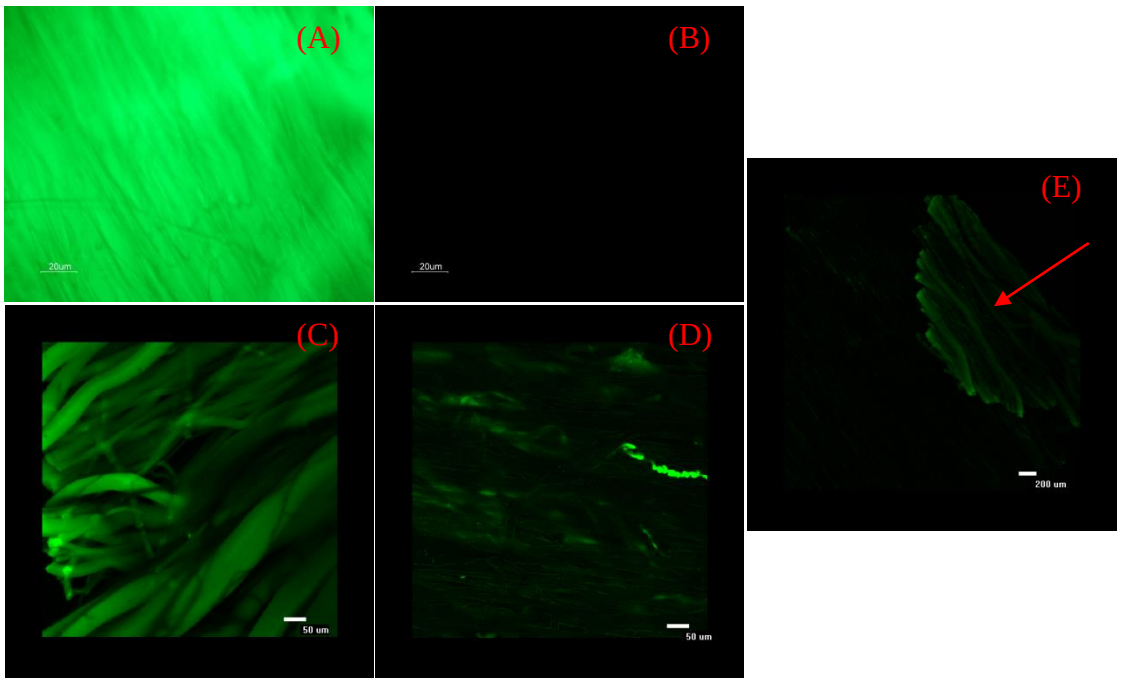

Figure 3.20 Fluorescent microscopy images of (A) pure gelatin control, (B) pure PCL control, (C) gelatin side of gelatin/PCL scaffold, (D) PCL side of gelatin/PCL scaffold, and (E) PCL side of gelatin/PCL scaffold with a corner folded over to show gelatin side (arrow) contrasted against the PCL. Images A-D taken at 200x magnification, E taken at 4x magnification. Scaffolds stained with Alexa Fluor 488.

controls are stained – a pure gelatin scaffold and a pure PCL scaffold. Since the dye only fluoresces when it binds to protein or protein derivatives, it is expected that the gelatin control fluoresces a bright green, and that the PCL shows no color. When looking at

separate sides of the gelatin/PCL scaffold there is a noticeable difference in the level of fluorescence from the gelatin side (Figure 3.20C) and PCL side (Figure 3.20D).The PCL fibers in the gelatin/PCL scaffold do have some fluorescence to them; however this is most likely due to two reasons: 1) fluorescence bleeding from the gelatin side of the scaffold behind the PCL fibers, and/or 2) spraying of gelatin solution on to the PCL fibers. The second reason is cause for suspicion if during co-electrospinning of the two solutions, infusion rate is cut to 0ml/hr for gelatin but voltage is still applied to the solution. It is possible for solution to spray, or even electrospin, when solution remains sitting in the conducting needle. This was phenomenon was easily observed for PCL, which would still produce fibers after infusion rate was cut to 0ml/hr and voltage continually supplied. Since this scaffold was an early trial of the electrospinning apparatus and procedure before moving onto the incorporation of NaCS, HA, and β-TCP, future scaffold production ensured that no voltage was supplied to the solution when infusion rate was cut to 0ml/hr.

3.3.1Presence of NaCS and Ceramic Particles

The detection of NaCS, HA, and β-TCP was carried out through FTIR analysis. The FTIR is also used to further distinguish the presences of two compositionally different halves of the scaffold by performing FTIR for each side of the scaffolds. Due to the thinness of the mats (which causes recording of molecular vibrations from the other side of the scaffold) and the number of functional components, it is difficult to clearly distinguish these components from the FTIR data – even after normalization. The bleeding of molecular vibrations from the opposite side of the scaffold not intended to be

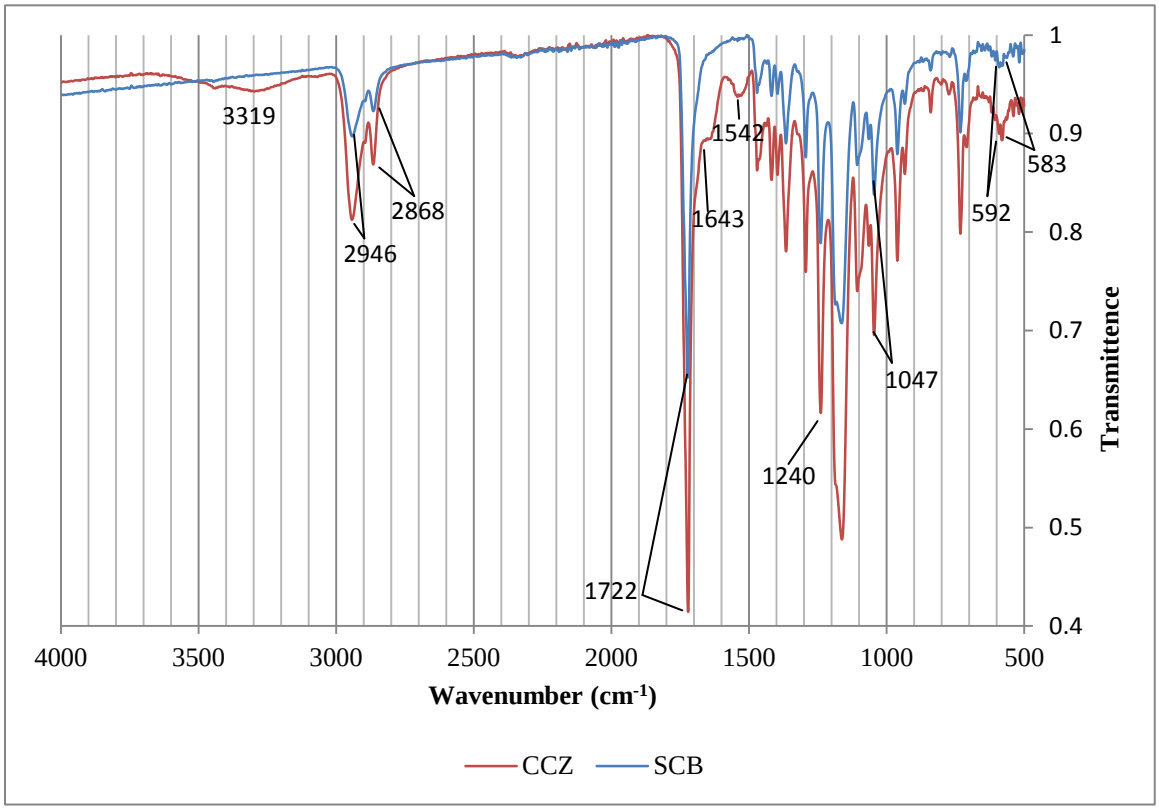

Figure 3.21 CCZ/SCB scaffold with normalized FTIR done for the CCZ and SCB sides. Functional groups are hard to discern within and between scaffolds sides due to the number of material components and insufficient scaffold thickness.

analyzed is seen most clearly in the FTIR of the CCZ/SCB scaffold (Figure 3.21). At 1722cm^{-1} is a carbonyl stretch; and at 2946 and 2868cm^{-1} are asymmetric and symmetric CH_2 stretches, respectively(Polini et al., 2011). These three FTIR peaks are characteristic of PCL. PCL is only present on the SCB half; still it appears in the FTIR of the CCZ half, which leads to the conclusion that the scaffold was too thin to allow for analysis of only one half and not the entire scaffold. The presence of gelatin on the CCZ half can be identified by the plateaued peak around 1643cm^{-1} representing C=O stretching, the broad peak around 3319cm^{-1} which is representative of N-H stretching, and the small peak around 1542cm^{-1} which is representative of C-N-H stretching (Hermanto, Sumarlin, & Fatimah, 2013). These three bonds represent the peptide link found between amino acids

to form the primary structure of proteins. While gelatin is not a protein, due to the loss of its secondary, tertiary, and quaternary superstructures, it still retains its primary structure of linked amino acids.

The presence of HA and β-TCP are indicated by phosphate peaks around 1047cm^{-1}, 592cm^{-1}, and 583cm^{-1}. However, the hydroxyl peaksat 3568cm^{-1}and 630cm^{-1}which differentiates HA from β-TCP cannot be identifiedhere (Patlolla et al., 2010). NaCs typically has peaks around roughly1250, 1530, 2850, and 3400cm^{-1}(Society, 2011). Only the 1250 peak is readily visible in this spectrum.

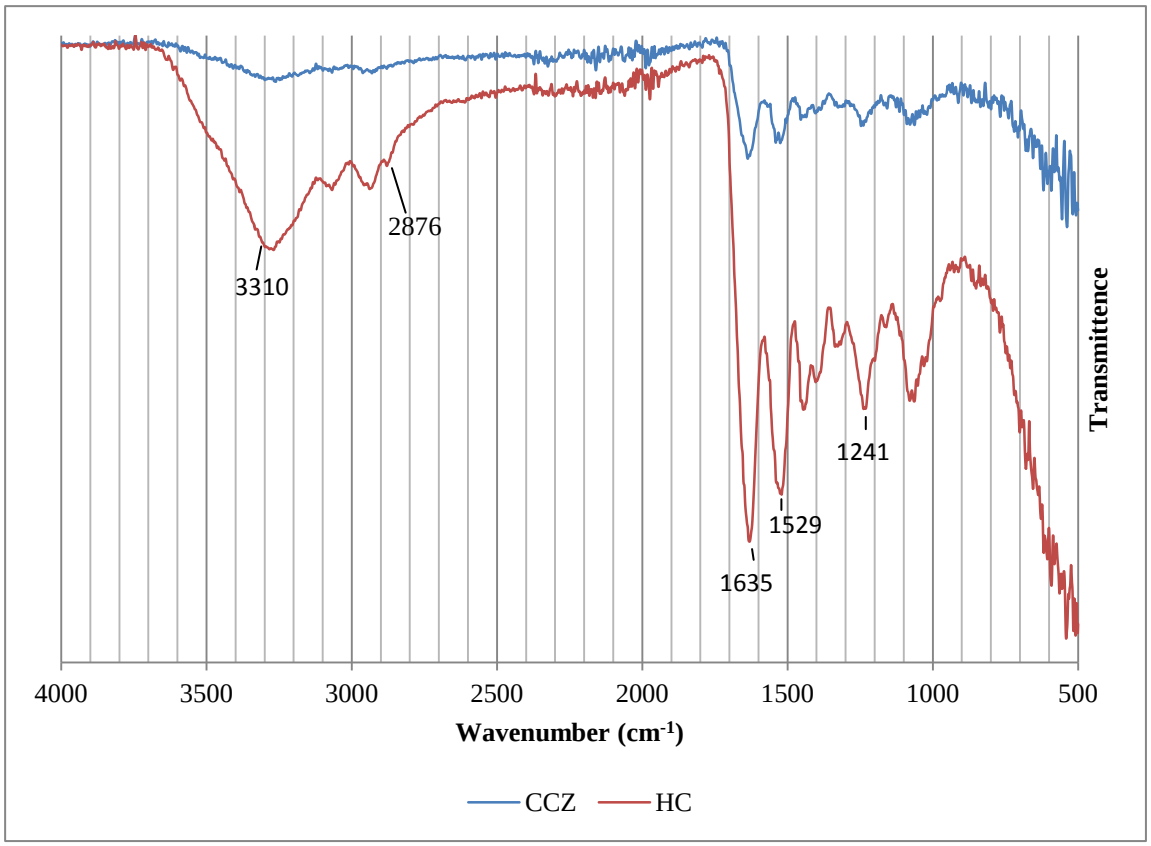

Figure 3.22 CCZ/HC scaffold with normalized FTIR done for the CCZ and HC sides. Functional groups are hard to discern within and between scaffolds sides due to the number of material components and insufficient scaffold thickness.

The CCZ/HC scaffold suffered from similar problems with FTIR bleeding between sides due to insufficient scaffold thickness. Gelatin is identified through C=O (1635cm^{-1}) and N-H stretching (3310cm^{-1}); and NaCS through its peaks at 1241cm^{-1}, 1529cm^{-1}, and 2876cm^{-1} (Figure 3.22). These are also seen in the CCZ half of the scaffold as well (Figure 3.23), where the 1541cm^{-1} C-N-H stretch peak is visible. A HA and β-TCP peak is identified at 1047cm-1. The remaining 592, 583, 3568, and 630cm^{-1} peaks for HA or β-TCP are not pronounced, even when the 500-1000cm^{-1} range is enlarged. It is possible that these peaks were drowned out by bonds in the fingerprint region, or that this section of scaffold analyzed was devoid of ceramic. It is possible that ceramic was not uniformly dispersed across the scaffold, leaving areas ceramic-free. In order to assess ceramic dispersion, SEM energy dispersive x-ray analysis would be required.

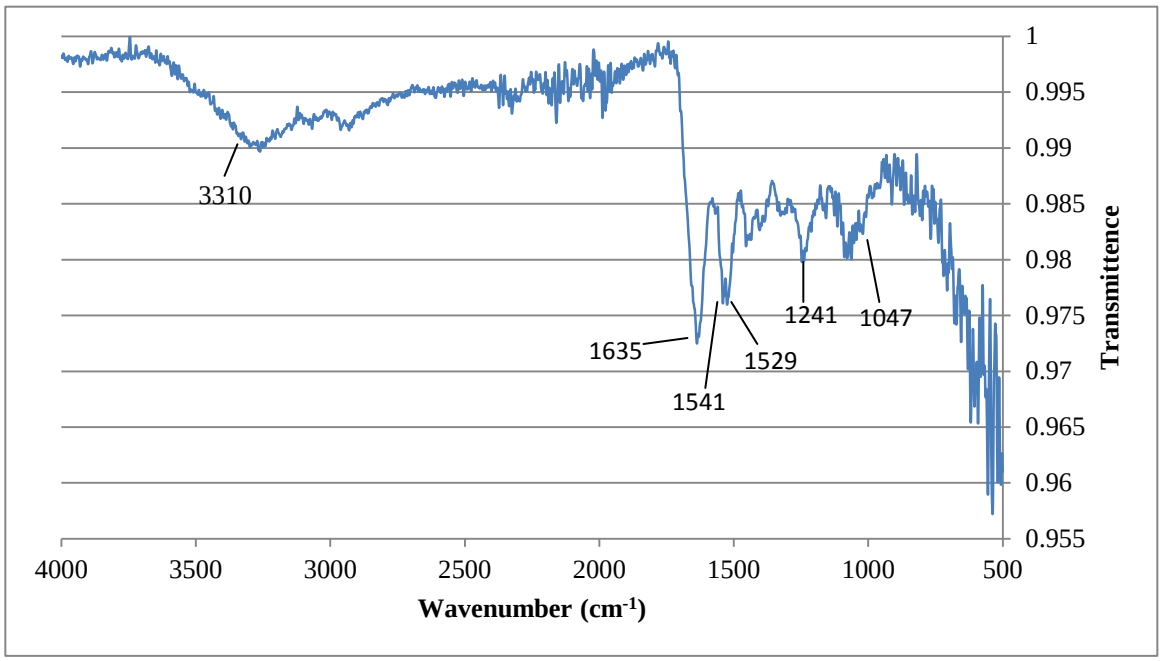

Figure 3.23 CCZ/HC scaffold with normalized FTIR done for the CCZ side.

3.4 Results Summary and Reflection

The main objective of this thesis was to fabricate an electrospinning apparatus capable of producing a heterogeneous fiber scaffold with a grade through its depth. What this thesis demonstrated was indeed, an electrospinning device capable of creating a heterogeneous fiber scaffold with two or more distinct fiber regions within it. These regions were distinct in their composition and/or fiber architecture, as seen in the SEM, light microscope, and fluorescence microscope images. These scaffolds had distinctly different fibers on either half of the same scaffold (i.e. gelatin based fiber on one half, PCL based on the other). Additionally, these fibers can have their orientation altered from one section of the scaffold to the other by adjusting the rotational speed of the mandrel throughout the electrospinning process. Electrospinning for 30 minutes onto a 15 rpm mandrel will create randomly aligned fibers, followed by spinning on to a 1000rpm mandrel to created aligned fibers. This yields two fiber sections with distinct fiber orientation. Additionally, gradually increasing the rotational speed of the mandrel from 15 to 1000rpm over the entire course of electrospinning can then create a slow transition from random to aligned fibers through the depth of the scaffold.

However, what was not explicitly demonstrated here was the presence of a grade through the depth of the scaffold, be it in fiber composition or fiber architecture. In order to verify the presence of such a grade, the graded interior region of the scaffold would need to be imaged. This would require the use of a confocal or confocal fluorescence microscope. This type of microscopy allows for viewing of thin slices of the specimen at different planes through its depth. Observing the grade between natural protein-derived fibers (such as gelatin) and synthetic polymers (such as PCL) can be done by a general

protein stain such as Alexa Fluor 488 and moving through successive viewing planes. Viewing the level of fluorescence generated by dye bound to gelatin, or viewing of the fluorescent fibers themselves, as the viewing plane shifted from the pure gelatin section to the pure PCL section would demonstrate the presence of a grade. If a single dye is not enough to distinguish two fiber types, each fiber type can be labeled separately. If using two fluorophores (fluorescent dyes), care must be taken to ensure that their emission ranges do not overlap significantly when one is more strongly excited than the other. This can be avoided by using alternative fluorophores or a different excitation laser (Murray, 2011).

Issues also arise when imaging a scaffold that is relatively thick (5-10μm or greater) due to background/out-of-focus light, differences in refractive index, and aberrations due to curved surfaces (Murray, 2011). It is important to choose an objective lens and aperture to create a working distance that matches the specimen thickness. For example, a 60x lens with a 1.4 aperture has a working distance of roughly 170μm. A thicker sample would require a larger working distance to view all sections of the scaffold; however this does not eliminate the aforementioned issues with imaging these thicker scaffolds. In cartilage regeneration, the created scaffold (such as the one proposed in this thesis) would aim to be around 2mm in thickness – similar to the thickness of native cartilage tissue. To image such a scaffold, it may need to be divided into thinner sections. If this is not possible, or the sections still remain too large, the sections can be imaged from both sides. If the image is still retains too much background light, additional methods can be used to clear up the images.

One technique is to use deconvolution. This is a computational-based method that aims to remove out-of-focus blur by first calculating the hypothetical structure of the subject that wishes to be imaged, and iteratively refining this hypothetical structure until it matches the observed image (Murray, 2011). There are issues in using this method, especially if the signal noise (due to refraction, for example) is greater than the contrast between the signal and the signal background, as this method will amplify noise. Since this is a computational method, there are inherent limitations in computational load. This is reduced by incorporating filters which attempt to smooth data, but these filters are accompanied by certain assumptions which aren't always true in compositionally complex specimens.

A second technique involves sandwiching the specimen between two small coverslips and imaging both sides. This method requires careful mounting, so as not to compress the specimen, while simultaneously attempting to eliminate any excess space between the specimen and the coverslips. This method has its limitations as well, primarily due to attenuation. Since the specimen is not homogeneous, differences in refractive index across the specimen will scatter laser illumination and emission – often limiting the acquisition of quality images to depths no more than 0.05mm (Murray, 2011).

The secondary, or sub-objective, of this thesis was to demonstrate the construction of a scaffold using the apparatus which mimics the heterogeneous ECM of the cartilage-bone interface. There are several criteria that must be met in order to satisfy this sub-objective: 1) the creation of a scaffold with distinguishable regions 2) the incorporation of the proper material components which mimic those found within

hyaline cartilage, calcified cartilage, and bone; 3) fiber diameters on the nano scale which mimic fibers within the target ECM in terms of facilitation ofcellular attachment, migration, and function; 4) uniform interfiber spacing which mimics that of the target ECM in terms of facilitating cellular attachment, migration, and function; 5) fiber orientation which mimics that found within the tissue(s) of interest; 6) a total scaffold thickness around 2mm, which is comparable to the thickness of hyaline cartilage tissue; and 7) a scaffold which has comparable mechanical properties to that of the tissue(s) of interest. The scaffold demonstrated here meets some of these criteria – others it meets partially or not at all.

This scaffold did have distinguishable regions in terms of fiber diameter, spacing, and material components as shown by the SEM and FTIR results. While these regions were distinct, it does not mean they were ideal in terms of the remaining criteria. All of the gelatin fibers had dimensions in the tens of micrometers, while the PCL fibers were in the high hundreds to thousands of nanometers.Interfiber spacing for all scaffold sections had a high standard of deviation, suggesting non-uniformity. The total thickness of the scaffold was in microns, nowhere close to the required 2mm thickness. Many of the short comings in these criteria are attributed to poor control of electrospinning parameters, primarily the humidity. The gelatin fibers suffered the most due to this lack of control. As previously mentioned in Section 3.1, the rapid evaporation of the solvent prevented the gelatin solution from forming a stable Taylor cone and subsequent elongation of the gelatin fibers upon ejection. By controlling the humidity so it resides within the range of 25-30%, these gelatin solutions should be able to properly electrospin. Further adjustments can be made as well to the throw distances. Typically, by increasing the

throw distance, the solution (PCL or gelatin based) is able to undergo further elongation, and thus increased reduction in final diameter when deposited onto the plate. Of course, increasing the throw distance also means adjusting the voltages applied to the solutions, as now the distance to the low potential ground is increased. Once these fibers can electrospin, without disruption of the Taylor cone which causes non-continuous electrospinning, the fibers should deposit more uniformly upon the surface of the mandrel. The continuous electrospinning also means that less polymer solution is wasted due to dripping or spraying, therefore allowing the creation of thicker electrospun mats. If one 10mL solution filled syringe is insufficient to achieve the required thickness, electrospinning can be temporarily halted and a newly filled syringe substituted.

In terms of fiber alignment, this scaffold achieved the intended random fiber alignment through all its sections. Upon reflection, it would be advantageous to, in addition to the compositional fiber grade, incorporate a fiber orientation grade through the depth of the scaffold. This would require a careful study of the exact mandrel rotational speed ranges that produce a specific level of alignment. The fibers would be observed under SEM, and fiber alignments assessed quantitatively by finding the angle several random fibers make relative to a defined axis. Statistical analysis would determine the mean angle and standard deviation from this mean. This information would then be used to rate scaffold samples on a pre-determined scale of alignment – for example, from 0, meaning completely random, to 10, meaning completely aligned.

Achieving mechanical properties comparable to that of natural tissue is extremely challenging, especially for a viscoelastic tissue such as cartilage. In cartilage, collagen II fibers bear a component of the mechanical stresses, but these fibers are within a fluid

matrix comprised of water (the major component of cartilage tissue) and proteoglycans. While collagen fibers are responsible for much of the tensile strength and stiffness of cartilage tissue, the water which surrounds these fibers is responsible for the compressive strength of cartilage. Some water can form a gel-like environment in small spaces within or between collagen fibers, while the remainder flows through the cartilage ECM upon compression. As water moves out of the cartilage ECM, the fixed charge density (due to the negatively charged GAGs bound to collagen IX fibers, which are subsequently bound to collagen II) increases, which in turn increases swelling pressure within the tissue, making further movement of water out the tissue increasingly (Portocarrero, 2010). This is because the inherently dipolar water (which also contains several cations such as sodium, calcium and potassium) must flow through small spaces between the gelatin fibers with bound GAGs against an increasing electrochemical gradient.

What is important to understand here is that there is a critical interaction between the collagen II fibers and the surrounding fluid or gel-like matrix, which is comprised of water; and that this interaction is facilitated through proteoglycans intermediately bound to collagen II fibers. It is this interaction that is responsible for the viscoelastic and very anisotropic mechanical behavior or cartilage tissue. Electrospinning a fiber scaffold alone is not enough to properly mimic the complex behavior of cartilage tissue. This electrospun scaffold must be contained within a hydrogel, but in such a way that the two components can interact mechanically. What this means is that when stress is placed upon the hydrogel, that the hydrogel properly transfers this stress to the fiber scaffold. Ideally this way in which this force is transmitted, as well as the maximum stresses able to be placed upon the fiber reinforced hydrogel, would rival that of natural cartilage.

Enabling this interaction between the fibers and hydrogel could be accomplished through the actual fabrication technique of the fiber reinforced hydrogel (i.e. how the fibers are incorporated or placed in the hydrogel), or through the addition of material components within the fibers or hydrogel which allow chemical bonding between the two structures.

The fabrication of these types of multifaceted scaffolds is something that many engineers have been attempting when it comes to mimicking complex heterogeneous tissues. As a result there have been many various approaches in creating these scaffolds. In a study done by Erisken et al., a hybrid twin-screw extrusion/electrospinning process was used to create a functionally graded scaffold which looked to mimic calcified cartilage and subchondral bone. This apparatus is a combination of a twin-screw extruder die with multiple flow channels for flow, and injection/feed ports for the introduction of various additives. The spinneret die is then attached to a high-voltage power supply to allow electrospinning onto a grounded plate. This apparatus has the potential to shape the ejecting polymer solution, break up large particle aggregates, vary solution temperatures over separate heat transfer zones, and perform a variety of operations (such as melting, conveying, etc.) (Erisken, Kalyon, & Wang, 2008).

Several other techniques for producing functionally graded scaffolds have been attempted as well. One method utilizes porogens, by stacking layers of power mixtures on top of one another, each with their own volume fractions or sizes. This can be achieved through multiple tape casting or slip casting, and varying the porogen used (Leong, Chua, Sudarmadji, & Yeong, 2008). A method done by Tampieri et al. created a scaffold with different porous zones by impregnating cellulosic sponges with two HA slurries with varying crystallinity, followed by sintering to remove the underlying sponge

(Leong et al., 2008). Zeschky et al. created a scaffold with a porosity grade by controlling the bubble nucleation, growth, and bubble rise in an oxycarbide ceramic foam (Leong et al., 2008). Harley et al. generated collagen-based cylindrical scaffolds with a radially aligned pore gradient by utilizing centrifugal force to separate liquid and solid phases in a suspension before rapid freeze drying and sublimation (Leong et al., 2008). Rapid prototyping techniques such as Theriform™ 3-D printing, finite difference method, and 3D fiber deposition are also used to achieve scaffolds with varying fiber composition, porosity, and pore size throughout.

The aforementioned methods all have the potential to produce scaffolds with varying composition and architecture, but these methods can be quite complex and the apparatuses often very expensive. This can be an issue for research laboratories that do not have the necessary funds to purchase this equipment. The beauty of the apparatus proposed by this thesis is in its ability to produce heterogeneous graded scaffolds simply and cheaply. If the scaffolds produced by this apparatus can perform equally well in cell studies as scaffolds produced by other methods, this may prove to be of enormous benefit to smaller, independent laboratories.

CHAPTER 4

CONCLUSION

The main objective of this thesiswas to develop an electrospinning apparatus setup capable of producing heterogeneous electrospun fiber scaffolds. Success of such a setup requires the resulting scaffold to have identifiably distinct regions, be it in material composition, fiber diameter, fiber orientation, or fiber spacing. The electrospinning setup proposed by this thesis, which consisted of a rotating mandrel and co-electrospinning of two polymer solutions, yielded fiber scaffolds with distinct halves. This is verified through the fluorescent microscopy images, which show a single fiber scaffold with two sides that are distinctly different in fiber material composition; through the SEM image analysis, which show scaffold halves with different fiber diameters and interfiber spacing; and through FTIR (tentatively), which shows scaffold halves with dissimilar spectrums, indicating a difference in additive material components.

Although not explicitly demonstrated here, scaffolds halves with different fiber orientations are easily obtainable as well. This is accomplished by electrospinning onto a slowly rotating mandrel (<50rpm) to achieve randomly aligned fibers, and then increasing the mandrel speed (>200rpm) to achieve aligned fibers. While not deeply investigated, it appears that increasing mandrel speeds yields scaffolds with smaller interfiber distances.

A secondary objective of this thesis was to apply this apparatus towards the creation of an electrospun fiber scaffold which mimics the cartilage-bone matrix interface. However, it’s difficult to say that this secondary objective has been sufficiently

met due to difficulties in electrospinning the gelatin based solutions in a low humidity environment. Typically, nanoscale fibers and an interfiber spacing ranging from 20-100μm is ideal for cell attachment, cell infiltration, and tissue in-growth (Patlolla et al., 2010). The fibers produced for the cartilage-bone matrix ECM mimic, on average, ranged from 1 to 13μm; and interfiber spacing, on average, ranged from 3 to 48μm. While the interfiber spacing is adequate, the fibers are in the thousands of nanometers – much too large this application. Even so, this is correctable by working in a humidity controlled environment and by adjusting electrospinning parameters such as throw distance, infusion rate, and applied voltage.

Outside fiber architecture, this scaffold does incorporate several important material components which mimic molecules naturally found in cartilage, calcified cartilage, and subchondral bone environments (as discussed in Chapter 2). Again, it is hard to say for certain how effective the current fiber solution compositions are without performing cell studies – something that, unfortunately, was not able to be achieved in the given time frame. Nevertheless, the scaffold produced does have three distinct regions tailored to specific zones at the cartilage-bone junction (Figure 1.2) – middle zone hyaline cartilage, calcified cartilage, and subchondral bone.

Through the production of an electrospinning setup capable of producing a single fiber scaffold with multiple distinct regions, more complex mimics of cellular ECMs can be achieved. This is especially useful for mimicking tissue environments such as the cartilage ECM, whose fiber architecture changes when moving from the articulating surface towards the subchondral bone; or for mimicking a tissue interface consisting of multiple cell types and environments.

CHAPTER 5

FUTURE DIRECTIONS

These graded, multi-region scaffolds could have great potential for the generation of tissues with complex architecture. Determining exactly how impactful these scaffolds could be would require additional characterization and long term cell growth and differentiation studies. To start, the scaffold presented here for a cartilage-bone interface ECM mimic would need to be reconstructed under a highly controlled environment in order to achieve smaller fiber diameters, uniform fiber spacing, and a thicker electrospun scaffold. This reconstructed scaffold would undergo FTIR analysis again in hopes of achieving a clearer FTIR spectrum for identification of material components on separate scaffold halves. SEM energy dispersive x-ray analysis would be performed as well in order to visualize the distribution of ceramic components across the scaffold. Uniform ceramic dispersion along fibers in the CCZ and SCB sections are desired to encourage all MSCs in these sections undergo partial calcification or endochondral ossification respectively. Thermal and tensile analysis would also be of interest to understand the rheological properties of this composite scaffold.

Further modification to these scaffolds can be done by varying or substituting material components, adjusting fiber alignment through the depth of the scaffold, adjusting the thickness of specific scaffold sections, or enveloping the scaffold in a hydrogel. It would be of interest to see how these changes may affect cell proliferation and differentiation.

Long term cell studies are paramount in determining the effectiveness of these types of scaffolds. However, there are a couple foreseeable problems that must be solved before cell studies can be carried out. The first is how to ensure proper cellular and nutrient infiltration throughout the scaffold. It is important to ensure that the scaffold is constructed with interfiber spacing large enough to accommodate cells between 5 and 20nm in diameter. Scaffolds with interfiber spacing smaller than the cell itself makes it difficult for cells to move into the scaffold center, thus forcing the majority to remain along the surface. A rotating wall vessel bioreactor can be used to ensure that culture media is adequately dispersed throughout the scaffold as well. This brings up the second issue: the required culture media for cellular differentiation. This is quite a big problem, especially when trying to differentiate two different cell types (chondrocytes and osteoblasts) within the same scaffold construct. Currently there is no culture medium that is simultaneously osteogenic and chondrogenic. Therefore, in order to ensure terminal differentiation a culture medium must be created which can accommodate this need. It could also be possible to make the scaffold sections extremely specialized (i.e. entrapment of specific growth factors) in order to lessen the dependence on culture medium for cell differentiation.

If the issues related to these scaffolds regarding cell studies are solved, it would interesting to observe differentiation of one cell type on one half of the scaffold, and differentiation of a second cell type on the other half (i.e. chondrocyte differentiation within the HC and CCZ scaffold sections, and osteoblast differentiation within the SCB section). In the case of the cartilage-bone interface, staining for cell nuclei, cell specific surface markers, collagen I, collagen II, collagen X, and proteoglycans (chondroitin 4-

sulfate, chondroitin 6-sulfate, and keratin sulfate) would aid in distinguishing mature terminally differentiated chondrocytes and osteoblasts. Long term studies would track changes in cell morphology, especially for chondrocytes within the CCZ undergoing endochondral ossification, and look for the formation of any kind of tidemark between the HC and CCZ sections.

A bold future application of this apparatus would be the development of a cartilage defect plug. If this apparatus can produce a heterogeneous scaffold, nearly identical to that of hyaline cartilage, and be incorporated within a hydrogel – creating a fiber reinforced hydrogel – this plug could be inserted within the defect and encourage the migration of cells from the subchondral bone up into the scaffold to begin tissue formation. There are still some large issues to overcome when developing this scaffold, primarily the mimicking of the mechanical nature of cartilage tissue as discussed in Section 3.4.

APPENDIX A

ELECTROSPINNING SYRINGE HOLDER CONSTRUCTION

In order to electrospin a graded scaffold, two solutions must be electrospun at the same time. This requires two non-conducting syringe stands to hold the syringes. The polyethylene syringe stand was constructed prior to the work done within this thesis. However, the wooden stand had to be constructed by hand. This involved dimensioning the 10 mL syringes used for the infusion pumps and for holding the polymer solution. In addition to holding the syringes, the stand must be adjustable – it must be able to rotate about its base, move laterally, and move vertically. The wooden syringe holder used in this thesis is adjustable in rotation and lateral movement, but not in height due to time constraints on construction. If height adjustments were crucial, a simple fix would be to replace the syringe base with one that had a greater height. Figures A.1 to A.8 are dimensioned reconstructions of the syringe holder, created in CreoParametrics 2.0. All dimensions are in millimeters. Higher resolution pictures are available upon request.

Figure A.1 Top view of the piece that holds the syringes themselves (front side on left). The bulges allow room for the syringe thumb presses. A square section is cut out towards the front to allow for easier removal of the syringe containing the polymer solution. A small hole is present on the front and back faces to allow the syringe tip to protrude.

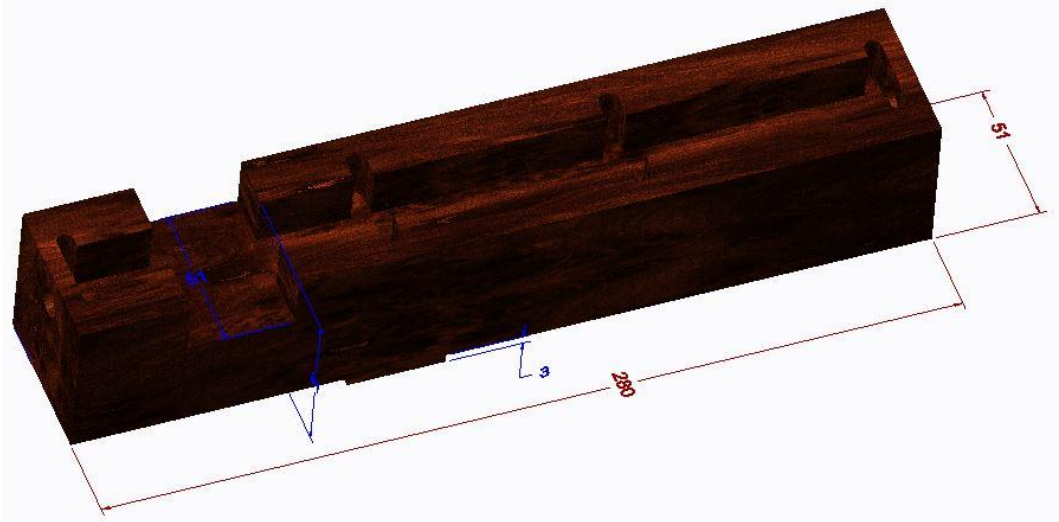

Figure A.2 Top/side view of the piece containing the syringe. The holes for the syringe tops are visible here. A rectangular protrusion extends from the bottom which serves to keep the piece in a track on the platform (Figure A.5).

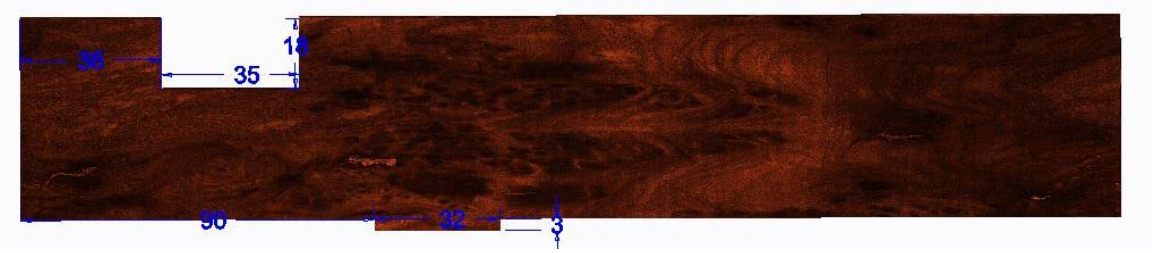

Figure A.3 Side view of the piece containing the syringe. Cutout and bottom protrusion are clearly visible.

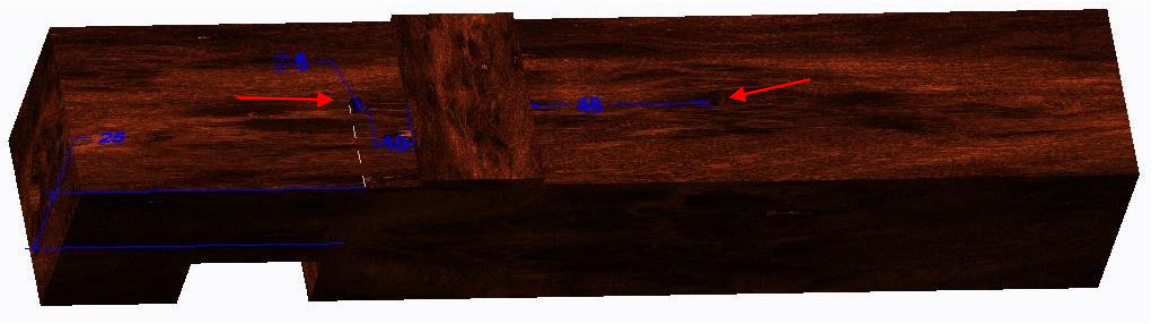

Figure A.4 Bottom view of syringe containing piece. Two holes (arrow) are present in the base to allow for fastening of the piece to the platform (Figure A.5).

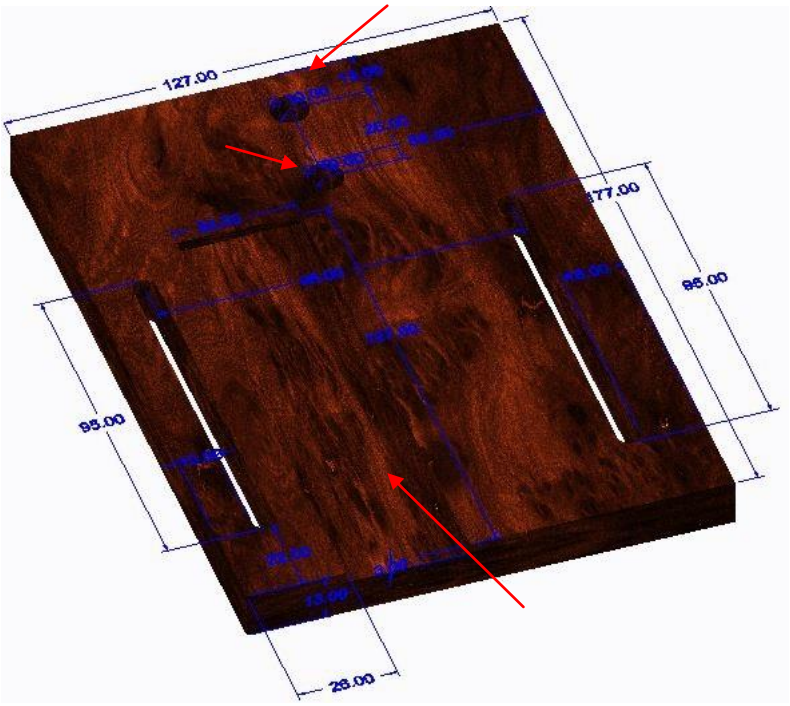

Figure A.5 Platform on which the syringe containing piece will sit. The notched groove (arrow) matches with the protrusion on the syringe containing piece and restricts movement to only one direction. The ovular cutouts allow for pegs to be inserted up through the platform and into the holes in the bottom of the syringe containing piece to lock its position in place. Two additional holes are present (arrow) to secure the platform to the pillar (Figure A.6).

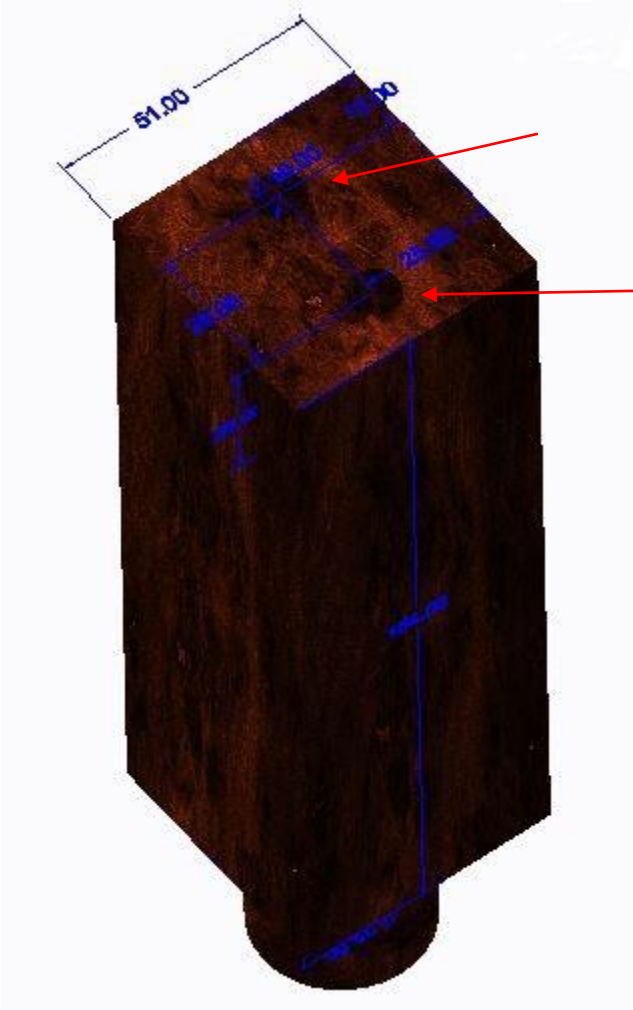

Figure A.6 Pillar which will form the connection between the platform and base. The rounded peg at the bottom allows the pillar, and subsequently the syringe platform, to rotate 360 degrees. Two holes (arrow) are present in the top to allow the platform to be secured to the pillar.

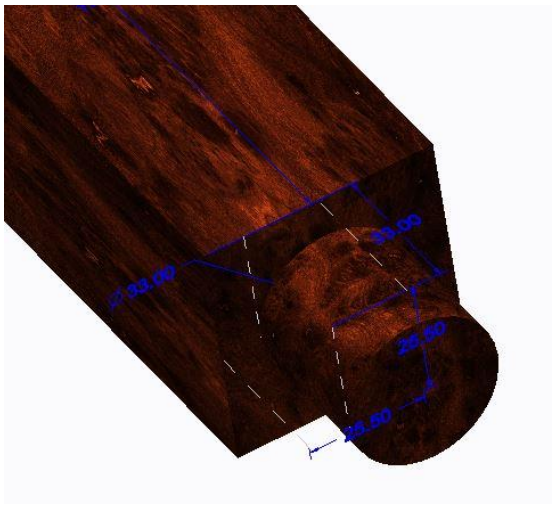

Figure A.7 Close up of the bottom of the pillar.

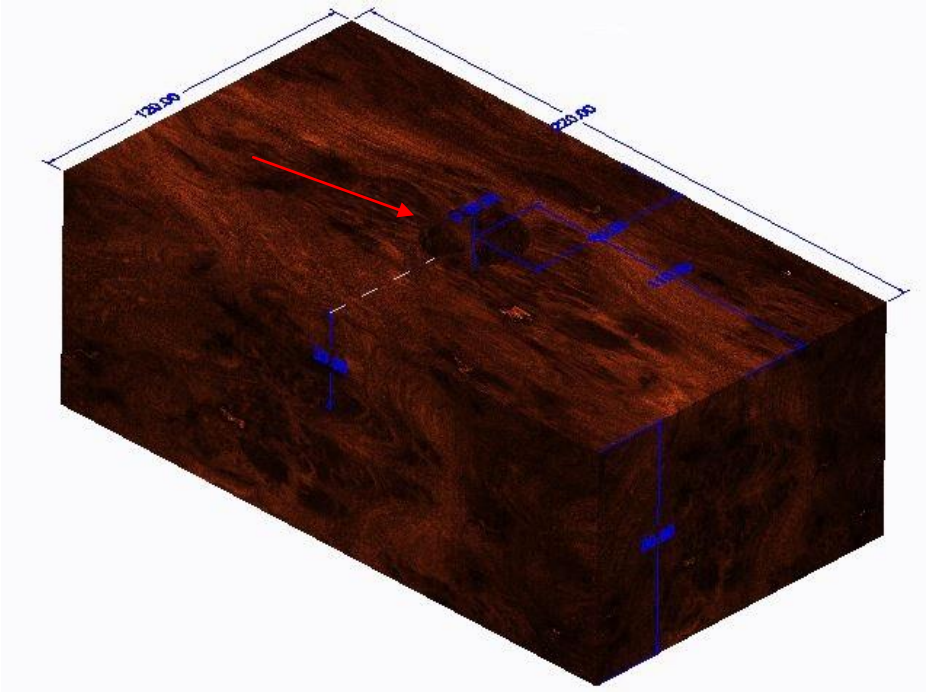

Figure A.8 Base of the syringe holder. The hole in the middle (arrow) allows for connection of the pillar to the base.

APPENDIX B

ELECTROSPINNING APPARATUS

In order to achieve scaffold graded through the depth, a grounded rotating mandrel was needed. This approach was chosen over placing two syringe holders side by side facing a static collection plate due to possible issues with interfering corona envelopes and fiber entanglement before reaching the grounding plate. A rotating grounding plate allows the syringe holders to be placed on opposites sides of the ground, anywhere from 10-60 cm apart, minimizing interference. This is especially useful when electrospinning solutions which require different voltage magnitudes. Electrospinning a solution which requires an applied voltage 50-60 kV (such as the gelatin-NaCS and gelatin-NaCS-HA/β-TCP solutions) side by side with a solution which requires an applied voltage of 15-20 kV (such as the PCL-HA/β-TCP solution) will often lead to fibers from the high voltage potential to ground to the neared low potential point – the adjacent lower voltage needle and attached alligator clip. Even though separating the two syringe holders while on the same side of the ground may prevent this, the two fibers may still tangle while on their way to the ground, as these fibers do maintain some residual charge after leaving the needle. Therefore, by keeping the syringe holders and solutions opposite each other and placing a ground directly in between, the closest site of low potential becomes the grounded mandrel instead of the other lower voltage syringe needle.

Pictures of the electrospinning setup as well as close-ups of the mandrel can be seen in Figures B.1-B.6. In this case, since the objective is to achieve random graded fiber mats, a toothed belt and gears are used to produce a much slower rotation of the

mandrel. Rubber expansion plugs are used to help align the gears in the same plane. Tape is added as extra insurance to keep the plugs in place as well as to offer additional shielding from solvent spray and fiber deposition on top of the polyethylene housing.

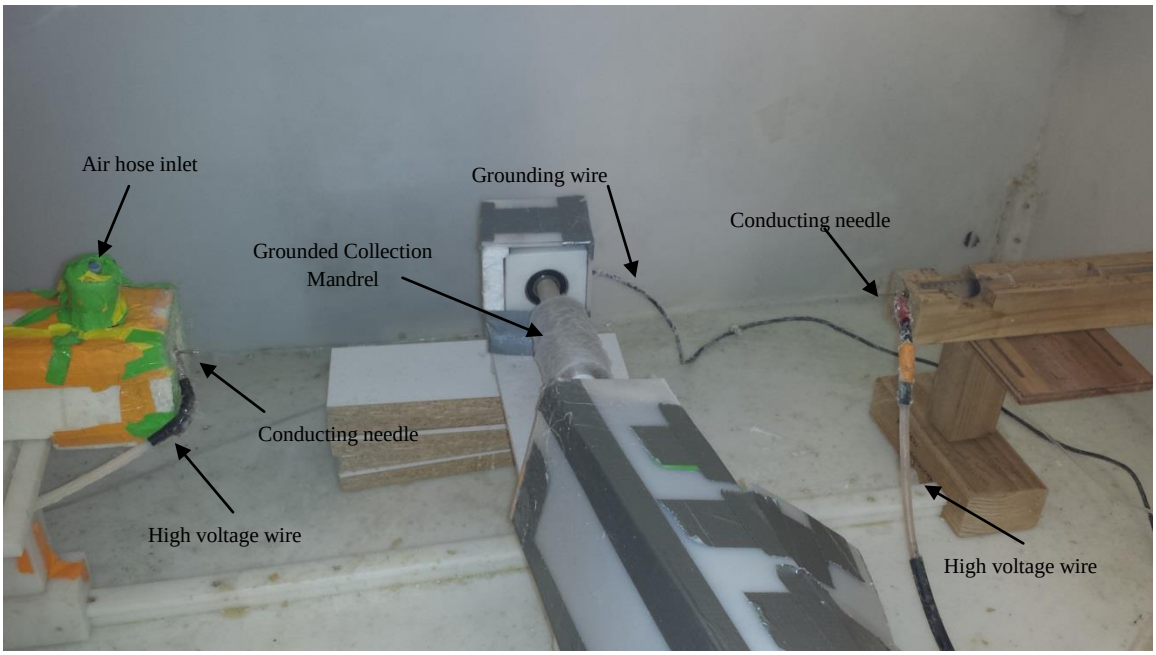

Figure B.1 Electrospinning setup within an enclosed polyethylene box. Solutions which require applied heat are electrospun using a Styrofoam enclosure with a small air hose inlet (left). Those that can be spun in ambient temperature do not require this enclosure (right). The rotating mandrel (middle) has its motor and ground attachment shield by non-conductive sheets of polyethylene. High voltage lines are clipped on to the metal needles on each syringe. Wooden planks are used to raise the mandrel up the plane of the needles.

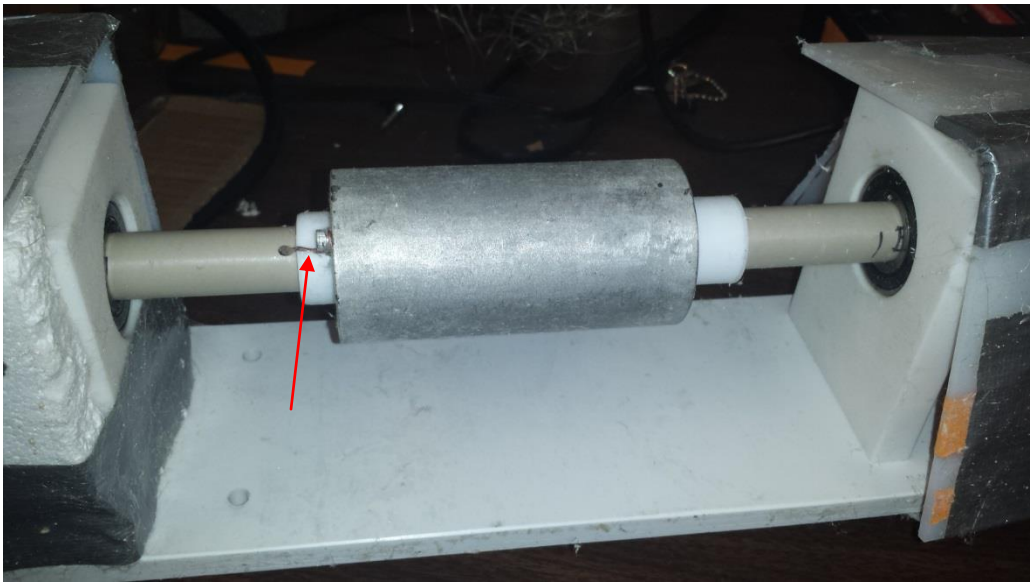

Figure B.2 Close up of mandrel collection plate. A small wire attaches to the side of the metal plate and runs through an insulated cylinder which connects to a slip ring on the left (covered in this photograph).

Figure B.3 Close up of the uncovered slip ring. The metallic portion of the slip ring (arrow) contacts the wire that runs from the mandrel in Figure B.2. A small eye hook protrudes from the slip ring (this hook contacts the underlying metal in the slip ring), which allows for the connection of the grounding wire.

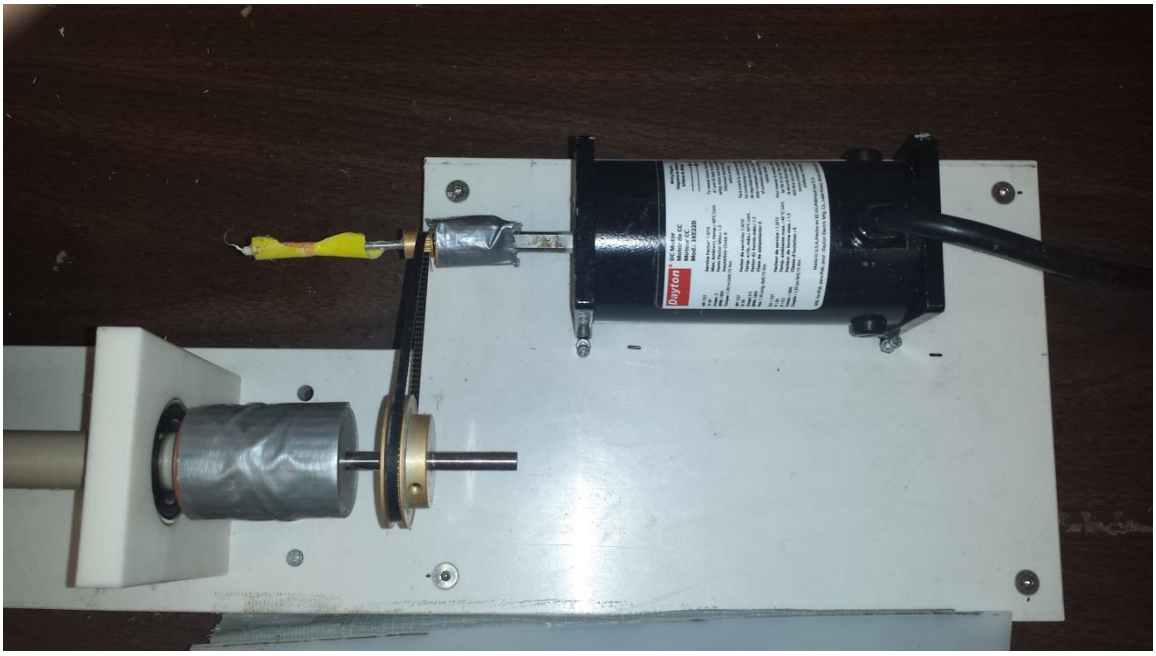

Figure B.4 Top view of motor connected to the rotating mandrel via toothed belt and gears. The motor has a maximum speed of 1800 rpm. A speed control knob (not shown) allows for adjustment. However, slow rotation cannot be obtained through setting the control knob to low speeds (lower than 300rpm) alone, as the motor does not produce any rotational motion. The toothed belt and gears allows for the motor to be set to a higher speed above this rotation threshold, and still achieve low speed mandrel rotation.

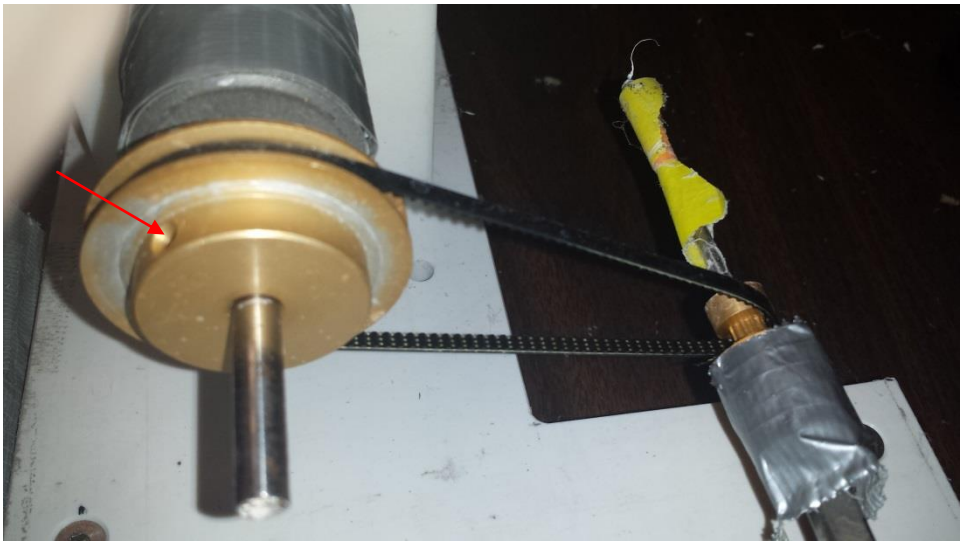

Figure B.5 Close up of the toothed belt and gears. Gears are secured on the protruding rods via a small screw and screw hole on the gear (arrow).

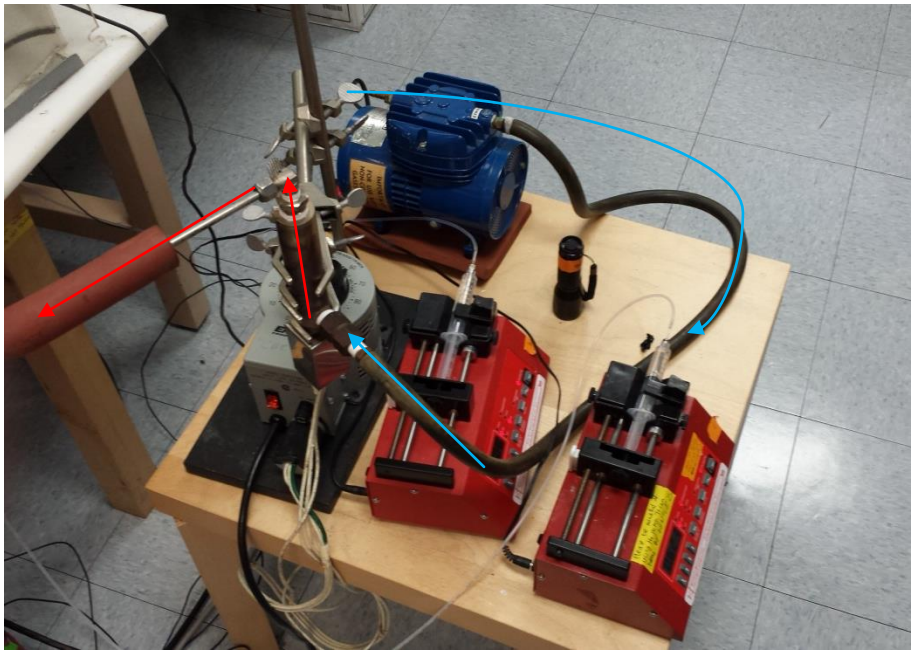

Figure B.6 Picture of NE-1000 programmable syringe pumps (*bottom right*) along with an air compressor (*top left*). The metal cylinder (*bottom left*) with attached electrical wires (white wires) allows the cylinder to heat up. These wires are plugged into an AC voltage regulator (*bottom left*) which allows for AC voltage adjustment to the metal cylinder, thus allowing for temperature control. A small air inlet on the bottom of the cylinder allows for room temperature air to enter the cylinder, heat up, and then exit through an insulated tube (arrows).

REFERENCES

Arkill, K. P., & Winlove, C. P. (2008). Solute transport in the deep and calcified zones of articular cartilage. *Osteoarthritis and Cartilage, 16*(6), 708-714. doi: http://dx.doi.org/10.1016/j.joca.2007.10.001

Barrilieaux, B., Phinney, D., Prockop, D., & O'Connor, K. (2006). Review: Ex Vivo Engineering of Living Tissues with Adult Stem Cells. *Tissue Engineering, 12*(11), 3007-3019.

Bogue, R. (1923). Conditions Affecting the Hydrolysis of Collagen to Gelatin. *Industrial and Engineering Chemistry, 15*(11), 1154-1159.

Bohlmann, J., Schneider, C., Andresen, H., & Buchholz, R. (2002). Optimized Production of Sodium Cellulose Sulfate (NaCS) for Microencapsulation of Cell Cultures. *Engineering in Life Sciences, 2*(12), 384-388.

Bozhilov, K. (2012). Brief Introduction to Scanning Electron Microscopy (SEM). 2014, from http://micron.ucr.edu/public/manuals/Sem-intro.pdf

Broom, N., & Poole, A. (1982). A Functional-Morphological Study of the Tidemark Region of Articular Cartilage Maintained in a Non-Viable Physiological Condition. *Journal of Anatomy, 135*(1), 65-82.

Buckwalter, J. A., Mow, V. C., & Ratcliffe, A. (1994). Restoration of Injured or Degenerated Articular Cartilage. *J Am Acad Orthop Surg, 2*(4), 192-201.

Bullough, P., & Jagannath, A. (1983). The Morphology of the Calcification Front in Articular Cartilage. *THe Bone & Joint Journal, 65-B*(1), 72-78.

Clarke, D., Johansson, C., Wilbertz, J., Veress, B., Nilsson, E., Karlstrom, H., . . . Frisen, J. (2000). Generalized Potential of Adult Neural Stem Cells. *Science 2, 288*(5471), 1660-1663. doi: 10.1126/science.288.5471.1660

Control, C. f. D. (2014). Arthritis. 2014, from http://www.cdc.gov/arthritis/data_statistics.htm

Cremer, M., Rosloniec, E., & Kang, A. (1998). The cartilage collagens: a review of their structure, organization, and role in the pathogenesis of experimental arthritis in animals and in human rheumatic disease. *Journal of Molecular Medicine, 76*, 275-288.

Dee, K., Puleo, D., & Bizios, R. (2002). *An Introduction to Tissue-Biomaterial Interactions*: John Wiley & Sons.

EMBL-EBI. Collagen alpha-1(II) chain (P02458). from http://www.ebi.ac.uk/interpro/protein/P02458

Erisken, C., Kalyon, D. M., & Wang, H. (2008). Functionally graded electrospun polycaprolactone and beta-tricalcium phosphate nanocomposites for tissue engineering applications. *Biomaterials, 29*(30), 4065-4073. doi: 10.1016/j.biomaterials.2008.06.022

Eyre, D. (2002). Collagen of articular cartilage. *Arthritis Res, 4*(1), 30-35.

Goldring, M. (2009). Cartilage and Chondrocytes. In G. Firestein (Ed.), *Kelley's Textbook of Rheumatology* (8th ed., Vol. 1, pp. 33-60): Elsevier

Gómez-Guillén, M. C., Giménez, B., López-Caballero, M. E., & Montero, M. P. (2011). Functional and bioactive properties of collagen and gelatin from alternative sources: A review. *Food Hydrocolloids, 25*(8), 1813-1827. doi: http://dx.doi.org/10.1016/j.foodhyd.2011.02.007

Haitang, Y., Qiang, T., & Heng, Z. (2014). Progress in Various Crosslinking Modification for Acellular Matrix. *Chinese Medical Journal, 127*(17), 3156-3164.

Hermanto, S., Sumarlin, L. O., & Fatimah, W. (2013). Differentiation of Bovine and Porcine Gelatin Based on Spectroscopic and Electrophoretic Analysis. *Journal of Food and Pharmaceutical Sciences, 1*, 68-73.

Hoemann, C., Lafantaisie-Favreau, C.-H., Lascau-Coman, V., Chen, G., & Guzman-Morales, J. (2012). The Cartilage-Bone Interface. *Journal of Knee Surgery, 25*, 85-98. doi: http://dx.doi.org/10.1055/s-0032-1319782

Huiskes, R. (1993). Stress Shielding and Bone Resorption in THA: Clinical Versus Computer-Simulation Studies. *Acta Orthopaedia Belgica, 59*, 118-129.

Izadifar, Z., Chen, X., & Kulyk, W. (2012). Strategic Design and Fabrication of Engineered Scaffolds for Articular Cartilage Repair. *Journal of Functional Biomaterials, 3*(4), 799-838. doi: 10.3390/jfb3040799

Kini, U., & Nandeesh, B. (2012). Physiology of Bone Formation, Remodeling, and MetabolismRadionuclide and Hybrid Bone Imaging (2012 ed., pp. 29-57): Springer.

Klemm, D., Schmauder, H.-P., & Heinze, T. (2004). *Comprehensive Cellulose Chemistry: Fundamentals and Analytical Methods* (Vol. 1).

Knudson, C., & Knudson, W. (2001). Cartilage Proteoglycans. *Cell & Developmental Biology, 12*, 69-78. doi: 10.1006/scdb.2000.0243

Knudson, W., & Loeser, R. (2002). CD44 and integrin matrix receptors participate in cartilage homeostasis. *Cellular and Molecular Life Sciences, 59*, 36-44.

Lane, L., & Bullough, P. (1980). Age-Related Changes in the Thickness of the Calcified Zone and the Number of Tidemarks in Adult Human Articular Cartilage. *Journal of Bone & Joint Surgery, 62-B*(3), 372-375.

Langer, R. V., Joseph. (1993). Tissue Engineering. *Science, 260*, 920-926.

Lanza, R., Langer, R., & Vacanti, J. (2013). *Principles of Tissue Engineering*: Academic Press.

Leong, K. F., Chua, C. K., Sudarmadji, N., & Yeong, W. Y. (2008). Engineering functionally graded tissue engineering scaffolds. *Journal of the Mechanical Behavior of Biomedical Materials, 1*(2), 140-152. doi: http://dx.doi.org/10.1016/j.jmbbm.2007.11.002

Li, D., & Xia, Y. (2004). Electrospinning of Nanofibers: Reinventing the Wheel? *Advanced Materials, 16*(14), 1151-1170. doi: 10.1002/adma.200400719

Loaiza, L. (2013). *Assessment of Gelatin Based Nano Fiber Reinforced Hydrogels as Mimics of the Cartilage ECM Using a Rotating Bioreactor*. (Masters of Science), New Jersey Institute of Technology.

Lu, X., & Mow, V. (2008). Biomechanics of Articular Cartilage and Determination of Material Properties. *Medicine & Science in Sports & Exercise, 40*(I), 193-199. doi: 10.1249/mss.0b013e31815cb1fc

Lukaszczyk, J., Janicki, B., & Frick, A. (2012). Investigation on Synthesis and Properties of Isosorbide based bis-GMA Analogue. *Journal of Materials Science, Materials in Medicine, 23*(5), 1149-1155. doi: 10.1007/s10856-012-4594-6

Lyons, T., McClure, S., Stoddart, R., & McClure, J. (2006). The Normal Human Chondro-Osseous Junctional Region: Evidence for Contact of Uncalcified Cartilage with Subchondral Bone and Marrow Spaces. *BMC Musculoskeletal Disorders, 7*(52). doi: 10.1186/1471-2474-7-52

Muir, H. (1978). Proteoglycans of Cartilage. *Journal Of Clinical Pathology, 31*(12), 67-81.

Murray, J. (2011). Methods for Imaging Thick Specimens: Confocal Microscopy, Deconvolution, and Structured Illumination. *Cold Spring Harbor Protocols*, 39. doi: http://dx.doi.org/10.1101/pdb.top066936

Oegema, T., Carpenter, R., Hofmeister, F., & Tompson, R. (1997). The Interaction of the Zone of Calcified Cartilage and Subchondral Bone in Osteoarthritis. *Microscopy Research and Technique, 37,* 324-332.

Ogose, A., Hotta, T., Kawashima, H., Kondo, N., Gu, W., Kamura, T., & Endo, N. (2004). Comparison of Hydroxyapatite and Beta Tricalcium Phosphate as Bone Substitutes After Excision of Bone Tumors. *Journal of Biomedical Materials Research Part B: Applied Biomaterials, 72B*(1), 94-101. doi: 10.1002/jbm.b.30136

Oprea, A.-M., Ciolacu, D., Neamtu, A., Mungui, O., Stoica, B., & Vasile, C. (2010). Cellulose/Chondroitin Sulfate Hydrogels: Synthesis, Drug Loading/Release Properties and Biocompatability. *Cellulose CHemistry and Technology, 44*(9), 369-378.

Oyefusi, A., Olanipekun, O., Neelgund, G. M., Peterson, D., Stone, J. M., Williams, E., . . . Oki, A. (2014). Hydroxyapatite grafted carbon nanotubes and graphene nanosheets: Promising bone implant materials. *Spectrochimica Acta Part A: Molecular and Biomolecular Spectroscopy, 132*(0), 410-416. doi: http://dx.doi.org/10.1016/j.saa.2014.04.004

Patlolla, A., Collins, G., & Livingston Arinzeh, T. (2010). Solvent-dependent properties of electrospun fibrous composites for bone tissue regeneration. *Acta Biomaterialia, 6*(1), 90-101. doi: http://dx.doi.org/10.1016/j.actbio.2009.07.028

Polini, A., Pisignano, D., Parodi, M., Quarto, R., & Scaglione, S. (2011). Osteoinduction of Human Mesenchymal Stem Cells by Bioactive Composite Scaffolds without Supplemental Osteogenic Growth Factors. *PLoS ONE, 6*(10), e26211. doi: 10.1371/journal.pone.0026211

Portocarrero, G. (2010). *Discovering the Path of Cartilage Regeneration: An Investigation of the Complexities of Nature's Ultimage Smart Material*. Biomedical Engineering. New Jersey Institute of Technology.

Reactome. (2013). Reactome: A Curated Pathway Database. Reactome Retrieved October 08, 2013 http://www.reactome.org/PathwayBrowser/#FOCUS_PATHWAY_ID=216083

Reusch, W. (2005). Infrared Spectroscopy. 2014, from http://www2.chemistry.msu.edu/faculty/reusch/VirtTxtJml/Spectrpy/InfraRed/infrared.htm

Roughley, P. (2006). The Structure and Function of Cartilage Proteoglycans. *European Cells and Materials, 12,* 92-101.

Shen, G. (2005). The role of type X collagen in facilitating and regulating endochondral ossification of articular cartilage. *Orthod Craniofac Res, 8*(1), 11-17. doi: 10.1111/j.1601-6343.2004.00308.x

Sherwood, L. (2007). Bone Growth. In M. Arbogast (Ed.), *Human Physiology from Cells to Systems* (7 ed., pp. 679-681): Yolanda Cossio.

Shier, Butler, & Lewis. (2009). Picture of compact bone: McGraw Hill.

Sigma-Aldrich. (2014). Polycaprolactone.

Sipe, J. (2002). Tissue Engineering and Reparative Medicine. *Annals New York Academy of Sciences, 961*, 1-9.

Society, C. (2011). Sodium Cellulose Sulfate. National Institute of Standards and Technology Retrieved 2014 http://webbook.nist.gov/cgi/cbook.cgi?ID=B6002718&Mask=80#IR-Spec

Takahashi, K., & Yamanaka, S. (2006). Induction of Pluripotent Stem Cells from Mouse Embryonic and Adult Fibroblast Cultures by Defined Factors. *Cell, 126*(4), 663-676. doi: http://dx.doi.org/10.1016/j.cell.2006.07.024

Thompson, C., Chase, G., Yarin, A., & Reneker, D. (2007). Effects of Parameters on Nanofiber Diameter Determined from Electrospinning Model. *Polymer, 48*, 6913-6922. doi: http://dx.doi.org/10.1016/j.polymer.2007.09.017

Tuckwell, D., Ayad, S., Grant, M., Takigawa, M., & Humphries, M. (1994). Conformation dependence of integrin-type II collagen binding. Inability of collagen peptides to support alpha 2 beta 1 binding, and mediation of adhesion to denatured collagen by a novel alpha 5 beta 1-fibronectin bridge. *Journal of Cell Science, 107*, 993-1005.

Tulla, M. (2007). *Collagen receptor integrins: evolution, ligand binding selectivity and the effect of activation.* University of Turku, Findland. Retrieved from https://jyx.jyu.fi/dspace/bitstream/handle/123456789/13173/9789513927660.pdf?sequence=1

UniProt. (2013a). P02458 (CO2A1_HUMAN). UniProtKB/Swiss-Prot Retrieved 2013 http://www.uniprot.org/uniprot/P02458#PRO_0000005730

UniProt. (2013b). P12931 (SRC_HUMAN). UniProtKB/Swiss-Prot Retrieved 2013 http://www.uniprot.org/uniprot/P12931

UniProt. (2013c). P28482 (MK01_HUMAN). UniProtKB/Swiss-Prot Retrieved 2013 http://www.uniprot.org/uniprot/P28482

UniProt. (2013d). P43405 (KSYK_HUMAN). UniProtKB/Swiss-Prot Retrieved 2013 http://www.uniprot.org/uniprot/P43405

UniProt. (2013e). P46109 (CRKL_HUMAN). UniProtKB/Swiss-Prot Retrieved 2013 http://www.uniprot.org/uniprot/P46109

UniProt. (2013f). P47736 (RPGP1_HUMAN). UniProtKB/Swiss-Prot Retrieved 2013 http://www.uniprot.org/uniprot/P47736

UniProt. (2013g). Q9Y490 (TLN1_HUMAN). UniProtKB/Swiss-Prot Retrieved 2013 http://www.uniprot.org/uniprot/Q9Y490

UniProt. (2013h). Q05397 (FAK1_HUMAN). UniProtKB/Swiss-Prot Retrieved 2013 http://www.uniprot.org/uniprot/Q05397

Wang, C. (2002). *Human Lysyl Hydroxylase Isoforms: Multifunctionality of human LH3 and the amino acids improtant for its collagen glycosyltransferase activities.* University of Oulu. Retrieved from http://herkules.oulu.fi/isbn9514267990/

White, D. J., Puranen, S., Johnson, M. S., & Heino, J. (2004). The collagen receptor subfamily of the integrins. *The International Journal of Biochemistry & Cell Biology, 36*(8), 1405-1410. doi: http://dx.doi.org/10.1016/j.biocel.2003.08.016

Woodruff, M. A., & Hutmacher, D. W. (2010). The return of a forgotten polymer—Polycaprolactone in the 21st century. *Progress in Polymer Science, 35*(10), 1217-1256. doi: http://dx.doi.org/10.1016/j.progpolymsci.2010.04.002

Wu, J. J., Lark, M. W., Chun, L. E., & Eyre, D. R. (1991). Sites of stromelysin cleavage in collagen types II, IX, X, and XI of cartilage. *J Biol Chem, 266*(9), 5625-5628.

Ying, Q.-L., Nichols, J., Chambers, I., & Smith, A. (2003). BMP Induction of Id Proteins Suppresses Differentiation and Sustains Embryonic Stem Cell Self-Renewal in Collaboration with STAT3. *Cell, 115*(3), 281-292. doi: http://dx.doi.org/10.1016/S0092-8674(03)00847-X

Young, S., Wong, M., Tabata, Y., & Mikos, A. G. (2005). Gelatin as a delivery vehicle for the controlled release of bioactive molecules. *Journal of Controlled Release, 109*(1–3), 256-274. doi: http://dx.doi.org/10.1016/j.jconrel.2005.09.023

Zeng, X., Danquah, M., Potumarthi, R., Cao, J., Chen, X. D., & Lu, Y. (2013). Characterization of Sodium Cellulose Sulphate/Poly-Dimethyl-Diallyl-Ammonium Chloride Biological Capsules for Immobilized Cultivation of Microalgae. *Journal of Chemical Technology and Biotechnology, 88*(4), 599-605. doi: 10.1002/jctb.3869

Zhang, Y., Wang, F., Tan, H., Chen, G., Guo, L., & Yang, L. (2012). Analysis of the Mineral Composition of the Human Calcified Cartilage Zone. *International Journal of Medical Sciences, 9*(5), 353-360. doi: 10.7150/ijms.4276